

**UCLA**

**UCLA Electronic Theses and Dissertations**

**Title**

Identification and functional analysis of an essential daughter bud assembly complex in *Toxoplasma gondii*

**Permalink**

<https://escholarship.org/uc/item/4qz307qk>

**Author**

Rios, Rebecca Pasquarelli

**Publication Date**

2024

Peer reviewed|Thesis/dissertation

UNIVERSITY OF CALIFORNIA

Los Angeles

Identification and functional analysis of an  
essential daughter bud assembly complex in *Toxoplasma gondii*

A dissertation submitted in partial satisfaction of the  
requirements for the degree Doctor of Philosophy  
in Molecular Biology

by

Rebecca Pasquarelli Rios

2024

© Copyright by

Rebecca Pasquarelli Rios

2024

## ABSTRACT OF THE DISSERTATION

Identification and functional analysis of an essential daughter bud assembly complex  
in the parasite *Toxoplasma gondii*

by

Rebecca Pasquarelli Rios

Doctor of Philosophy in Molecular Biology

University of California, Los Angeles, 2024

Professor Peter John Bradley, Chair

*Toxoplasma gondii* is a single-celled obligate intracellular parasite which is estimated to infect 30% of the global human population. While *T. gondii* infections are typically asymptomatic in healthy individuals, they can cause life-threatening complications in immunocompromised individuals and congenitally infected neonates. As current treatments are toxic and do not clear the lifelong chronic infection, a deeper understanding of parasite biology is needed to identify novel targets for therapeutic intervention. As a member of the phylum Apicomplexa, *T. gondii* contains several unique organelles which play critical roles in facilitating the parasite's lytic cycle, which causes the acute phase of disease. One of these unique apicomplexan organelles is the inner membrane complex (IMC), which lies directly underneath the parasite's plasma membrane and is composed of a series of flattened vesicles supported by an underlying cytoskeletal network. The IMC plays essential roles throughout the *T. gondii* lytic cycle by serving as the platform for the molecular machinery that controls parasite motility, stabilizing the apical complex which facilitates host cell invasion, and acting as a scaffold for developing daughter cells during parasite replication.

*T. gondii* replicates using a unique form of internal budding called endodyogeny, in which two daughter buds are formed within the cytoplasm of a single maternal cell. Endodyogeny can be divided into four steps: bud initiation, elongation, constriction, and maturation. During this process, IMC components are added to the developing daughter cell scaffold in a tightly regulated, sequential manner. While many of the components of the IMC are known to be important for parasite fitness, most are maintained in mature parasites and play critical roles in other phases of the lytic cycle besides replication. Several IMC proteins have been identified which are found only in the IMC of daughter buds, but most are dispensable or have only moderate impacts on parasite fitness. The identification of IMC32, a daughter-specific IMC protein which recruits during bud initiation and is essential for endodyogeny, led us to hypothesize that other unidentified daughter-specific IMC proteins coordinate with IMC32 to lay the foundation of the daughter cell scaffold.

Here, we report the discovery of an essential daughter bud assembly complex which lays the foundation for the daughter IMC in *T. gondii*. Using proximity labelling and protein-protein interaction screens, we identify two novel proteins, IMC43 and BCC0, as binding partners of IMC32. We analyze the function of each of these proteins using conditional knockdown systems which reveal that both IMC43 and BCC0 are essential for endodyogeny. We additionally use deletion analyses and functional complementation to identify which regions of IMC43 and BCC0 are essential for localization and function. By employing pairwise yeast two-hybrid assays, we determine which regions of IMC32, IMC43, and BCC0 are involved in complex formation. Finally, we assess how loss of each complex component affects each of the others. These data allow us to develop a hierarchical model for complex assembly in which BCC0 depends on IMC32 for its localization during bud initiation, and IMC32 in turn depends on IMC43 for its localization later during bud elongation. Together, this work expands our understanding of how nascent daughter buds are assembled during endodyogeny and yields ample opportunities for future studies into the function and regulation of these essential proteins in both *T. gondii* and other parasites.

The dissertation of Rebecca Pasquarelli Rios is approved.

Elissa A. Hallem

Kent L. Hill

Patricia J. Johnson

Jorge Torres

Peter John Bradley, Committee Chair

University of California, Los Angeles

2024

# Table of Contents

Abstract.....	ii
Committee.....	iv
List of Figures .....	vii
List of Tables.....	ix
Acknowledgements.....	x
Vita.....	xiii
Chapter 1: Introduction .....	1
1.1 <i>Toxoplasma gondii</i> is an important human pathogen .....	2
1.1.1 Prevalence and transmission .....	2
1.1.2 Clinical manifestations and treatment .....	3
1.2 <i>Toxoplasma gondii</i> is an apicomplexan parasite .....	5
1.2.1 The phylum Apicomplexa .....	5
1.2.2 Morphological features of apicomplexan parasites .....	6
1.2.3 Cell division in apicomplexan parasites.....	9
1.3 The <i>Toxoplasma gondii</i> inner membrane complex .....	11
1.3.1 Structure of the inner membrane complex .....	11
1.3.2 Subdomains of the inner membrane complex.....	13
1.3.3 Functions of the inner membrane complex .....	16
1.4 Endodyogeny in <i>Toxoplasma gondii</i> .....	17
1.4.1 Sequential recruitment of daughter IMC proteins.....	17
1.4.2 Regulation of endodyogeny.....	21
1.5 Overview of the dissertation.....	24
1.6 References.....	27
Chapter 2: Identification of IMC43, a novel IMC protein that collaborates with IMC32 to form an essential daughter bud assembly complex in <i>Toxoplasma gondii</i> .....	40
2.1 Abstract.....	41
2.2 Introduction .....	42
2.3 Results.....	43
2.3.1 IMC43 is a component of the early daughter cell scaffold.....	43
2.3.2 IMC43 is an essential protein involved in endodyogeny .....	44
2.3.3 IMC43 contains an essential functional domain near the C-terminus of the protein .....	46
2.3.4 Identification of IMC43 binding partners using TurboID and Y2H screening.....	47

2.3.5	TGGT1_297120 encodes a novel IMC protein with a dynamic localization that is dependent on IMC43 .....	50
2.3.6	IMC43 regulates the organization of IMC32 in the daughter cell scaffold .....	50
2.4	Discussion.....	52
2.5	Materials and methods.....	56
2.6	Acknowledgments.....	62
2.7	References.....	62
2.8	Supplemental Material .....	67
Chapter 3: BCC0 collaborates with IMC32 and IMC43 to form the <i>Toxoplasma gondii</i> essential daughter bud assembly complex.....		78
3.1	Abstract.....	79
3.2	Introduction .....	80
3.3	Results.....	81
3.3.1	Identification of candidate IMC32 binding partners .....	81
3.3.2	BCC0 depends on IMC32 and IMC43 for its localization to the daughter IMC .....	83
3.3.3	Residues 701-877 are essential for BCC0 localization and function.....	85
3.3.4	Residues 1-899 are sufficient for BCC0 function .....	85
3.3.5	BCC0's essential domain binds to IMC32's coiled-coil domains.....	87
3.4	Discussion.....	88
3.5	Materials and methods.....	93
3.6	Acknowledgments.....	98
3.7	References.....	98
3.8	Supplemental Material .....	103
Chapter 4: Conclusions and Future Directions .....		113
4.1	Conclusions .....	114
4.2	Future Directions.....	116
4.3	References.....	120

## List of Figures

Figure 1-1: Cellular structure of <i>Toxoplasma gondii</i> .....	7
Figure 1-2: <i>T. gondii</i> replicates by endodyogeny .....	9
Figure 1-3: The inner membrane complex of <i>T. gondii</i> .....	12
Figure 1-4: <i>T. gondii</i> IMC subdomains .....	14
Figure 1-5: Sequential recruitment of IMC proteins during endodyogeny .....	18
Figure 2-1: TGGT1_238895 localizes to the daughter IMC body and is recruited at the earliest stages of endodyogeny .....	44
Figure 2-2: IMC43 is essential for parasite replication and survival.....	45
Figure 2-3: Assessment of key structures involved in endodyogeny .....	47
Figure 2-4: Deletion analyses reveal regions involved in IMC43 localization and function .....	48
Figure 2-5: TurboID and Y2H screens yield 30 candidate IMC43 binding partners .....	49
Figure 2-6: IMC44 is a novel IMC protein which depends on IMC43 binding for regulation of its dynamic localization .....	51
Figure 2-7: IMC43 binding is required for maintenance of IMC32 during later stages of endodyogeny .....	53
Figure 2-8: Summary .....	54
Figure 2-S1: Conservation and secondary structure predictions for TGGT1_238895.....	67
Figure 2-S2: IFA showing successful targeting of the IMC43 locus using CRISPR/Cas9 .....	69
Figure 2-S3: Western blots showing depletion and complementation of IMC43 <sup>AID</sup> .....	70
Figure 2-S4: Most IMC43 deletion constructs localize normally to the daughter IMC .....	71
Figure 2-S5: Most IMC43 deletion constructs rescue the morphological and replication defects observed upon depletion of IMC43 .....	72
Figure 2-S6: IMC44 is dispensable for the <i>T. gondii</i> lytic cycle and does not impact IMC43 localization.....	73
Figure 2-S7: Most IMC43 deletion constructs rescue the mislocalization of IMC44 caused by depletion of IMC43 .....	74
Figure 2-S8: Depletion of IMC32 has no effect on IMC43 localization .....	75

Figure 2-S9: Most IMC43 deletion constructs rescue the mislocalization of IMC32 caused by depletion of IMC43 .....	76
Figure 3-1: TurboID and Y2H screens identify BCC0 as a candidate IMC32 binding partner.....	82
Figure 3-2: BCC0 requires both IMC32 and IMC43 for its localization to the daughter IMC .....	83
Figure 3-3: BCC0 knockdown does not affect the localization of IMC32 or IMC43 .....	84
Figure 3-4: BCC0 residues 701-877 are required for localization and residues 170-375 have a minor impact on function.....	86
Figure 3-5: BCC0 residues 701-877 are essential for function.....	88
Figure 3-6: BCC0 residues 1-899 are sufficient for function .....	89
Figure 3-7: BCC0 residues 570-899 bind to IMC32's C-terminal coiled-coil domains .....	90
Figure 3-8: Summary .....	91
Figure 3-S1: The AID system does not provide a sufficient knockdown for analysis of BCC0 function.....	103
Figure 3-S2: Conservation and secondary structure predictions for BCC0 .....	104
Figure 3-S3: Most BCC0 deletion constructs localize normally .....	107
Figure 3-S4: Validation of BCC0 knockout for strains depicted in Fig 3-4 .....	108
Figure 3-S5: ATc treatment is toxic to wild-type <i>T. gondii</i> .....	110
Figure 3-S6: Localization and PCR verification for strains depicted in Fig 3-6.....	111
Figure 4-1: Updated timeline of the sequential recruitment of IMC proteins during endodyogeny .....	114

## List of Tables

Table 2-S1: Full IMC43 <sup>TurboID</sup> mass spectrometry results.....	77
Table 2-S2: Full IMC43 Y2H screen results.....	77
Table 2-S3: Oligonucleotides used in this study.....	77
Table 3-S1: Full IMC32 <sup>TurboID</sup> mass spectrometry results.....	112
Table 3-S2: Full IMC32 Y2H screen results.....	112
Table 3-S3: Oligonucleotides used in this study.....	112
Table 3-S4: Raw data for quantification of western blot and plaque assays .....	112

## Acknowledgements

First, I would like to thank my advisor, Dr. Peter Bradley, who has been an incredible mentor to me for the past five years. His infectious enthusiasm and dedication to fostering a positive work environment made the Bradley lab a wonderful place to learn and work. I deeply appreciate the countless hours we spent together troubleshooting experiments, working on fellowship proposals and manuscripts, and practicing presentations. I'm very grateful that I had the opportunity to complete my PhD in his lab. I would also like to thank all the members of the Bradley lab who I have had the pleasure of working with. Peter Back and Amara Thind were both my friends and my mentors. Peter Back and I worked together on several projects, and he was always willing to provide me with advice or perspective about science, graduate school, or life in general. Amara was a great friend who I could always count on to make me laugh or commiserate with me over the stresses of graduate school. I'm grateful that I had the chance to work with both of them. Juan Torres and Andrew Ly trained me during my rotation and I'm thankful for their time and help. Juan also initiated the IMC32 project which my dissertation builds upon. I'm very grateful to the members of my thesis committee, Dr. Elissa Hallem, Dr. Kent Hill, Dr. Patricia Johnson, and Dr. Jorge Torres, for their support and guidance throughout the years. I would also like to thank Jihui Sha and James Wohlschlegel who have been collaborators on all of my papers.

I would also like to acknowledge the people who inspired me to pursue a PhD in the first place. My undergraduate research advisor Dr. Robert Reenan was generous enough to hire me as a paid undergraduate laboratory technician, which allowed me to spend my time learning in the lab rather than working in the dining hall. He was a great teacher and a joy to work with, and being in his lab is what made me realize I wanted to pursue a career in scientific research. During my time in the Reenan lab, I primarily worked with Victoria St. Amand. She was exceptionally kind, patient, and generous with her time and knowledge, and I'm grateful for her mentorship and training. Dr. Christopher de Graffenried and Dr. Richard Bungiro introduced me to the fascinating

field of molecular parasitology and supported me by writing my letters of recommendation for graduate school, which I am very thankful for. I would also like to thank my high school chemistry teacher, Meredith Bizragane. Her class was what made me first discover my love of science, and her encouragement gave me the confidence to pursue it in college.

I would like to thank my dad, Raymond Pasquarelli, who instilled in me my work ethic and drive. He has been a loving and supportive father and has always helped me in any way that he could. I'm very grateful for his support. Finally, I am deeply grateful to my amazing husband, Isaiah Rios. His encouragement throughout both my undergraduate and graduate studies gave me the confidence and strength to keep going even when it was hard. He kept me grounded and always managed to make me laugh no matter how stressed I was. I'm incredibly lucky to have him and our adorable dog Beans in my life.

The figures in Chapter 1 contain images which were reprinted or adapted from published work. The electron micrograph in Figure 1-1A is reprinted from Dubey et al. 1998 with permission from the American Society for Microbiology for the purpose of this dissertation (license ID 1485357-1). The diagrams in Figure 1-1B and 1-3C are adapted from Katris et al. 2014, which is an open access article distributed under the terms of the [Creative Commons Attribution 4.0 International License](#). The electron micrograph in Figure 1-2A is reprinted from Striepen et al. 2000, which is an open access article distributed under the terms of the [Creative Commons Attribution-NonCommercial-ShareAlike 4.0 International License](#). The diagrams in Figure 1-5 and 4-1 are adapted from Gubbels et al. 2020, which is an open access article distributed under the terms of the [Creative Commons Attribution 4.0 International License](#). The electron micrograph in Figure 1-3A was generated by Josh Beck during his time in the Bradley lab (unpublished). Figure 1-3B was created with BioRender.

Chapter 2 was originally published in *PLOS Pathogens* and is reprinted here under the terms of the [Creative Commons Attribution 4.0 International License](#).

Pasquarelli RR, Back PS, Sha J, Wohlschlegel JA, Bradley PJ. Identification of IMC43, a novel IMC protein that collaborates with IMC32 to form an essential daughter bud assembly complex in *Toxoplasma gondii*. *PLoS Pathog*. 2023;19: e1011707.

<https://doi.org/10.1371/journal.ppat.1011707> PMID: 37782662

Peter S. Back performed the initial localization of IMC44 and generated the IMC44 knockout strain. Jihui Sha and James A. Wohlschlegel performed the mass spectrometric analysis of biotinylated proteins. Peter J. Bradley was the principal investigator. This work was supported by NIH grants AI123360 to Peter J. Bradley and GM089778 to James A. Wohlschlegel. Rebecca R. Pasquarelli and Peter S. Back were supported by the Ruth L. Kirschstein National Research Service Award GM007185 and UCLA Molecular Biology Institute Whitcome Fellowship. Rebecca R. Pasquarelli was additionally supported by the Ruth L. Kirschstein National Research Service Award AI007323.

Chapter 3 was originally published in *PLOS Pathogens* and is reprinted here under the terms of the [Creative Commons Attribution 4.0 International License](#).

Pasquarelli RR, Sha J, Wohlschlegel JA, Bradley PJ. BCC0 collaborates with IMC32 and IMC43 to form the *Toxoplasma gondii* essential daughter bud assembly complex. *PLoS Pathog* 20(7): e1012411. <https://doi.org/10.1371/journal.ppat.1012411> PMID: 39024411

Jihui Sha and James A. Wohlschlegel performed the mass spectrometric analysis of biotinylated proteins. Peter J. Bradley was the principal investigator. This work was supported by NIH grants AI123360 to Peter J. Bradley and GM153408 to James A. Wohlschlegel. Rebecca R. Pasquarelli was supported by the Ruth L. Kirschstein National Research Service Awards GM007185 and AI007323, as well as the UCLA Molecular Biology Institute Whitcome Fellowship.

## Vita

### Education

---

2019 Bachelor of Science in Biology, with Honors, Brown University

### Research

---

2020 – 2024 Graduate Student Researcher, Laboratory of Dr. Peter Bradley  
Department of Microbiology, Immunology, and Molecular Genetics, UCLA

Spring 2020 Rotating Graduate Student Researcher, Laboratory of Dr. Elissa Hallem  
Department of Microbiology, Immunology, and Molecular Genetics, UCLA

Winter 2020 Rotating Graduate Student Researcher, Laboratory of Dr. Peter Bradley  
Department of Microbiology, Immunology, and Molecular Genetics, UCLA

Fall 2020 Rotating Graduate Student Researcher, Laboratory of Dr. Kent Hill  
Department of Microbiology, Immunology, and Molecular Genetics, UCLA

2016 – 2019 Undergraduate Student Researcher, Laboratory of Dr. Robert Reenan  
Department of Molecular Biology, Cellular Biology, and Biochemistry,  
Brown University

### Submitted Manuscripts

---

August 2024 **Pasquarelli RR**, Quan JJ, Cheng ES, Yang V, Britton TA, Sha J, Wohlschlegel JA, Bradley PJ. "Characterization and functional analysis of *Toxoplasma* Golgi-associated proteins identified by proximity labelling." *Under review at mBio*.

### Publications

---

July 2024 **Pasquarelli RR**, Sha J, Wohlschlegel JA, Bradley PJ. "BCC0 collaborates with IMC32 and IMC43 to form the *Toxoplasma gondii* essential daughter bud assembly complex" *PLOS Pathogens*.

October 2023 **Pasquarelli RR**, Back PS, Sha J, Wohlschlegel JA, Bradley PJ. "Identification of IMC43, a novel IMC protein that collaborates with IMC32 to form an essential daughter bud assembly complex in *Toxoplasma gondii*." *PLOS Pathogens*.

January 2023 Back PS, Moon AS, **Pasquarelli RR**, Bell HN, Torres JA, Chen AL, Sha J, Vashisht AA, Wohlschlegel JA, Bradley PJ. "IMC29 Plays an Important Role in *Toxoplasma* Endodyogeny and Reveals New Components of the Daughter-Enriched IMC Proteome." *mBio*.

October 2021 Chern JH, **Pasquarelli RR**, Moon AS, Chen AL, Sha J, Wohlschlegel JA, Bradley PJ. "A Novel *Toxoplasma* Inner Membrane Complex Suture-

Associated Protein Regulates Suture Protein Targeting and Colocalizes with Membrane Trafficking Machinery.” *mBio*.

February 2021 Torres JA, **Pasquarelli RR**, Back PS, Moon AS, Bradley PJ.  
“Identification and Molecular Dissection of IMC32, a Conserved *Toxoplasma* Inner Membrane Complex Protein That Is Essential for Parasite Replication.” *mBio*.

#### Honors and Awards

---

2024 Sidney Charles Rittenberg Award, UCLA Department of Microbiology, Immunology, and Molecular Genetics

2022 John-Eiserling-Lengyel Teaching Excellence Award, UCLA Molecular Biology Institute

2022 Best Talk Award, 16<sup>th</sup> Biennial International Congress on Toxoplasmosis

2018 Undergraduate Teaching and Research Award, Brown University Office of Biology Undergraduate Education

#### Grants and Fellowships

---

2021 and 2023 Microbial Pathogenesis Training Grant (Ruth L. Kirschstein National Research Service Award AI007323), UCLA

2021 – 2023 Whitcome Predoctoral Fellowship, UCLA Molecular Biology Institute

2020 Cell and Molecular Biology Training Grant (Ruth L. Kirschstein National Research Service Award GM007185), UCLA

#### Selected Presentations

---

2023 “IMC43 plays an essential role in formation of the *T. gondii* daughter IMC.” 34<sup>th</sup> Annual Molecular Parasitology Meeting. Poster Presentation.

2022 “Identification and characterization of IMC53, a novel early daughter IMC protein which plays an essential role in endodyogeny.” 16<sup>th</sup> Biennial International Congress on Toxoplasmosis. Oral presentation. Awarded “Best Talk.”

2022 “Identification and characterization of IMC53, a novel early daughter inner membrane complex protein which plays an essential role in *Toxoplasma* replication.” 33<sup>rd</sup> Annual Molecular Parasitology Meeting. Oral Presentation.

2020 “Identification and Functional Analysis of Parasite-Specific Golgi Proteins in *Toxoplasma gondii*.” Southern California Eukaryotic Pathogens Symposium. Poster presentation.

## **Chapter 1:**

### Introduction

## 1.1 *Toxoplasma gondii* is an important human pathogen

### 1.1.1 Prevalence and transmission

*Toxoplasma gondii* is an obligate intracellular parasite which can infect nearly any nucleated cell within any warm-blooded animal [1]. Most *T. gondii* infections are acquired by ingesting an encysted form of the parasite [2]. First, ingestion of raw or undercooked meat derived from a *Toxoplasma*-infected animal can result in infection from tissue cysts, which contain hundreds of *T. gondii* parasites surrounded by a hardy cyst wall. Another infectious form of the parasite is oocysts, the result of the parasite's sexual cycle which occurs in the gut of its definitive host, members of the Felidae family. Oocysts are shed in the feces of these animals and can be accidentally ingested through contaminated food or water, or through the care of domestic cats. Due to their protective bilayered wall, oocysts can persist and remain infectious in moist environments for up to a year [3]. Once tissue cysts or oocysts are ingested, they are released within the gut where they first infect epithelial cells and then disseminate throughout the body by infecting leukocytes in the circulatory system [4]. In addition to oral transmission, *T. gondii* can be transmitted vertically from a pregnant woman to her developing fetus. This can only occur when the mother acquires a primary *T. gondii* infection during pregnancy, allowing the parasite to travel through the circulatory system and cross the placenta prior to the development of a protective immune response [5].

Currently, it is estimated that approximately 30% of the global human population is infected with *T. gondii* [6,7]. Prevalence in specific countries varies greatly depending on factors such as climate, diet, and sanitation. Countries in the Far East including South Korea and Japan have the lowest seroprevalence of less than 10%, whereas countries in South America and Africa which have tropical climates, such as Costa Rica and Nigeria, have seroprevalences greater than 70% [6]. Since infection is often acquired through ingestion of raw or undercooked meat, countries

that incorporate these foods into their diets tend to have higher rates of infection. For example, seroprevalence in France is estimated at 54%. In the United States, prevalence is relatively low at 11%. Given its high prevalence, global distribution, and wide range of host species, *T. gondii* is considered to be the most successful parasite in existence.

### **1.1.2 Clinical manifestations and treatment**

The clinical manifestations and health outcomes for a *T. gondii* infection vary depending on the route of infection and immune status of the host [2]. For healthy adults and children who acquire the infection orally, the acute infection typically consists of mild flu-like symptoms such as fever, aches, and lymphadenopathy. During this phase of the disease, a rapidly replicating form of the parasite called tachyzoites disseminates throughout the body by infecting leukocytes in the circulatory system [8]. These symptoms typically resolve on their own within weeks as the body mounts a protective immune response against the pathogen, resulting in the destruction of most tachyzoites [9]. However, a small percentage of tachyzoites avoid immune clearance by differentiating into a slowly replicating form called bradyzoites, which form hardy tissue cysts within muscle and brain tissue [10]. These tissue cysts can persist for many decades, resulting in lifelong chronic infection. In healthy individuals, the chronic infection is typically asymptomatic, although in rare cases the parasite can invade the eye (a site of immune privilege) and cause tissue destruction, a condition called ocular toxoplasmosis [11]. This most often occurs in the elderly due to a waning immune response, or in individuals who have a genetic predisposition linked to HLA type, polymorphisms in toll-like receptor genes, or altered expression levels of certain cytokines [12]. If left untreated, ocular toxoplasmosis can lead to retinal scarring or blindness [11].

While *Toxoplasma* infection in immunocompetent individuals usually does not pose a serious risk, immunocompromised individuals experience potentially fatal disease due to the

body's inability to clear tachyzoites. This can occur either when an already immunocompromised person acquires a primary infection, or when a previously healthy person with a chronic infection becomes immunocompromised later in life, causing the parasite to recrudesce by converting from the bradyzoite form to the tachyzoite form [13]. Toxoplasmosis is best known for causing severe disease in patients with acquired immunodeficiency syndrome (AIDS). In these patients, replication of tachyzoites in neural tissue can lead to the formation of lesions in the brain leading to toxoplasmic encephalitis, which is fatal if left untreated. While the incidence of AIDS has declined greatly in recent decades due to the success of antiretroviral therapies, toxoplasmic encephalitis is still the leading cause of brain lesions in patients with HIV [14]. Another high-risk group which has even worse outcomes are solid organ, bone marrow, or hematopoietic stem cell transplant patients. In these patients, the parasite is often disseminated throughout the body rather than being primarily restricted to the central nervous system, and mortality ranges from 38-67% even with treatment [15].

Another group which can experience serious or life-threatening disease are neonates who become infected in utero due to vertical transmission. Neonates are at risk of becoming infected if their mother either acquires a primary infection during pregnancy or becomes immunocompromised during pregnancy, resulting in reactivation of a chronic infection [16]. While 75% of infected newborns are subclinical at birth, 14-85% of these patients develop complications months or years later [5]. The classic triad of congenital toxoplasmosis is chorioretinitis, intracranial calcifications, and hydrocephalus. In severe cases, neonates can additionally exhibit fever, hepatosplenomegaly, jaundice, convulsions, and abnormal cerebrospinal fluid. Clinical manifestations of congenital toxoplasmosis vary greatly depending on how early in development the infection is acquired. Neonates who become infected during the first trimester experience the most severe disease and are at increased risk for spontaneous abortion, while those infected

during the second or third trimester have a higher rate of survival and typically experience less severe complications [17].

Currently, there is no vaccine to protect against *T. gondii* infection and no treatments exist that can clear the chronic infection. Acute infections can be treated using drugs that target the folate pathway involved in DNA synthesis. The most commonly used therapy for toxoplasmosis is pyrimethamine, which targets the dihydrofolate reductase enzyme, combined with sulfonamides, which target the dihydropteroate synthetase enzyme [15]. Since these drugs target both parasite and human enzymes, they cause severe side effects due to myelotoxicity. However, these effects can be significantly reduced by addition of folinic acid. This treatment regimen can additionally be prescribed for women who become infected during pregnancy, but is teratogenic and thus cannot be used during the first trimester [18,19]. In Europe, Canada, and Mexico, women diagnosed with a new *T. gondii* infection during the first trimester are treated with spiramycin to prevent transmission to the developing fetus. However, it is still considered an experimental drug in the United States and requires special permission from the Food & Drug Administration [20]. Furthermore, spiramycin is ineffective for established congenital infections due to its inability to cross the placenta [15]. Therefore, early diagnosis is crucial for preventing disease in these patients. Together, *T. gondii*'s high global prevalence, serious disease in vulnerable populations, and lack of preventative and curative therapies underscores the need for a deeper understanding of apicomplexan biology.

## **1.2 *Toxoplasma gondii* is an apicomplexan parasite**

### **1.2.1 The phylum Apicomplexa**

*T. gondii* is a member of the Apicomplexa, a phylum of over 6,000 protozoan parasites [21]. All members of the phylum are obligate intracellular parasites which undergo a lytic cycle

(host cell invasion, intracellular replication, and egress) during one or more stages of their life cycles. Other important human pathogens within the phylum include species within the genera *Plasmodium* and *Cryptosporidium*. *Plasmodium spp.* are the causative agents of malaria, which is endemic in 84 countries and caused over 600,000 deaths in 2021 [22,23]. *Cryptosporidium spp.* are the second leading cause of moderate to severe diarrhea in infants, leading to growth stunting [24,25]. The phylum also includes several important veterinary pathogens which cause economic loss in the livestock industry. These include *Eimeria spp.* which causes chicken coccidiosis and *Neospora caninum* which causes abortion in cattle [26–28]. Historically, most apicomplexan parasites have been difficult to study due to a lack of in vitro culture systems and inability to achieve stable transfection. *T. gondii* is highly experimentally tractable and has a robust set of molecular tools for genetic and functional analysis, making it an excellent model system for studying less tractable apicomplexan parasites [29,30].

### **1.2.2 Morphological features of apicomplexan parasites**

The defining feature of the Apicomplexa is the apical complex, an assemblage of structural and secretory elements at the apex of the cell which facilitates the process of host cell invasion (Figure 1-1) [21]. The *T. gondii* apical complex consists of multiple components: the apical polar ring, conoid, and two preconoidal rings [31]. The apical polar ring serves as a microtubule organizing center from which an array of 22 subpellicular microtubules originate. The conoid sits atop the apical polar ring and is a hollow, barrel-shaped structure made of tubulin filaments. The preconoidal rings sit apical to the conoid, and within the conoid there are an additional two interconoidal microtubules.

The apical complex serves as the site of exocytosis for proteins involved in parasite motility and host cell invasion [32,32,33]. These proteins are held within specialized apicomplexan organelles called micronemes and rhoptries [34]. Micronemes are small organelles which

accumulate in the cytoplasm towards the apical end of the cell. These organelles contain transmembrane adhesin proteins which are released onto the surface of the parasite plasma membrane by exocytosis upon initial contact with a host cell [35]. Microneme proteins facilitate gliding motility by attaching to both the host cell plasma membrane and the parasite's actin-myosin motor, which is called the glideosome. The rhoptries are club-shaped organelles which are tethered to the apex of the cell. After a parasite attaches, the rhoptries release a series of proteins which form the moving junction, a ring-shaped structure through which the parasite travels as it invaginates the host cell plasma membrane during invasion [36]. In addition to serving as an anchor for the parasite to penetrate the host cell, the moving junction serves as a molecular sieve which strips host cell proteins off the plasma membrane as the parasite invades, rendering

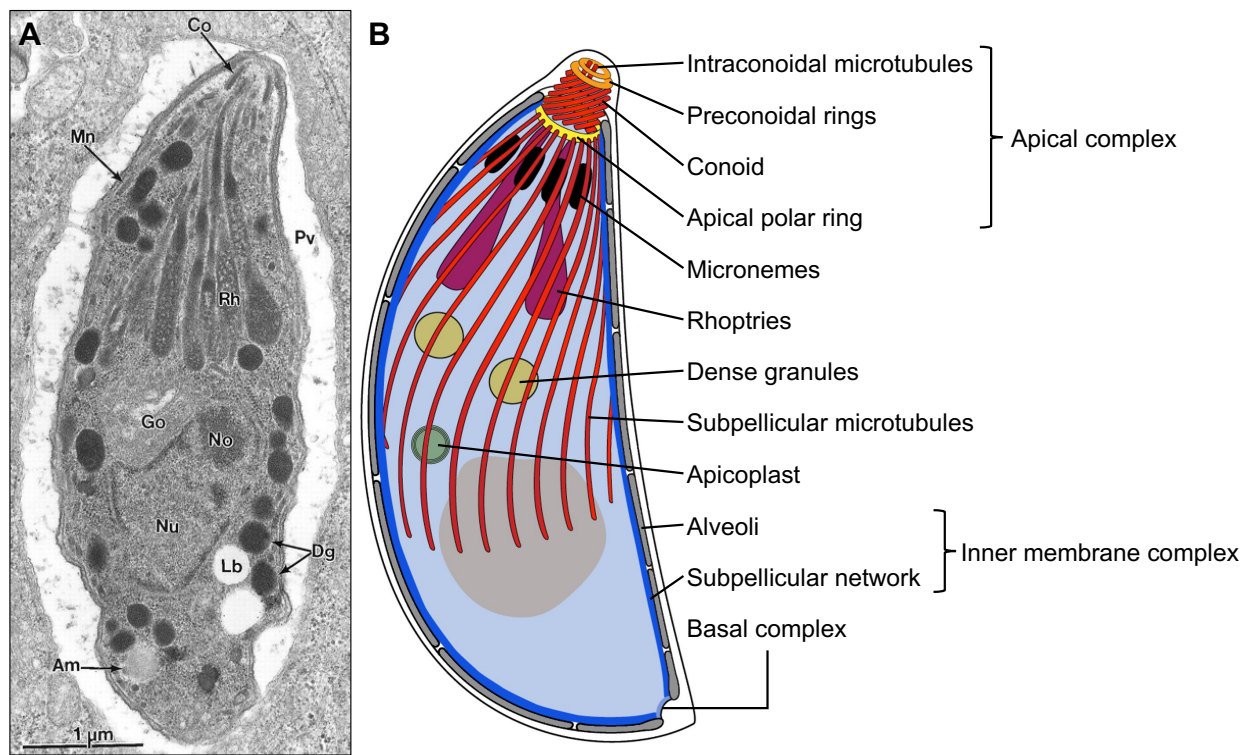


**Figure 1-1. Cellular structure of *Toxoplasma gondii*.** A) Transmission electron micrograph showing a single intracellular *T. gondii* tachyzoite. Key structural features and organelles are labelled. Am = amylopectin granule; Co = conoid; Dg = dense granule; Go = Golgi apparatus; Mn = microneme; No = nucleolus, Nu = nucleus; Pv = parasitophorous vacuole; Rh = rhoptry. Reprinted from Dubey et al. 1998. B) Diagram of a *T. gondii* tachyzoite. Key structural features and organelles are labelled. Adapted from Katris et al. 2014.

the resulting parasitophorous vacuole nonfusogenic due to its lack of host cell receptors [37]. After invasion is complete, a third wave of secretory proteins are released from the dense granules to facilitate vacuolar remodeling and modulation of the host cell [38].

In addition to secretory organelles, another unique feature of apicomplexans is a non-photosynthetic plastid called the apicoplast which primarily functions in the biosynthesis of isoprenoids, fatty acids, and heme. [39]. The apicoplast is surrounded by four membranes and contains a 35 kB circular genome. Therefore, it is believed to be derived from a secondary endosymbiotic event in which an ancestral eukaryote engulfed and retained another eukaryote that had previously engulfed a photosynthetic prokaryote [40]. Despite the fact that it has its own genome, most apicoplast-localizing proteins are nuclear-encoded and must be transported to the organelle via the secretory pathway. Due to its prokaryotic origins and essential functions, the apicoplast is an ideal target for therapeutics [41,42].

Finally, another unique feature of the apicomplexans is the inner membrane complex (IMC), a peripheral membrane system which lies beneath the parasite plasma membrane. The IMC is composed of two structures: a series of flattened vesicles called alveoli and an underlying cytoskeletal network composed of intermediate filament-like proteins called alveolins [43]. While this structure is referred to as the IMC only in the apicomplexans, the alveoli are the defining feature of Alveolata, the superphylum encompassing the apicomplexans as well as the free-living dinoflagellates and ciliates [44]. The IMC plays crucial roles throughout the life cycles of these parasites by stabilizing the apical complex, serving as the platform for the glideosome, and acting as a scaffold for developing daughter cells during parasite replication [43]. The structure and function of the IMC in *T. gondii* will be discussed in detail in Section 1.3.

### 1.2.3 Cell division in apicomplexan parasites

Apicomplexan parasites replicate asexually using a variety of unique budding mechanisms in which the IMC acts as a scaffold for nascent daughter buds. Across all forms of apicomplexan cell division, the daughter IMC is assembled adjacent to the centrosome and grows in an apical to basal direction [45,46]. The various modes of apicomplexan cell division are defined as either internal or external budding mechanisms. The key feature that distinguishes internal budding mechanisms from external budding mechanisms is the time at which the maternal cytoskeleton is degraded [47]. Parasites which replicate using external budding mechanisms degrade the maternal cytoskeleton immediately after host cell invasion [48]. During internal budding, on the other hand, the maternal cytoskeleton is maintained throughout the process of cell division and is only degraded just before the emergence of nascent daughter buds (Figure 1-2) [49].

The two forms of internal budding employed by apicomplexan parasites are endodyogeny, in which two daughter buds are formed within the cytoplasm of a single maternal cell, and endopolygeny, in which more than two buds are formed. Endopolygeny can further be divided into two forms: endopolygeny with karyokinesis, in which the nucleus is divided after each DNA

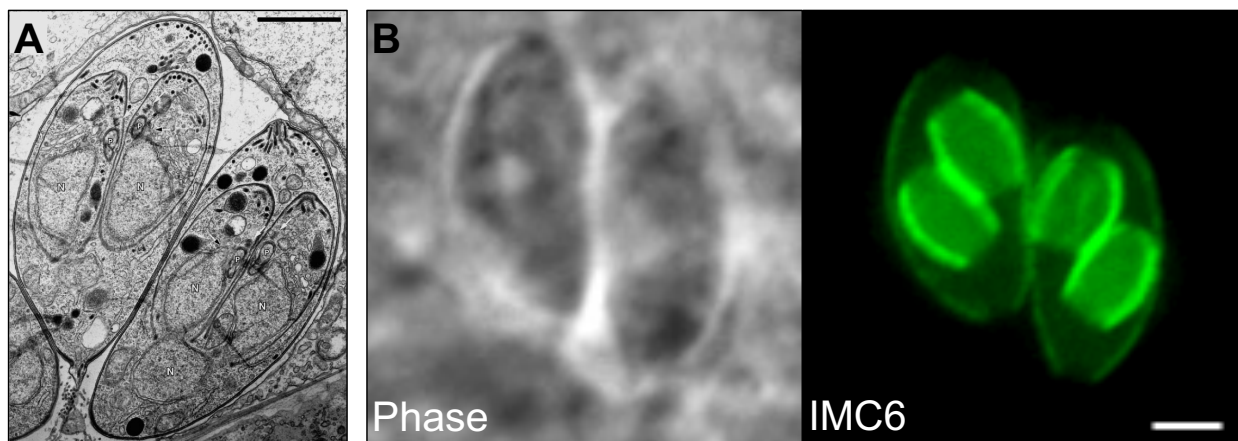


**Figure 1-2. *T. gondii* replicates by endodyogeny.** A) Transmission electron micrograph showing two intracellular *T. gondii* tachyzoites dividing by endodyogeny. Each parasite contains two nearly mature daughter buds. Scale bar is approximately 1 μm. Reprinted from Striepen et al. 2000. B) Phase contrast and immunofluorescence assay (IFA) showing two dividing *T. gondii* tachyzoites, each containing two nearly mature daughter buds stained with antibodies detecting the alveolin IMC6. Scale bar = 2 μm.

replication cycle, or endopolygony without karyokinesis, in which the maternal cell maintains one large polyploid nucleus until the final round of DNA replication is complete [47]. Most parasites within the subclass Coccidia (excluding *Eimeria spp.*) use both endodyogony and one of the forms of endopolygony at different stages of their life cycles. These include *T. gondii* as well as parasites from the genera *Hammondia*, *Neospora*, *Besnoitia*, *Cystoisospora*, and *Sarcocystis*. For example, *T. gondii* divides by endodyogony in intermediate hosts and endopolygony with karyokinesis in its definitive host prior to entering its sexual replication cycle [47,50]. The process of endodyogony in *T. gondii* tachyzoites will be discussed in detail in Section 1.4.

The most well-studied form of external budding is schizogony in *Plasmodium spp.* During schizogony, the maternal cell undergoes multiple rounds of DNA replication followed by nuclear division, with the final round of nuclear division being paired with the budding of all nascent daughter cells off of the maternal plasma membrane simultaneously [47]. The number of buds produced by schizogony varies greatly depending on the life cycle stage and species of *Plasmodium*. For example, blood-stage *P. falciparum* produces 8-32 buds per round of schizogony, whereas liver-stage *P. falciparum* can produce up to 90,000 [51,52]. In addition to *Plasmodium spp.*, schizogony is also employed by parasites in the genera *Eimeria* and *Cryptosporidium* [53,54]. Some species of *Babesia* and *Theileria* employ other forms of external budding referred to as “binary fission,” which produces two daughter cells, and “multiple fission,” which produces four daughter cells [47,55].

The ability of apicomplexan parasites to produce such a large number of daughter cells per round of cell division is due to their unique bipartite centrosome which enables separate regulation of the nuclear and budding cycles [46,56]. The inner core of the centrosome, marked by CEP250-L1, is positioned close to the nuclear membrane in contact with the centrocone, a specialized nuclear pore complex through which the mitotic spindle is formed. Together, the centrosome inner core and centrocone form a complete spindle pole complex which facilitates

karyokinesis with an intact nuclear membrane, a process called closed mitosis [57–59]. The outer core of the centrosome, marked by the centrin protein Cen1, is positioned adjacent to the inner core but farther from the nuclear membrane. The function of the outer core is to initiate budding. The inner and outer core are both duplicated during each nuclear cycle, but the outer core only becomes activated during the budding cycle [46]. In parasites that undergo endodyogeny, the nuclear and budding cycles occur simultaneously. However, in parasites that produce more than two daughter buds through either endopolygeny or schizogony, multiple nuclear cycles occur independently before the budding cycle is activated.

### **1.3 The *Toxoplasma gondii* inner membrane complex**

#### **1.3.1 Structure of the inner membrane complex**

The IMC of *T. gondii* lies directly underneath the parasite's plasma membrane and is comprised of two layers (Figure 1-3). The first layer is a series of vesicles called alveoli which are flattened against the interior of the plasma membrane [60]. The alveoli are rectangular in shape and are arranged in a quilt-like pattern with the edges of adjacent alveoli tightly sutured together. At the apex of the parasite, a single cone-shaped vesicle called the apical cap encircles the apical complex. Some proteins that associate with the alveoli are integral membrane proteins containing one or more transmembrane domains, such as the glideosome components GAP40 and GAP50 [61]. Others, such as ISP1-4 and the glideosome component GAP45, are tethered to the membrane by lipid modifications such as palmitoylation or myristoylation [62–64]. The second layer is a mesh-like network of intermediate filament-like proteins called alveolins, which is referred to as the subpellicular network [65]. The alveolins are a family of 14 proteins (IMC1 and IMC3-15) which are defined by the presence of a conserved proline and valine-rich alveolin domain [44,66]. Additional detergent-insoluble proteins such as PHIL1, ILP1, and many other IMC

proteins associate with the subpellicular network via protein-protein interactions [67–69]. The IMC is further divided into three subdomains: the apical cap, IMC body, and basal complex, which will be discussed in Section 1.3.2.

Underneath the IMC there is an array of 22 highly stable subpellicular microtubules (SPMTs) which originate from the apical polar ring and extend towards the basal end of the parasite, ending at approximately two-thirds the length of the cell [70]. Freeze-fracture electron microscopy studies have shown that the cytoplasmic-facing side of the alveoli is dotted with

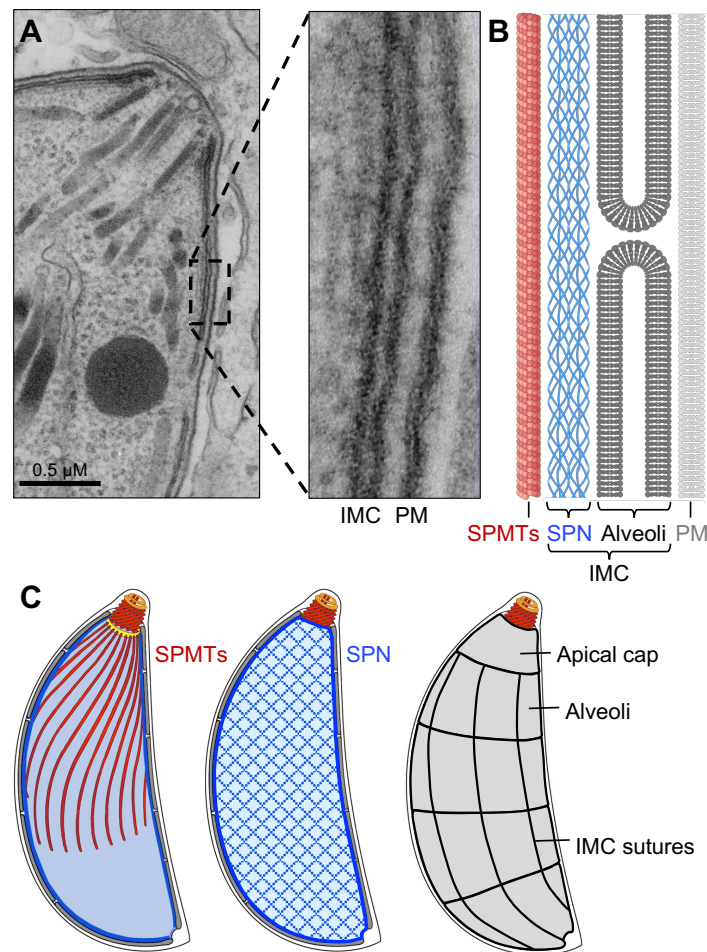


**Figure 1-3. The inner membrane complex of *T. gondii*.** A) Transmission electron micrograph showing the positioning of the IMC underneath the plasma membrane of *T. gondii*. Inset shows the boxed region zoomed in. Credit: Josh Beck, Bradley Lab. B) Diagram showing the structure of the IMC. C) Diagram showing the organization of the subpellicular microtubules, subpellicular network, and alveoli in a *T. gondii* tachyzoite. IMC = inner membrane complex. PM = plasma membrane. SPN = subpellicular network. SPMTs = subpellicular microtubules. Adapted from Katris et al. 2014.

intramembranous particles (IMPs) which are arranged in rows that stretch longitudinally along the entire length of the parasite [71]. While most of the IMPs are arranged in single rows, there are 22 double-rows which are separated with 32 nm periodicity, which matches the periodicity of the 22 subpellicular microtubules. Thus, the IMPs are hypothesized to be involved in tethering the subpellicular microtubules to the alveoli. Cryogenic electron tomography studies in *Plasmodium* sporozoites have also demonstrated the existence of protein linkers with 32 nm periodicity spanning between the IMC and subpellicular microtubules [72]. It has been hypothesized that the IMPs are either a component of the IMC-SPMT linker or the site at which they dock to the alveoli. The protein composition of the IMPs and linkers has not been definitively proven, although recent studies have demonstrated that depletion of the integral alveolar protein GAPM1a leads the SPMTs to become disorganized and subsequently depolymerized [73]. GAPM proteins have been shown to form oligomeric complexes that associate with components of both the glideosome and the subpellicular network [74]. Together this data supports the hypothesis that GAPM proteins are part of the IMPs and/or IMC-SPMT linkers, although further studies are needed to definitively prove this.

### **1.3.2 Subdomains of the inner membrane complex**

Within the IMC there are three distinct subdomains: the apical cap, IMC body, and basal complex (Figure 1-4). Each subdomain has distinct protein components and functions. The apical cap is defined by the cone-shaped vesicle at the apex of the parasite. The proteins ISP1 and AC1-13 have been shown to localize to the IMC only in this region [62,67,75–78]. Interestingly, restriction to the apical cap region is not only seen in membrane-associated proteins. The alveolin IMC11 as well as the detergent insoluble proteins AC9 and AC10 localize to the apical cap, demonstrating that the IMC subdomains exist even within the subpellicular network. Proteins within this region have been shown to be important for host cell invasion [66,75,78].

The central body portion of the IMC contains many proteins with diverse functions including most of the alveolins, ISP2-4, and components of the glideosome [62,64,66]. Smaller subregions within the IMC body appear to be delineated by the alveoli, as ISP2 and 4 localize to only the top two-thirds of the IMC body [62]. In addition to the proteins which localize to the entire IMC body, some proteins localize specifically to the junctions between the individual alveolar plates, termed the IMC sutures. The proteins ISC1-7 localize to both the longitudinal and transverse sutures, whereas the proteins TSC1 (also called CBAP or SIP) and TSC2-5 localize only to the transverse sutures [67,79–81]. The S-acyltransferase DHHC14 also localizes to both the longitudinal and transverse sutures, but only in daughter buds [82]. Interestingly, the sutures are defined not only by the alveoli but also the subpellicular network underlying the sutures. While ISC3, ISC6, TSC5, and TSC6 all contain transmembrane domains which tether them to the alveoli, ISC1, ISC2, ISC4, ISC5, and TSC1-4 are all firmly associated with the cytoskeleton [67,80,81,83]. The suture proteins are thought to be important for physically tethering adjacent alveoli to each other, ultimately maintaining the structure of the IMC. This is supported by data showing that disruption of either ISC3 or TSC1 results in aberrant parasite morphology leading to

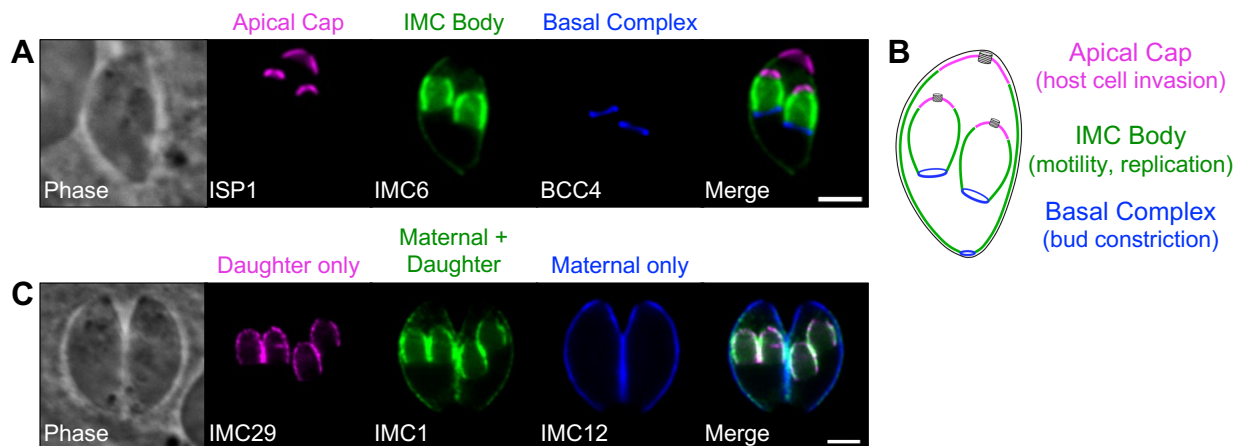


**Figure 1-4. *T. gondii* IMC subdomains.** A) IFA showing a single dividing *T. gondii* tachyzoite stained for markers of the apical cap (ISP1), IMC body (IMC6), and basal complex (BCC4). B) Diagram depicting the location and function of the three subdomains of the IMC. C) IFA showing the localization of daughter only (IMC29), maternal and daughter (IMC1), and maternal only (IMC12) IMC proteins. Scale bars = 2µm.

defects in both in vitro growth and in vivo virulence [80,81,83]. More recently it has been demonstrated that both the micropore and the apical annuli, structures which are hypothesized to be involved in endocytosis and exocytosis, respectively, are consistently located at the IMC sutures [84–90]. Thus, the suture proteins may play a role in positioning or stabilizing these structures.

The ring-shaped opening at the basal end of the IMC is termed the basal complex. Unlike the apical cap, this region of the IMC is not defined by a specific alveolar plate. The basal complex consists of two distinct components: the basal inner ring (BIR) and the basal inner collar (BIC). The BIR is directly attached to the IMC, whereas the BIC is separated from the IMC and extends through the opening of the IMC at the posterior end of the cell where it contacts the plasma membrane [66]. The alveolins IMC5, 8, 9, and 13 have been shown to localize to the basal complex. Interestingly, there appear to be additional subregions within the basal complex. The basal complex marker MORN1 appears at the most apical region of the basal complex. IMC5 and IMC8 are closely colocalized in a slightly smaller ring just basal to MORN1, and IMC9 and IMC13 are present in an even smaller ring basal to that [91]. The main function of the basal complex is to act as a contractile ring during cytokinesis, although the molecular mechanism by which this is achieved remains unclear. The role of basal complex localizing alveolins is also a mystery, as IMC5, 8, 9, and 13 are all predicted to be dispensable for parasite fitness [92].

While many proteins localize to only one of the IMC subdomains, this is not the case for all IMC proteins. For example, IMC39 localizes to both the apical cap and the upper two-thirds of the IMC body while PHIL1, the glideosome components GAP40/50, and the alveolins IMC1 and IMC4 localize to the entire IMC [63,66,69,76]. Finally, in addition to localizing to distinct subdomains, IMC proteins can differ in whether they are present in the maternal IMC, daughter IMC, or both.

### 1.3.3 Functions of the inner membrane complex

The IMC has three critical functions which are essential for all apicomplexan life cycles. First, it acts as a scaffold for developing daughter buds during cell division. This process will be discussed in detail in Section 1.4. Second, the IMC is the platform for the glideosome, which is the actin-myosin motor that powers gliding motility in these parasites. Host cell attachment and motility are required for both host cell invasion and egress. Thus, ablation of the glideosome is lethal. The glideosome is anchored in the IMC by GAP40 and GAP50, which are integral membrane proteins embedded in the membranes of the alveoli, and GAP45, which is tethered to both the alveoli and the plasma membrane by palmitoylation [63]. These proteins connect to MyoA, a class XIVa myosin motor, which in turn binds to short actin filaments that are present in the space between the alveoli and the plasma membrane [61]. When the parasite senses it has come in contact with a host cell, adhesin proteins secreted from the micronemes are distributed across the surface of the parasite's plasma membrane via their transmembrane domains. The N-terminus of the adhesins is displayed on the surface of the parasite plasma membrane and binds to receptors on the surface of the host cell. The C-terminal portion interacts with the actin filaments underneath the parasite's plasma membrane. The MyoA motor is regulated by its own phosphorylation and by the light chains MLC1 and ELC1/2, which change conformation in response to phosphorylation and  $\text{Ca}^{2+}$  binding, respectively [93–95]. Movement of the myosin motor translocates the actin filaments in an apical-to-basal direction, propelling the parasite forward along the surface of the host cell.

In addition to the classical GAP40/GAP50/GAP45/MyoA glideosome, alternative configurations exist within the apical cap and basal complex subdomains of the IMC. In the apical cap, GAP45 is replaced with GAP70 and an additional myosin motor called MyoH associates with the conoid [32,63]. In the basal complex, GAP80 replaces GAP45 and MyoC acts as the motor [96,97]. There appears to be significant functional redundancy among these glideosome

configurations. Disruption of MyoA has been shown to cause MyoC to relocate to the body of the IMC. While these parasites exhibit a severe defect in invasion, they remain motile. Disruption of the basal complex-resident GAP80 has also been shown to be functionally compensated by GAP45 [97].

While the IMC's roles in motility and replication have been known for many years, a third function for the apical cap subdomain of the IMC was only recently discovered [75,77,78,98,99]. AC9 and AC10, two proteins that are restricted to the subpellicular network underlying the apical cap, were shown to be essential for stabilizing the apical complex. These studies demonstrated that AC10 recruits AC9 to the apical cap, which in turn recruits the MAP kinase ERK7. Loss of any of these three proteins has been shown to cause loss of the conoid and disorganization of the subpellicular microtubules in maternal cells but not nascent daughter buds. ERK7 has also been shown to control the localization of the ubiquitin ligase CSAR1, excluding it from the maternal apical cap until daughter buds reach maturation [100]. The prevailing model is that AC9 and AC10 serve as a scaffold to hold ERK7 in place in the apical cap, allowing it to exclude CSAR1 from this region, ultimately preventing the premature degradation of the apical complex.

## **1.4 Endodyogeny in *Toxoplasma gondii***

### **1.4.1 Sequential recruitment of daughter IMC proteins**

As discussed in Section 1.2.3, the human-infecting form of *T. gondii* divides asexually using a mode of internal budding called endodyogeny in which the IMC acts as a scaffold for two developing daughter buds. During endodyogeny, components of the IMC are synthesized and added to the developing daughter cell scaffold sequentially in a “just in time” manner [101]. The process of endodyogeny occurs in four steps: bud initiation, elongation, constriction, and maturation (Figure 1-5). Centrosome duplication marks the initiation of budding, at which point

the apical complex begins to form and several IMC proteins are added to the newly formed daughter buds, including the alveolin IMC15, the daughter IMC proteins IMC29, IMC32 and BCC0, the apical cap proteins AC1/5/9/10, the ubiquitin ligase FBXO1, and the basal complex components BCC3/4 [49,66,67,75–78,102–104]. These proteins are trafficked to the IMC by the GTPase Rab11b [105]. During bud initiation, the nascent daughter buds appear as two small rings just adjacent to the centrosomes. The daughter bud conoids are anchored to the outer core of the

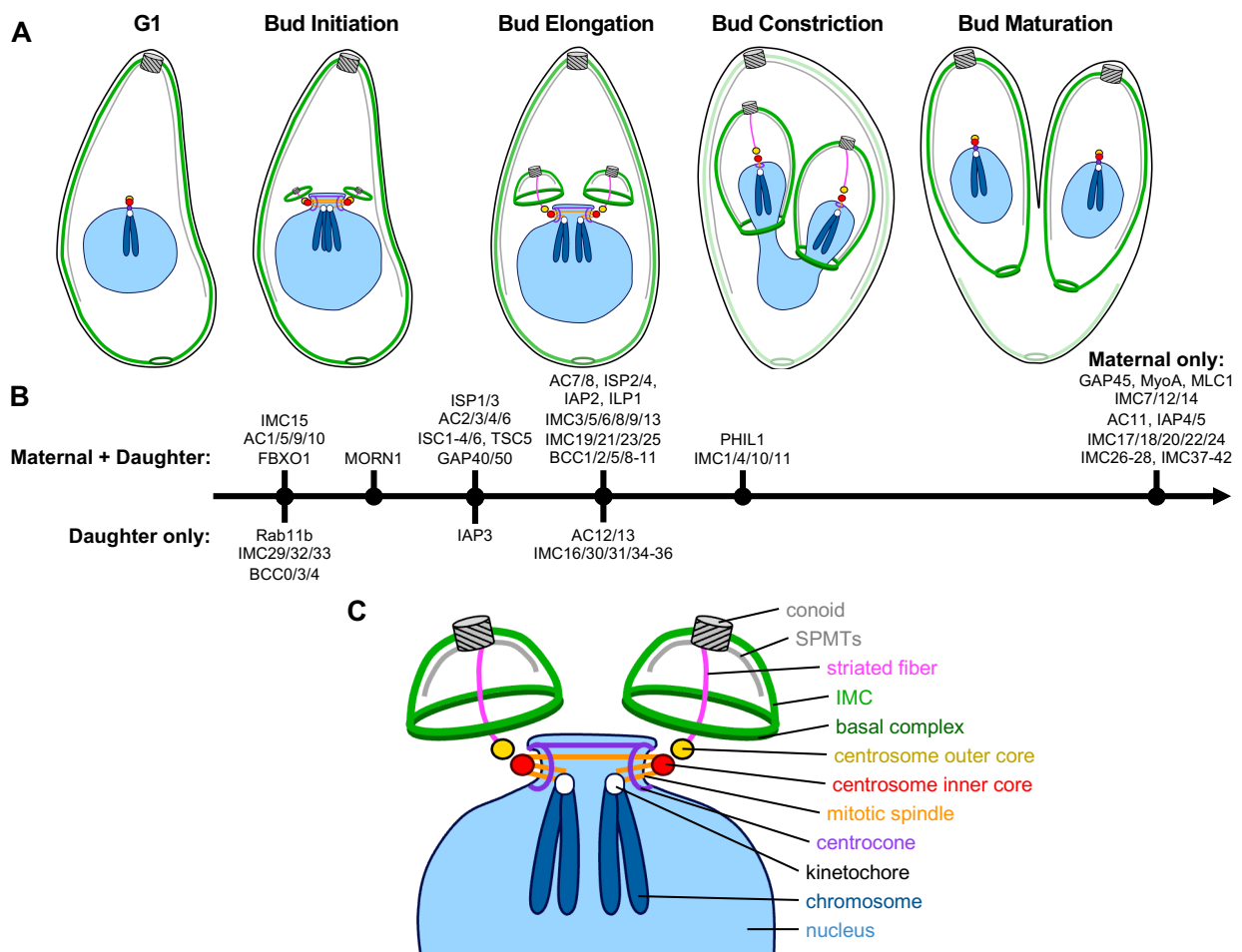


**Figure 1-5. Sequential recruitment of IMC proteins during endodyogeny.** A) Diagram showing the process of a single *T. gondii* cell dividing by endodyogeny. B) Timeline showing the sequential recruitment of proteins to the developing daughter cell scaffold. Each node represents the approximate point at which each listed protein is recruited relative to the stages of endodyogeny depicted in panel A. C) Magnified diagram of the daughter cell scaffold during the bud elongation stage of endodyogeny. Key structures are labelled. SPMTs = subpellicular microtubules. IMC = inner membrane complex. Diagrams in panels A and C are adapted from Gubbels et al. 2020.

centrosome by a fiber composed of polymerized striated fiber assembly proteins [106]. Interestingly, at this point IMC32 and BCC0 are present in a series of five distinct puncta which are arranged symmetrically around the daughter bud ring [103,104]. The basis of this five-fold symmetry remained a mystery until a recent study demonstrated that during bud initiation, the 22 subpellicular microtubules originally appear as five bundles of microtubules in a 4 + 4 + 4 + 4 + 6 configuration [107,108]. While IMC32 and BCC0 have not been colocalized with these early microtubule bundles, it seems likely that their shared symmetry might indicate a functional relationship. Finally, while MORN1 is expressed and visible in the centrocone throughout the cell cycle, it only recruits to the nascent daughter basal complex at the end of bud initiation [58,103].

After bud initiation is complete, the daughter buds begin to elongate in an apical-to-basal fashion, driven by polymerization of the subpellicular microtubules [109]. During this stage the daughter bud becomes dome-shaped and the apical cap, IMC body, and basal complex subdomains of the IMC are better resolved. At the very start of bud elongation when the daughter bud scaffold is still very small, a group of proteins including the membrane-associated proteins ISP1/3, the apical cap proteins AC2/3/4/6, the sutures proteins ISC1-4/6 and TSC5, the glideosome components GAP40/50, and the daughter IMC-associated protein IAP3 are recruited [49,62,67,76,83]. IAP3 displays a novel localization in which it appears to associate with a small region on the inner face of each daughter bud which colocalizes with the dividing apicoplast as it is segregated into each daughter bud [76,110]. The function of IAP3 has not yet been explored, but its negative phenotype score in a genome-wide CRISPR/Cas9 knockout screen and its association with the apicoplast at this point in cell division suggests it may play an important role in tethering the organelle to the daughter IMC to ensure it is properly segregated [92,111]. As the daughter bud elongates further, more proteins are recruited to the developing IMC. These include many proteins which are ultimately maintained in the IMC of mature parasites after the completion of cell division, such as ILP1 and many of the alveolins [62–64,66,67,76,103,112,113]. In addition,

several proteins which are found only in the daughter IMC are recruited at this point, including the daughter apical cap proteins AC12/13 and the daughter IMC body proteins IMC16/30/31/34-36 [76,77,114,115]. Finally, late in bud elongation when the daughter buds are close to reaching their final size, PHIL1 and the alveolins IMC1/4/10/11 are recruited [66,69]. During the process of bud elongation, the nucleus begins to elongate and become partitioned into the two daughter buds with the nuclear membrane still intact.

Once the daughter buds are close to reaching their final size, the third phase of endodyogeny, bud constriction, begins. At this point the basal complex of the nascent daughter buds becomes smaller in diameter, the nucleus is divided, and all organelles except for the mitochondrion are packaged into the daughter buds [111]. The molecular mechanism governing bud constriction remains unclear, but several key players have been identified. Disruption of either MORN1 or BCC4 has been shown to cause severe defects in growth and morphology including an inability to separate the basal ends of nascent daughter buds, resulting in the formation of “multi-headed” parasites [103,116,117]. Loss of the myosin motor MyoJ or the centrin protein Cen2 was also shown to result in incomplete bud constriction, but surprisingly this led to only minor defects in growth [118]. Notably, several proteins which originally recruit to the body of the IMC are relocalized to the basal complex at a later stage of endodyogeny. The alveolins IMC5/8/9/13 are recruited to the body of the IMC during bud elongation, transition to the basal complex during bud constriction, and are retained in the mature basal complex after cell division is complete [66]. BCC3, on the other hand, initially localizes to the IMC sutures of daughter buds during bud initiation, transitions to the basal complex during late bud elongation, and is then removed from the IMC as the buds emerge [103]. The functional relevance of these dynamically localizing IMC proteins is unclear, as all five of them are likely to be dispensable based on their phenotype scores [92].

Once the buds have reached their final size, the maternal IMC, apical complex, and subpellicular microtubules are degraded, marking the beginning of the final stage of endodyogeny, bud maturation. As the buds mature, the plasma membrane of the maternal cell is attached to the IMC of the nascent daughter cells. The process of adopting the maternal plasma membrane is dependent on the GTPase Rab11A and coincides with the assembly of the glideosome as GAP45, MyoA, and MLC1 are recruited [61,105]. Other IMC proteins which are found only in mature parasites, such as the alveolins IMC7/12/14, are added during bud maturation as well [66,67,76,77,83]. At this stage, the C-terminus of the alveolin IMC1 is cleaved and the alveolins become cross-linked in a detergent insoluble protein meshwork [119]. The mitochondrion is also partitioned into the two nascent daughter buds very late in endodyogeny as the buds begin to emerge [111]. After emergence, the cytoplasm of the two daughter cells remain connected through the residual body at the basal end of each cell, in which the maternal cytoskeleton accumulates and is subsequently degraded [100,118].

#### **1.4.2 Regulation of endodyogeny**

As discussed in Section 1.2.3, cell division in apicomplexan parasites is coordinated by the unique bipartite centrosome which consists of an outer core that facilitates the budding cycle and an inner core that facilitates the nuclear cycle [46]. The separation of the centrosome into two cores allows these parasites to separately regulate karyokinesis and cytokinesis, therefore allowing multiple rounds of karyokinesis to occur prior to the initiation of budding [120]. *T. gondii* tachyzoites undergoing endodyogeny produce only two buds per round of cell division, thus the nuclear and budding cycles occur simultaneously. Regardless, the two cycles are still regulated by different mechanisms.

DNA microarray and single-cell RNA sequencing analysis in *T. gondii* have demonstrated that many genes are transcriptionally regulated in a “just in time” temporal manner [101,121]. For

components of the daughter IMC, their expression typically peaks in S-phase just prior to their deposition onto the developing daughter cell scaffold. IMC components which are added to the IMC only during bud emergence typically peak later, towards the end of cytokinesis. The largest family of transcription factors in apicomplexan parasites are the 67 Apicomplexan Apetala 2 (ApiAP2) proteins [122,123]. Aside from the Apicomplexa, Apetala 2 transcription factors are only found in plants. Thus, it has been hypothesized that they are of cyanobacterium origin and were introduced into the Apicomplexa from the secondary endosymbiotic event that produced the apicoplast.

While most of the ApiAP2 transcription factors have not yet been studied, several have been linked to cell division in *T. gondii*. First, DNA synthesis appears to be regulated by AP2XII-2, as loss of this transcription factor was shown to result in growth defects due to slower progression through S-phase [124]. AP2XII-2 was also found to associate with the transcriptional silencers HDAC3 and MORC at the promoters of genes expressed by sexually committed parasites, but relatively few genes were found to be actively suppressed by this complex [125]. Regulation of the budding cycle during endodyogeny has been shown to be coordinated by AP2IX-5 [113,126]. Depletion of AP2IX-5 was shown to cause defects in IMC formation and organelle morphology despite normal centrosome duplication and nuclear division. AP2IX-5 was also shown to bind to and activate the promoters for hundreds of genes involved in budding, including the daughter IMC components ISP1 and IMC29. Finally, heterodimers of AP2XI-5 and AP2X-5 were found to bind to and activate the promoters of genes encoding secretory proteins which are packaged into the micronemes and rhoptries of nascent daughter buds during S/M phase [127,128].

Currently, it remains unknown how the correct ApiAP2 transcription factors are activated or suppressed at the appropriate point in the cell cycle. In most eukaryotic systems, cyclin (Cyc) proteins bind to and activate cyclin-dependent kinases (Cdk) which then phosphorylate

transcription factors to modulate gene expression. *T. gondii* encodes ten Cdk-related kinases (Crk), eight of which are expressed in tachyzoites and localize to either the cytoplasm or the nucleus [129]. However, the typical transcription factors such as E2F and RB which are phosphorylated by Cdks in other eukaryotes are missing from the genomes of apicomplexan parasites [56]. Thus, it has been hypothesized that ApiAP2 transcription factors may act as Crk effectors, although no experimental evidence has demonstrated this. Functional analysis of the Crks and cyclins has suggested that Crk5 controls DNA licensing at the onset of S-phase, Crk4-Cyc4 controls centrosome duplication, Crk6-Cyc1 controls assembly of the mitotic spindle, and Crk1-CycL controls budding [129–132].

Several other kinases have been shown to play important roles in centrosome regulation during endodyogeny. MAPK-L1 has been shown to both prevent overduplication of the centrosomes and secure the physical connection between the nucleus and the daughter cytoskeleton [46]. Loss of MAPK2, on the other hand, was shown to cause cell cycle arrest prior to centrosome duplication [133]. Nek1, a NIMA-related protein kinase, was shown to be required for separation of the centrosomes after duplication [45]. Interestingly, loss of this protein led to the formation of a single daughter bud on top of the unseparated centrosomes. Finally, loss of the calcium-dependent protein kinase CDPK7 has been shown to affect duplication and positioning of the centrosomes which led to defects in budding [134].

Finally, phosphorylation of proteins that make up the structural foundation of the nascent daughter buds appears to be important in ensuring proper bud assembly. The aurora kinase Ark3 was shown to exhibit a dynamic localization in which it is absent from mature parasites, recruits to the outer core of the centrosome during bud initiation, then relocalizes to a small region on the inner face of the nascent daughter buds during bud elongation, similar to IAP3 [46,76,135]. Despite its localization to the centrosome, depletion of Ark3 did not affect centrosome duplication or nuclear division. However, Ark3-depleted parasites did exhibit severe defects in budding and

IMC morphology, suggesting it may regulate IMC proteins during endodyogeny. The plant-like protein phosphatase PPKL has been shown to enrich at the daughter cell scaffold during endodyogeny, and its depletion lead to severe defects in IMC morphology and stability of the subpellicular microtubules despite normal centrosome duplication and nuclear division [136]. Depletion of PPKL also led to increased phosphorylation of the microtubule-associated protein SPM1, leading to the hypothesis that dephosphorylation of SPM1 by PPKL stabilizes the growing subpellicular microtubules during endodyogeny. Interestingly, Crk1 was also found to be differentially phosphorylated in PPKL-depleted parasites, suggesting a functional connection between these two regulatory proteins. During bud constriction, the basal complex component MORN1 appears to be regulated by the haloacid dehalogenase (HAD) phosphatase HAD2a, as genetic disruption of either protein results in a unique “multi-headed” phenotype in which parasites fail to separate their basal ends at the completion of endodyogeny [116,117,137]. A similar phenotype was observed upon pharmacological inhibition of MAPK-L1, and loss of this kinase was also shown to affect the positioning of the basal complex on nascent daughter buds [46,138]. This could suggest that MAPK-L1 also plays a role in regulating the basal complex, although more direct investigation will be necessary to explore this.

## **1.5 Overview of the dissertation**

During endodyogeny, IMC components are added to the nascent daughter cell scaffold in a sequential manner. While many components of the IMC have been identified, most are recruited after budding has already been initiated and are dispensable for parasite fitness. Several daughter-specific IMC proteins have been discovered, including the apical cap proteins AC12/13, the IMC body proteins IMC16/29-36 and BCC0, IAP3, and the basal complex proteins BCC3/4 [66,76,77,79,103,104,114,115]. IMC32 was the first essential daughter IMC protein ever

identified, and it was only recently reported by our lab [104]. During bud initiation, IMC32 localizes to a series of five puncta which are arranged symmetrically around the ring-shaped daughter buds. These five puncta extend into a series of five stripes which extend longitudinally along the body of the daughter IMC during bud elongation and are removed during bud maturation. The discovery of IMC32 highlighted the critical importance of early recruiting daughter-specific IMC proteins in providing the foundation for building the daughter cell scaffold during endodyogeny. This was further supported by our functional analysis of the early recruiting daughter-specific IMC protein IMC29. While not essential, IMC29 was shown to be critical for endodyogeny, as its disruption led to severe defects in IMC morphology and replication rate [76]. The importance of IMC32 and IMC29 led us to hypothesize that more unidentified, early recruiting daughter-specific IMC proteins must exist which coordinate with IMC32 and/or IMC29 to lay the foundation of the daughter cell scaffold. This hypothesis became the focus of this dissertation.

In our studies of IMC29, we performed proximity labelling experiments which identified several of the daughter IMC proteins mentioned above [76]. We selected one of these genes for further functional analysis based on its low phenotype score in a genome-wide CRISPR/Cas9 knockout screen, which indicates that it is likely to be important or essential for parasite fitness [92]. In Chapter 2, we report the identification and functional analysis of this gene, which we name IMC43 [139]. We demonstrate that IMC43 recruits to the body of the daughter IMC during bud initiation, and it is essential for parasite replication and survival. Using both proximity labelling and direct protein-protein interaction screening, we identify 30 candidate IMC43-binding partners and validate two of them: a novel, dynamically localizing daughter IMC protein which we name IMC44, and the essential early daughter protein IMC32. Using deletion analyses and protein-protein interaction assays, we determine that IMC43 contains an essential interaction domain near its C-terminus which directly binds to both IMC44 and IMC32 and controls both of their localizations.

As IMC43 and IMC32 are both essential, this work reveals the existence of an essential daughter bud assembly complex which lays the foundation of the IMC during endodyogeny.

In Chapter 3, we use IMC32 as bait in proximity labelling and protein-protein interaction screens to identify a third component of this complex: the essential early daughter IMC protein BCC0, which was additionally identified by Engelberg et al. [103]. We demonstrate that BCC0 localizes to the early daughter cell scaffold with the same five-fold symmetry which we observed for IMC32. Deletion analyses reveal that only a small region of BCC0 is required for its localization and function. Using protein-protein interaction assays, we demonstrate that the essential domain of BCC0 directly binds to IMC32 at its essential C-terminal coiled-coil domains. We additionally show that BCC0 depends on the presence of both IMC32 and IMC43 for its localization, leading to a hierarchical model of recruitment. Together, this work identifies an essential daughter bud assembly complex and dissects its organization and function, revealing how the foundation of the early daughter cell scaffold is laid during replication of the important human pathogen *T. gondii*.

## 1.6 References

1. Tenter AM, Heckeroth AR, Weiss LM. *Toxoplasma gondii*: from animals to humans. *International Journal for Parasitology*. 2000;30: 1217–1258. [https://doi.org/10.1016/S0020-7519\(00\)00124-7](https://doi.org/10.1016/S0020-7519(00)00124-7) PMID: 11113252
2. Montoya JG, Liesenfeld O. Toxoplasmosis. *Lancet*. 2004;363: 1965–1976. [https://doi.org/10.1016/S0140-6736\(04\)16412-X](https://doi.org/10.1016/S0140-6736(04)16412-X) PMID: 15194258
3. Jones JL, Parise ME, Fiore AE. Neglected parasitic infections in the United States: toxoplasmosis. *Am J Trop Med Hyg*. 2014;90: 794–799. <https://doi.org/10.4269/ajtmh.13-0722> PMID: 24808246
4. Jones EJ, Korcsmaros T, Carding SR. Mechanisms and pathways of *Toxoplasma gondii* transepithelial migration. *Tissue Barriers*. 2017;5: e1273865. <https://doi.org/10.1080/21688370.2016.1273865> PMID: 28452683
5. McAuley JB. Congenital Toxoplasmosis. *J Pediatric Infect Dis Soc*. 2014;3 Suppl 1: S30-35. <https://doi.org/10.1093/jpids/piu077> PMID: 25232475
6. Flegr J, Prandota J, Sovičková M, Israili ZH. Toxoplasmosis - a global threat. Correlation of latent toxoplasmosis with specific disease burden in a set of 88 countries. *PLoS One*. 2014;9: e90203. <https://doi.org/10.1371/journal.pone.0090203> PMID: 24662942
7. Pappas G, Roussos N, Falagas ME. Toxoplasmosis snapshots: global status of *Toxoplasma gondii* seroprevalence and implications for pregnancy and congenital toxoplasmosis. *Int J Parasitol*. 2009;39: 1385–1394. <https://doi.org/10.1016/j.ijpara.2009.04.003> PMID: 19433092
8. Randall LM, Hunter CA. Parasite dissemination and the pathogenesis of toxoplasmosis. *Eur J Microbiol Immunol (Bp)*. 2011;1: 3–9. <https://doi.org/10.1556/EuJMI.1.2011.1.3> PMID: 24466431
9. Weiss LM, Dubey JP. Toxoplasmosis: A history of clinical observations. *Int J Parasitol*. 2009;39: 895–901. <https://doi.org/10.1016/j.ijpara.2009.02.004> PMID: 19217908
10. Dubey JP, Lindsay DS, Speer CA. Structures of *Toxoplasma gondii* tachyzoites, bradyzoites, and sporozoites and biology and development of tissue cysts. *Clin Microbiol Rev*. 1998;11: 267–299. <https://doi.org/10.1128%2Fcmr.11.2.267> PMID: 9564564
11. Holland GN. Ocular toxoplasmosis: a global reassessment. Part I: epidemiology and course of disease. *Am J Ophthalmol*. 2003;136: 973–988. <https://doi.org/10.1016/j.ajo.2003.09.040> PMID: 14644206
12. Fernández C, Jaimes J, Ortiz MC, Ramírez JD. Host and *Toxoplasma gondii* genetic and non-genetic factors influencing the development of ocular toxoplasmosis: A systematic review. *Infect Genet Evol*. 2016;44: 199–209. <https://doi.org/10.1016/j.meegid.2016.06.053> PMID: 27389360

13. Daher D, Shaghlil A, Sobh E, Hamie M, Hassan ME, Moumneh MB, et al. Comprehensive Overview of *Toxoplasma gondii*-Induced and Associated Diseases. *Pathogens*. 2021;10: 1351. <https://doi.org/10.3390/pathogens10111351> PMID: 34832507
14. Marra CM. Central nervous system infection with *Toxoplasma gondii*. *Handb Clin Neurol*. 2018;152: 117–122. <https://doi.org/10.1016/B978-0-444-63849-6.00009-8> PMID: 29604970
15. Konstantinovic N, Guegan H, Stājner T, Belaz S, Robert-Gangneux F. Treatment of toxoplasmosis: Current options and future perspectives. *Food Waterborne Parasitol*. 2019;15: e00036. <https://doi.org/10.1016/j.fawpar.2019.e00036> PMID: 32095610
16. Montoya JG, Remington JS. Management of *Toxoplasma gondii* infection during pregnancy. *Clin Infect Dis*. 2008;47: 554–566. <https://doi.org/10.1086/590149> PMID: 18624630
17. Kalantari N, Gorgani-Firouzjaee T, Moulana Z, Chehrazi M, Ghaffari S. *Toxoplasma gondii* infection and spontaneous abortion: A systematic review and meta-analysis. *Microb Pathog*. 2021;158: 105070. <https://doi.org/10.1016/j.micpath.2021.105070> PMID: 34186117
18. Tari RM, Diallo A, Kouame E, Assogba P, Badjabaissi E, Povi L-E, et al. Assessment of the Teratogenic Effect of Sulfadoxine-Pyrimethamine on the Chicken Embryo. *J Toxicol*. 2022;2022: 2995492. <https://doi.org/10.1155/2022/2995492> PMID: 35340707
19. Dunay IR, Gajurel K, Dhakal R, Liesenfeld O, Montoya JG. Treatment of Toxoplasmosis: Historical Perspective, Animal Models, and Current Clinical Practice. *Clin Microbiol Rev*. 2018;31: e00057-17. <https://doi.org/10.1128/CMR.00057-17> PMID: 30209035
20. Montoya JG, Laessig K, Fazeli MS, Siliman G, Yoon SS, Drake-Shanahan E, et al. A fresh look at the role of spiramycin in preventing a neglected disease: meta-analyses of observational studies. *Eur J Med Res*. 2021;26: 143. <https://doi.org/10.1186/s40001-021-00606-7> PMID: 34895348
21. Votýpka J, Modrý D, Oborník M, Šlapeta J, Lukeš J. Apicomplexa. In: Archibald JM, Simpson AGB, Slamovits CH, Margulis L, Melkonian M, Chapman DJ, et al., editors. *Handbook of the Protists*. Cham: Springer International Publishing; 2017. pp. 1–58. [https://doi.org/10.1007/978-3-319-32669-6\\_20-1](https://doi.org/10.1007/978-3-319-32669-6_20-1)
22. Mackintosh CL, Beeson JG, Marsh K. Clinical features and pathogenesis of severe malaria. *Trends Parasitol*. 2004;20: 597–603. <https://doi.org/10.1016/j.pt.2004.09.006> PMID: 15522670
23. World Malaria Report 2022. Geneva, Switzerland: World Health Organization; 2022.
24. Bouzid M, Hunter PR, Chalmers RM, Tyler KM. *Cryptosporidium* Pathogenicity and Virulence. *Clinical Microbiology Reviews*. 2013;26: 115–134. <https://doi.org/10.1128/CMR.00076-12> PMID: 23297262

25. Sow SO, Muhsen K, Nasrin D, Blackwelder WC, Wu Y, Farag TH, et al. The Burden of Cryptosporidium Diarrheal Disease among Children < 24 Months of Age in Moderate/High Mortality Regions of Sub-Saharan Africa and South Asia, Utilizing Data from the Global Enteric Multicenter Study (GEMS). *PLoS Negl Trop Dis*. 2016;10: e0004729. <https://doi.org/10.1371/journal.pntd.0004729> PMID: 27219054
26. Dubey JP. Review of Neospora caninum and neosporosis in animals. *Korean J Parasitol*. 2003;41: 1–16. <https://doi.org/10.3347/kjp.2003.41.1.1> PMID: 12666725
27. Kivaria FM. Estimated direct economic costs associated with tick-borne diseases on cattle in Tanzania. *Trop Anim Health Prod*. 2006;38: 291–299. <https://doi.org/10.1007/s11250-006-4181-2> PMID: 17137131
28. Sharman PA, Smith NC, Wallach MG, Katrib M. Chasing the golden egg: vaccination against poultry coccidiosis. *Parasite Immunol*. 2010;32: 590–598. <https://doi.org/10.1111/j.1365-3024.2010.01209.x> PMID: 20626814
29. Kim K, Weiss LM. *Toxoplasma gondii*: the model apicomplexan. *International Journal for Parasitology*. 2004;34: 423–432. <https://doi.org/10.1016/j.ijpara.2003.12.009> PMID: 15003501
30. Meissner M, Klaus K. What new cell biology findings could bring to therapeutics: is it time for a phenome-project in *Toxoplasma gondii*? *Mem Inst Oswaldo Cruz*. 2009;104: 185–189. <https://doi.org/10.1590/s0074-02762009000200010> PMID: 19430642
31. Katris NJ, van Dooren GG, McMillan PJ, Hanssen E, Tilley L, Waller RF. The apical complex provides a regulated gateway for secretion of invasion factors in *Toxoplasma*. *PLoS Pathog*. 2014;10: e1004074. <https://doi.org/10.1371/journal.ppat.1004074> PMID: 24743791
32. Graindorge A, Fréchal K, Jacot D, Salamun J, Marq JB, Soldati-Favre D. The Conoid Associated Motor MyoH Is Indispensable for *Toxoplasma gondii* Entry and Exit from Host Cells. *PLoS Pathog*. 2016;12: e1005388. <https://doi.org/10.1371/journal.ppat.1005388> PMID: 26760042
33. Long S, Brown KM, Drewry LL, Anthony B, Phan IQH, Sibley LD. Calmodulin-like proteins localized to the conoid regulate motility and cell invasion by *Toxoplasma gondii*. Soldati-Favre D, editor. *PLoS Pathog*. 2017;13: e1006379. <https://doi.org/10.1371/journal.ppat.1006379> PMID: 28475612
34. Lebrun M, Carruthers VB, Cesbron-Delauw M-F. Chapter 14 - *Toxoplasma* secretory proteins and their roles in parasite cell cycle and infection. In: Weiss LM, Kim K, editors. *Toxoplasma gondii* (Third Edition). Academic Press; 2020. pp. 607–704. <https://doi.org/10.1016/B978-0-12-815041-2.00014-1>
35. Dubois DJ, Soldati-Favre D. Biogenesis and secretion of micronemes in *Toxoplasma gondii*. *Cell Microbiol*. 2019;21: e13018. <https://doi.org/10.1111/cmi.13018> PMID: 30791192

36. Boothroyd JC, Dubremetz J-F. Kiss and spit: the dual roles of *Toxoplasma* rhoptries. *Nat Rev Microbiol*. 2008;6: 79–88. <https://doi.org/10.1038/nrmicro1800> PMID: 18059289
37. Mordue DG, Håkansson S, Niesman I, Sibley LD. *Toxoplasma gondii* resides in a vacuole that avoids fusion with host cell endocytic and exocytic vesicular trafficking pathways. *Exp Parasitol*. 1999;92: 87–99. <https://doi.org/10.1006/expr.1999.4412> PMID: 10366534
38. Griffith MB, Pearce CS, Heaslip AT. Dense granule biogenesis, secretion, and function in *Toxoplasma gondii*. *J Eukaryot Microbiol*. 2022;69: e12904. <https://doi.org/10.1111/jeu.12904> PMID: 35302693
39. McFadden GI, Yeh E. The apicoplast: now you see it, now you don't. *Int J Parasitol*. 2017;47: 137–144. <https://doi.org/10.1016/j.ijpara.2016.08.005> PMID: 27773518
40. Arisue N, Hashimoto T. Phylogeny and evolution of apicoplasts and apicomplexan parasites. *Parasitol Int*. 2015;64: 254–259. <https://doi.org/10.1016/j.parint.2014.10.005> PMID: 25451217
41. Kennedy K, Crisafulli EM, Ralph SA. Delayed Death by Plastid Inhibition in Apicomplexan Parasites. *Trends Parasitol*. 2019;35: 747–759. <https://doi.org/10.1016/j.pt.2019.07.010> PMID: 31427248
42. Soldati D. The apicoplast as a potential therapeutic target in and other apicomplexan parasites. *Parasitol Today*. 1999;15: 5–7. [https://doi.org/10.1016/s0169-4758\(98\)01363-5](https://doi.org/10.1016/s0169-4758(98)01363-5) PMID: 10234168
43. Harding CR, Frischknecht F. The Riveting Cellular Structures of Apicomplexan Parasites. *Trends in Parasitology*. 2020;36: 979–991. <https://doi.org/10.1016/j.pt.2020.09.001> PMID: 33011071
44. Gould SB, Tham W-H, Cowman AF, McFadden GI, Waller RF. Alveolins, a new family of cortical proteins that define the protist infrakingdom Alveolata. *Mol Biol Evol*. 2008;25: 1219–1230. <https://doi.org/10.1093/molbev/msn070> PMID: 18359944
45. Chen C-T, Gubbels M-J. The *Toxoplasma gondii* centrosome is the platform for internal daughter budding as revealed by a Nek1 kinase mutant. *Journal of Cell Science*. 2013;126: 3344–3355. <https://doi.org/10.1242/jcs.123364> PMID: 23729737
46. Suvorova ES, Francia M, Striepen B, White MW. A Novel Bipartite Centrosome Coordinates the Apicomplexan Cell Cycle. Pellman D, editor. *PLoS Biol*. 2015;13: e1002093. <https://doi.org/10.1371/journal.pbio.1002093> PMID: 25734885
47. Gubbels M-J, Keroack CD, Dangoudoubiyam S, Worliczek HL, Paul AS, Bauwens C, et al. Fussing About Fission: Defining Variety Among Mainstream and Exotic Apicomplexan Cell Division Modes. *Front Cell Infect Microbiol*. 2020;10: 269. <https://doi.org/10.3389/fcimb.2020.00269> PMID: 32582569
48. Ferreira JL, Heincke D, Wichers JS, Liffner B, Wilson DW, Gilberger T-W. The Dynamic Roles of the Inner Membrane Complex in the Multiple Stages of the Malaria Parasite.

- Front Cell Infect Microbiol. 2020;10: 611801. <https://doi.org/10.3389/fcimb.2020.611801>  
PMID: 33489940
49. Ouologuem DT, Roos DS. Dynamics of the *Toxoplasma gondii* inner membrane complex. *Journal of Cell Science*. 2014; jcs.147736. <https://doi.org/10.1242/jcs.147736> PMID: 24928899
  50. Ferguson DJ, Hutchison WM, Dunachie JF, Siim JC. Ultrastructural study of early stages of asexual multiplication and microgametogony of *Toxoplasma gondii* in the small intestine of the cat. *Acta Pathol Microbiol Scand B Microbiol Immunol*. 1974;82: 167–181. <https://doi.org/10.1111/j.1699-0463.1974.tb02309.x> PMID: 4528099
  51. Roques M, Bindschedler A, Beyeler R, Heussler VT. Same, same but different: Exploring *Plasmodium* cell division during liver stage development. *PLoS Pathog*. 2023;19: e1011210. <https://doi.org/10.1371/journal.ppat.1011210> PMID: 36996035
  52. Vaughan AM, Kappe SHI. Malaria Parasite Liver Infection and Exoerythrocytic Biology. *Cold Spring Harb Perspect Med*. 2017;7: a025486. <https://doi.org/10.1101/cshperspect.a025486> PMID: 28242785
  53. Dubremetz JF, Elsner YY. Ultrastructural study of schizogony of *Eimeria bovis* in cell cultures. *J Protozool*. 1979;26: 367–376. <https://doi.org/10.1111/j.1550-7408.1979.tb04639.x> PMID: 536929
  54. English ED, Guérin A, Tandel J, Striepen B. Live imaging of the *Cryptosporidium parvum* life cycle reveals direct development of male and female gametes from type I meronts. *PLoS Biol*. 2022;20: e3001604. <https://doi.org/10.1371/journal.pbio.3001604> PMID: 35436284
  55. Fawcett DW, Conrad PA, Grootenhuis JG, Morzaria SP. Ultrastructure of the intraerythrocytic stage of *Theileria* species from cattle and waterbuck. *Tissue Cell*. 1987;19: 643–655. [https://doi.org/10.1016/0040-8166\(87\)90071-1](https://doi.org/10.1016/0040-8166(87)90071-1) PMID: 3122362
  56. White MW, Suvorova ES. Apicomplexa Cell Cycles: Something Old, Borrowed, Lost, and New. *Trends in Parasitology*. 2018;34: 759–771. <https://doi.org/10.1016/j.pt.2018.07.006> PMID: 30078701
  57. Brooks CF, Francia ME, Gissot M, Croken MM, Kim K, Striepen B. *Toxoplasma gondii* sequesters centromeres to a specific nuclear region throughout the cell cycle. *Proc Natl Acad Sci U S A*. 2011;108: 3767–3772. <https://doi.org/10.1073/pnas.1006741108> PMID: 21321216
  58. Gubbels M-J, Vaishnav S, Boot N, Dubremetz J-F, Striepen B. A MORN-repeat protein is a dynamic component of the *Toxoplasma gondii* cell division apparatus. *J Cell Sci*. 2006;119: 2236–2245. <https://doi.org/10.1242/jcs.02949> PMID: 16684814
  59. Tomasina R, Gonzalez FC, Martins-Duarte ÉS, Bastin P, Gissot M, Francia ME. Separate To Operate: the Centriole-Free Inner Core of the Centrosome Regulates the Assembly of the Intranuclear Spindle in *Toxoplasma gondii*. *mBio*. 2022;13: e0185922. <https://doi.org/10.1128/mbio.01859-22> PMID: 36069445

60. Porchet E, Torpier G. [Freeze fracture study of *Toxoplasma* and *Sarcocystis* infective stages (author's transl)]. *Z Parasitenkd.* 1977;54: 101–124. <https://doi.org/10.1007/BF00380795> PMID: 415447
61. Gaskins E, Gilk S, DeVore N, Mann T, Ward G, Beckers C. Identification of the membrane receptor of a class XIV myosin in *Toxoplasma gondii*. *J Cell Biol.* 2004;165: 383–393. <https://doi.org/10.1083/jcb.200311137> PMID: 15123738
62. Beck JR, Rodriguez-Fernandez IA, Cruz de Leon J, Huynh M-H, Carruthers VB, Morrisette NS, et al. A Novel Family of *Toxoplasma* IMC Proteins Displays a Hierarchical Organization and Functions in Coordinating Parasite Division. Soldati-Favre D, editor. *PLoS Pathog.* 2010;6: e1001094. <https://doi.org/10.1371/journal.ppat.1001094> PMID: 20844581
63. Frénal K, Polonais V, Marq J-B, Stratmann R, Limenitakis J, Soldati-Favre D. Functional dissection of the apicomplexan glideosome molecular architecture. *Cell Host Microbe.* 2010;8: 343–357. <https://doi.org/10.1016/j.chom.2010.09.002> PMID: 20951968
64. Fung C, Beck JR, Robertson SD, Gubbels M-J, Bradley PJ. *Toxoplasma* ISP4 is a central IMC sub-compartment protein whose localization depends on palmitoylation but not myristoylation. *Mol Biochem Parasitol.* 2012;184: 99–108. <https://doi.org/10.1016/j.molbiopara.2012.05.002> PMID: 22659420
65. Mann T, Beckers C. Characterization of the subpellicular network, a filamentous membrane skeletal component in the parasite *Toxoplasma gondii*. *Molecular and Biochemical Parasitology.* 2001;115: 257–268. [https://doi.org/10.1016/S0166-6851\(01\)00289-4](https://doi.org/10.1016/S0166-6851(01)00289-4) PMID: 11420112
66. Anderson-White BR, Ivey FD, Cheng K, Szatanek T, Lorestani A, Beckers CJ, et al. A family of intermediate filament-like proteins is sequentially assembled into the cytoskeleton of *Toxoplasma gondii*: IMC proteins in *Toxoplasma* cell division. *Cellular Microbiology.* 2011;13: 18–31. <https://doi.org/10.1111/j.1462-5822.2010.01514.x> PMID: 20698859
67. Chen AL, Kim EW, Toh JY, Vashisht AA, Rashoff AQ, Van C, et al. Novel components of the *Toxoplasma* inner membrane complex revealed by BiOLD. *Mbio.* 2015;6: e02357-14. <https://doi.org/10.1128/mbio.02357-14> PMID: 25691595
68. Choi CP, Moon AS, Back PS, Jami-Alahmadi Y, Vashisht AA, Wohlschlegel JA, et al. A photoactivatable crosslinking system reveals protein interactions in the *Toxoplasma gondii* inner membrane complex. *PLoS Biol.* 2019;17: e3000475. <https://doi.org/10.1371/journal.pbio.3000475> PMID: 31584943
69. Gilk SD, Raviv Y, Hu K, Murray JM, Beckers CJM, Ward GE. Identification of Phil1, a novel cytoskeletal protein of the *Toxoplasma gondii* pellicle, through photosensitized labeling with 5-[<sup>125</sup>I]iodonaphthalene-1-azide. *Eukaryot Cell.* 2006;5: 1622–1634. <https://doi.org/10.1128/EC.00114-06> PMID: 17030994

70. Anderson-White B, Beck JR, Chen C-T, Meissner M, Bradley PJ, Gubbels M-J. Cytoskeleton assembly in *Toxoplasma gondii* cell division. *Int Rev Cell Mol Biol*. 2012;298: 1–31. <https://doi.org/10.1016/B978-0-12-394309-5.00001-8> PMID: 22878103
71. Morrissette NS, Murray JM, Roos DS. Subpellicular microtubules associate with an intramembranous particle lattice in the protozoan parasite *Toxoplasma gondii*. *J Cell Sci*. 1997;110 ( Pt 1): 35–42. <https://doi.org/10.1242/jcs.110.1.35> PMID: 9010782
72. Kudryashev M, Lepper S, Stanway R, Bohn S, Baumeister W, Cyrklaff M, et al. Positioning of large organelles by a membrane-associated cytoskeleton in *Plasmodium* sporozoites. *Cellular Microbiology*. 2010;12: 362–371. <https://doi.org/10.1111/j.1462-5822.2009.01399.x> PMID: 19863555
73. Harding CR, Gow M, Kang JH, Shortt E, Manalis SR, Meissner M, et al. Alveolar proteins stabilize cortical microtubules in *Toxoplasma gondii*. *Nat Commun*. 2019;10: 401. <https://doi.org/10.1038/s41467-019-08318-7> PMID: 30674885
74. Bullen HE, Tonkin CJ, O'Donnell RA, Tham W-H, Papenfuss AT, Gould S, et al. A Novel Family of Apicomplexan Glideosome-associated Proteins with an Inner Membrane-anchoring Role. *Journal of Biological Chemistry*. 2009;284: 25353–25363. <https://doi.org/10.1074/jbc.M109.036772> PMID: 19561073
75. Back PS, O'Shaughnessy WJ, Moon AS, Dewangan PS, Hu X, Sha J, et al. Ancient MAPK ERK7 is regulated by an unusual inhibitory scaffold required for *Toxoplasma* apical complex biogenesis. *Proc Natl Acad Sci USA*. 2020;117: 12164–12173. <https://doi.org/10.1073/pnas.1921245117> PMID: 32409604
76. Back PS, Moon AS, Pasquarelli RR, Bell HN, Torres JA, Chen AL, et al. IMC29 Plays an Important Role in *Toxoplasma* Endodyogeny and Reveals New Components of the Daughter-Enriched IMC Proteome. *mBio*. 2023;14: e0304222. <https://doi.org/10.1128/mbio.03042-22> PMID: 36622147
77. Dos Santos Pacheco N, Tosetti N, Krishnan A, Haase R, Maco B, Suarez C, et al. Revisiting the Role of *Toxoplasma gondii* ERK7 in the Maintenance and Stability of the Apical Complex. *mBio*. 2021;12: e0205721. <https://doi.org/10.1128/mBio.02057-21> PMID: 34607461
78. Tosetti N, Dos Santos Pacheco N, Bertiaux E, Maco B, Bournonville L, Hamel V, et al. Essential function of the alveolin network in the subpellicular microtubules and conoid assembly in *Toxoplasma gondii*. *eLife*. 2020;9: e56635. <https://doi.org/10.7554/eLife.56635> PMID: 32379047
79. Chen AL, Moon AS, Bell HN, Huang AS, Vashisht AA, Toh JY, et al. Novel insights into the composition and function of the *Toxoplasma* IMC sutures. *Cell Microbiol*. 2016;19: e12678. <https://doi.org/10.1111/cmi.12678> PMID: 27696623
80. Lentini G, Kong-Hap M, El Hajj H, Francia M, Claudet C, Striepen B, et al. Identification and characterization of *Toxoplasma* SIP, a conserved apicomplexan cytoskeleton protein involved in maintaining the shape, motility and virulence of the parasite. *Cell Microbiol*. 2015;17: 62–78. <https://doi.org/10.1111/cmi.12337> PMID: 25088010

81. Tilley LD, Krishnamurthy S, Westwood NJ, Ward GE. Identification of TgCBAP, a novel cytoskeletal protein that localizes to three distinct subcompartments of the *Toxoplasma gondii* pellicle. *PLoS One*. 2014;9: e98492. <https://doi.org/10.1371/journal.pone.0098492> PMID: 24887026
82. Dogga SK, Frénal K. Two palmitoyl acyltransferases involved sequentially in the biogenesis of the inner membrane complex of *Toxoplasma gondii*. *Cellular Microbiology*. 2020;22. <https://doi.org/10.1111/cmi.13212> PMID: 32329212
83. Chen AL, Moon AS, Bell HN, Huang AS, Vashisht AA, Toh JY, et al. Novel insights into the composition and function of the *Toxoplasma* IMC sutures. *Cellular Microbiology*. 2017;19: e12678. <https://doi.org/10.1111/cmi.12678> PMID: 27696623
84. Chelaghma S, Ke H, Barylyuk K, Krueger T, Koreny L, Waller RF. Apical annuli are specialised sites of post-invasion secretion of dense granules in *Toxoplasma*. *Elife*. 2024;13: e94201. <https://doi.org/10.7554/eLife.94201> PMID: 38270431
85. Chern JH, Pasquarelli RR, Moon AS, Chen AL, Sha J, Wohlschlegel JA, et al. A Novel *Toxoplasma* Inner Membrane Complex Suture-Associated Protein Regulates Suture Protein Targeting and Colocalizes with Membrane Trafficking Machinery. *mBio*. 2021;12: e02455-21. <https://doi.org/10.1128/mBio.02455-21> PMID: 34634933
86. Díaz-Martin RD, Sandoval Rodriguez FE, González Pozos S, Gómez de León CT, Mondragón Castelán M, Mondragón Flores R. A comprehensive ultrastructural analysis of the *Toxoplasma gondii* cytoskeleton. *Parasitol Res*. 2022;121: 2065–2078. <https://doi.org/10.1007/s00436-022-07534-3> PMID: 35524789
87. Engelberg K, Chen C, Bechtel T, Sánchez Guzmán V, Drozda AA, Chavan S, et al. The apical annuli of *Toxoplasma gondii* are composed of coiled-coil and signalling proteins embedded in the inner membrane complex sutures. *Cellular Microbiology*. 2020;22. <https://doi.org/10.1111/cmi.13112> PMID: 31470470
88. Hu K, Johnson J, Florens L, Fraunholz M, Suravajjala S, DiLullo C, et al. Cytoskeletal components of an invasion machine--the apical complex of *Toxoplasma gondii*. *PLoS Pathog*. 2006;2: e13. <https://doi.org/10.1371/journal.ppat.0020013> PMID: 16518471
89. Koreny L, Mercado-Saavedra BN, Klinger CM, Barylyuk K, Butterworth S, Hirst J, et al. Stable endocytic structures navigate the complex pellicle of apicomplexan parasites. *Nature Communications*. 2023;14: 2167. <https://doi.org/10.1038/s41467-023-37431-x> PMID: 37061511
90. Nichols BA, Chiappino ML, Pavesio CE. Endocytosis at the micropore of *Toxoplasma gondii*. *Parasitol Res*. 1994;80: 91–98. <https://doi.org/10.1007/BF00933773> PMID: 8202461
91. Gubbels M-J, Ferguson DJP, Saha S, Romano JD, Chavan S, Primo VA, et al. *Toxoplasma gondii*'s Basal Complex: The Other Apicomplexan Business End Is Multifunctional. *Front Cell Infect Microbiol*. 2022;12: 882166. <https://doi.org/10.3389/fcimb.2022.882166> PMID: 35573773

92. Sidik SM, Huet D, Ganesan SM, Huynh M-H, Wang T, Nasamu AS, et al. A Genome-wide CRISPR Screen in *Toxoplasma* Identifies Essential Apicomplexan Genes. *Cell*. 2016;166: 1423-1435.e12. <https://doi.org/10.1016/j.cell.2016.08.019> PMID: 27594426
93. Bookwalter CS, Kelsen A, Leung JM, Ward GE, Trybus KM. A *Toxoplasma gondii* class XIV myosin, expressed in Sf9 cells with a parasite co-chaperone, requires two light chains for fast motility. *J Biol Chem*. 2014;289: 30832–30841. <https://doi.org/10.1074/jbc.M114.572453> PMID: 25231988
94. Nebel T, Prieto JH, Kapp E, Smith BJ, Williams MJ, Yates JR, et al. Quantitative in vivo analyses reveal calcium-dependent phosphorylation sites and identifies a novel component of the *Toxoplasma* invasion motor complex. *PLoS Pathog*. 2011;7: e1002222. <https://doi.org/10.1371/journal.ppat.1002222> PMID: 21980283
95. Tang Q, Andenmatten N, Hortua Triana MA, Deng B, Meissner M, Moreno SNJ, et al. Calcium-dependent phosphorylation alters class XIVa myosin function in the protozoan parasite *Toxoplasma gondii*. *Mol Biol Cell*. 2014;25: 2579–2591. <https://doi.org/10.1091/mbc.E13-11-0648> PMID: 24989796
96. Delbac F, Sanger A, Neuhaus EM, Stratmann R, Ajioka JW, Tournel C, et al. *Toxoplasma gondii* myosins B/C: one gene, two tails, two localizations, and a role in parasite division. *J Cell Biol*. 2001;155: 613–623. <https://doi.org/10.1083/jcb.200012116> PMID: 11706051
97. Frenal K, Marq J-B, Jacot D, Polonais V, Soldati-Favre D. Plasticity between MyoC- and MyoA-glideosomes: an example of functional compensation in *Toxoplasma gondii* invasion. *PLoS Pathog*. 2014;10: e1004504. <https://doi.org/10.1371/journal.ppat.1004504> PMID: 25393004
98. Back PS, O’Shaughnessy WJ, Moon AS, Dewangan PS, Reese ML, Bradley PJ. Multivalent Interactions Drive the *Toxoplasma* AC9:AC10:ERK7 Complex To Concentrate ERK7 in the Apical Cap. *mBio*. 2022;13: e0286421. <https://doi.org/10.1128/mbio.02864-21> PMID: 35130732
99. O’Shaughnessy WJ, Hu X, Beraki T, McDougal M, Reese ML. Loss of a conserved MAPK causes catastrophic failure in assembly of a specialized cilium-like structure in *Toxoplasma gondii*. *Mol Biol Cell*. 2020;31: 881–888. <https://doi.org/10.1091/mbc.E19-11-0607> PMID: 32073987
100. O’Shaughnessy WJ, Hu X, Henriquez SA, Reese ML. *Toxoplasma* ERK7 protects the apical complex from premature degradation. *J Cell Biol*. 2023;222: e202209098. <https://doi.org/10.1083/jcb.202209098> PMID: 37027006
101. Behnke MS, Wootton JC, Lehmann MM, Radke JB, Lucas O, Nawas J, et al. Coordinated progression through two subtranscriptomes underlies the tachyzoite cycle of *Toxoplasma gondii*. *PLoS One*. 2010;5: e12354. <https://doi.org/10.1371/journal.pone.0012354> PMID: 20865045
102. Baptista CG, Lis A, Deng B, Gas-Pascual E, Dittmar A, Sigurdson W, et al. *Toxoplasma* F-box protein 1 is required for daughter cell scaffold function during parasite replication.

- Gubbels M-J, editor. PLoS Pathog. 2019;15: e1007946.  
<https://doi.org/10.1371/journal.ppat.1007946> PMID: 31348812
103. Engelberg K, Bechtel T, Michaud C, Weerapana E, Gubbels M-J. Proteomic characterization of the *Toxoplasma gondii* cytokinesis machinery portrays an expanded hierarchy of its assembly and function. Nat Commun. 2022;13: 4644.  
<https://doi.org/10.1038/s41467-022-32151-0> PMID: 35941170
  104. Torres JA, Pasquarelli RR, Back PS, Moon AS, Bradley PJ. Identification and Molecular Dissection of IMC32, a Conserved *Toxoplasma* Inner Membrane Complex Protein That Is Essential for Parasite Replication. mBio. 2021;12: e03622-20.  
<https://doi.org/10.1128/mBio.03622-20> PMID: 33593973
  105. Agop-Nersesian C, Egarter S, Langsley G, Foth BJ, Ferguson DJP, Meissner M. Biogenesis of the Inner Membrane Complex Is Dependent on Vesicular Transport by the Alveolate Specific GTPase Rab11B. Sibley LD, editor. PLoS Pathog. 2010;6: e1001029.  
<https://doi.org/10.1371/journal.ppat.1001029> PMID: 20686666
  106. Francia ME, Jordan CN, Patel JD, Sheiner L, Demerly JL, Fellows JD, et al. Cell Division in Apicomplexan Parasites Is Organized by a Homolog of the Striated Rootlet Fiber of Algal Flagella. Ward GE, editor. PLoS Biol. 2012;10: e1001444.  
<https://doi.org/10.1371/journal.pbio.1001444> PMID: 23239939
  107. Li Z, Du W, Yang J, Lai D-H, Lun Z-R, Guo Q. Cryo-Electron Tomography of *Toxoplasma gondii* Indicates That the Conoid Fiber May Be Derived from Microtubules. Adv Sci (Weinh). 2023;10: e2206595. <https://doi.org/10.1002/adv.202206595> PMID: 36840635
  108. Padilla LFA, Murray JM, Hu K. The initiation and early development of the tubulin-containing cytoskeleton in the human parasite *Toxoplasma gondii*. Mol Biol Cell. 2024;35: ar37. <https://doi.org/10.1091/mbc.E23-11-0418> PMID: 38170577
  109. Shaw MK, Compton HL, Roos DS, Tilney LG. Microtubules, but not actin filaments, drive daughter cell budding and cell division in *Toxoplasma gondii*. Journal of Cell Science. 2000;113: 1241–1254. <https://doi.org/10.1242/jcs.113.7.1241> PMID: 10704375
  110. Striepen B, Crawford MJ, Shaw MK, Tilney LG, Seeber F, Roos DS. The plastid of *Toxoplasma gondii* is divided by association with the centrosomes. J Cell Biol. 2000;151: 1423–1434. <https://doi.org/10.1083/jcb.151.7.1423> PMID: 11134072
  111. Nishi M, Hu K, Murray JM, Roos DS. Organellar dynamics during the cell cycle of *Toxoplasma gondii*. Journal of Cell Science. 2008;121: 1559–1568.  
<https://doi.org/10.1242/jcs.021089> PMID: 18411248
  112. Lorestani A, Ivey FD, Thirugnanam S, Busby MA, Marth GT, Cheeseman IM, et al. Targeted proteomic dissection of *Toxoplasma* cytoskeleton sub-compartments using MORN1. Cytoskeleton (Hoboken). 2012;69: 1069–1085.  
<https://doi.org/10.1002/cm.21077> PMID: 23027733

113. Wang C, Hu D, Tang X, Song X, Wang S, Zhang S, et al. Internal daughter formation of *Toxoplasma gondii* tachyzoites is coordinated by transcription factor TgAP2IX-5. *Cellular Microbiology*. 2021;23. <https://doi.org/10.1111/cmi.13291> PMID: 33217129
114. Butler C. Novel Cell Cycle Proteins In Apicomplexan Parasites. University of South Florida, Tampa. 2014. Available: <https://digitalcommons.usf.edu/etd/5195>
115. Butler CL, Lucas O, Wuchty S, Xue B, Uversky VN, White M. Identifying novel cell cycle proteins in Apicomplexa parasites through co-expression decision analysis. *PLoS One*. 2014;9: e97625. <https://doi.org/10.1371/journal.pone.0097625> PMID: 24841368
116. Heaslip AT, Dzierszynski F, Stein B, Hu K. TgMORN1 is a key organizer for the basal complex of *Toxoplasma gondii*. *PLoS Pathog*. 2010;6: e1000754. <https://doi.org/10.1371/journal.ppat.1000754> PMID: 20140195
117. Lorestani A, Sheiner L, Yang K, Robertson SD, Sahoo N, Brooks CF, et al. A *Toxoplasma* MORN1 null mutant undergoes repeated divisions but is defective in basal assembly, apicoplast division and cytokinesis. *PLoS One*. 2010;5: e12302. <https://doi.org/10.1371/journal.pone.0012302> PMID: 20808817
118. Frénal K, Jacot D, Hammoudi P-M, Graindorge A, Maco B, Soldati-Favre D. Myosin-dependent cell-cell communication controls synchronicity of division in acute and chronic stages of *Toxoplasma gondii*. *Nat Commun*. 2017;8: 15710. <https://doi.org/10.1038/ncomms15710> PMID: 28593938
119. Mann T, Gaskins E, Beckers C. Proteolytic processing of TgIMC1 during maturation of the membrane skeleton of *Toxoplasma gondii*. *J Biol Chem*. 2002;277: 41240–41246. <https://doi.org/10.1074/jbc.M205056200> PMID: 12177058
120. Gubbels M-J, Coppens I, Zarringhalam K, Duraisingh MT, Engelberg K. The Modular Circuitry of Apicomplexan Cell Division Plasticity. *Front Cell Infect Microbiol*. 2021;11: 670049. <https://doi.org/10.3389/fcimb.2021.670049> PMID: 33912479
121. Xue Y, Theisen TC, Rastogi S, Ferrel A, Quake SR, Boothroyd JC. A single-parasite transcriptional atlas of *Toxoplasma gondii* reveals novel control of antigen expression. *Elife*. 2020;9: e54129. <https://doi.org/10.7554/elife.54129> PMID: 32065584
122. Balaji S, Babu MM, Iyer LM, Aravind L. Discovery of the principal specific transcription factors of Apicomplexa and their implication for the evolution of the AP2-integrase DNA binding domains. *Nucleic Acids Res*. 2005;33: 3994–4006. <https://doi.org/10.1093/nar/gki709> PMID: 16040597
123. Zarringhalam K, Ye S, Lou J, Rezvani Y, Gubbels M-J. Cell cycle-regulated ApiAP2s and parasite development: the *Toxoplasma* paradigm. *Curr Opin Microbiol*. 2023;76: 102383. <https://doi.org/10.1016/j.mib.2023.102383> PMID: 37898053
124. Srivastava S, White MW, Sullivan WJ. *Toxoplasma gondii* AP2XII-2 Contributes to Proper Progression through S-Phase of the Cell Cycle. *mSphere*. 2020;5: e00542-20. <https://doi.org/10.1128/mSphere.00542-20> PMID: 32938695

125. Srivastava S, Holmes MJ, White MW, Sullivan WJ. *Toxoplasma gondii* AP2XII-2 Contributes to Transcriptional Repression for Sexual Commitment. *mSphere*. 2023;8: e0060622. <https://doi.org/10.1128/msphere.00606-22> PMID: 36786611
126. Khelifa AS, Guillen Sanchez C, Lesage KM, Huot L, Mouveaux T, Pericard P, et al. TgAP2IX-5 is a key transcriptional regulator of the asexual cell cycle division in *Toxoplasma gondii*. *Nat Commun*. 2021;12: 116. <https://doi.org/10.1038/s41467-020-20216-x> PMID: 33414462
127. Lesage KM, Huot L, Mouveaux T, Courjol F, Saliou J-M, Gissot M. Cooperative binding of ApiAP2 transcription factors is crucial for the expression of virulence genes in *Toxoplasma gondii*. *Nucleic Acids Res*. 2018;46: 6057–6068. <https://doi.org/10.1093/nar/gky373> PMID: 29788176
128. Walker R, Gissot M, Huot L, Alayi TD, Hot D, Marot G, et al. *Toxoplasma* transcription factor TgAP2XI-5 regulates the expression of genes involved in parasite virulence and host invasion. *J Biol Chem*. 2013;288: 31127–31138. <https://doi.org/10.1074/jbc.M113.486589> PMID: 24025328
129. Alvarez CA, Suvorova ES. Checkpoints of apicomplexan cell division identified in *Toxoplasma gondii*. *PLoS Pathog*. 2017;13: e1006483. <https://doi.org/10.1371/journal.ppat.1006483> PMID: 28671988
130. Hawkins LM, Naumov AV, Batra M, Wang C, Chaput D, Suvorova ES. Novel CRK-Cyclin Complex Controls Spindle Assembly Checkpoint in *Toxoplasma* Endodyogeny. *mBio*. 2021;13: e0356121. <https://doi.org/10.1128/mbio.03561-21> PMID: 35130726
131. Hawkins LM, Wang C, Chaput D, Batra M, Marsilia C, Awshah D, et al. The Crk4-Cyc4 complex regulates G2/M transition in *Toxoplasma gondii*. *EMBO J*. 2024. <https://doi.org/10.1038/s44318-024-00095-4> PMID: 38600241
132. Naumov A, Kratzer S, Ting L-M, Kim K, Suvorova ES, White MW. The *Toxoplasma* Centrocone Houses Cell Cycle Regulatory Factors. *mBio*. 2017;8: e00579-17. <https://doi.org/10.1128/mBio.00579-17> PMID: 28830940
133. Hu X, O'Shaughnessy WJ, Beraki TG, Reese ML. Loss of the Conserved Alveolate Kinase MAPK2 Decouples *Toxoplasma* Cell Growth from Cell Division. *mBio*. 2020;11: e02517-20. <https://doi.org/10.1128/mBio.02517-20> PMID: 33173004
134. Morlon-Guyot J, Berry L, Chen C-T, Gubbels M-J, Lebrun M, Daher W. The *Toxoplasma gondii* calcium-dependent protein kinase 7 is involved in early steps of parasite division and is crucial for parasite survival. *Cell Microbiol*. 2014;16: 95–114. <https://doi.org/10.1111/cmi.12186> PMID: 24011186
135. Berry L, Chen C-T, Reininger L, Carvalho TG, El Hajj H, Morlon-Guyot J, et al. The conserved apicomplexan Aurora kinase TgArk3 is involved in endodyogeny, duplication rate and parasite virulence. *Cellular Microbiology*. 2016;18: 1106–1120. <https://doi.org/10.1111/cmi.12571> PMID: 26833682

136. Yang C, Doud EH, Sampson E, Arrizabalaga G. The protein phosphatase PPKL is a key regulator of daughter parasite development in *Toxoplasma gondii*. *mBio*. 2023;14: e0225423. <https://doi.org/10.1128/mbio.02254-23> PMID: 37877735
137. Engelberg K, Ivey FD, Lin A, Kono M, Lorestani A, Faugno-Fusci D, et al. A MORN1-associated HAD phosphatase in the basal complex is essential for *Toxoplasma gondii* daughter budding. *Cellular Microbiology*. 2016;18: 1153–1171. <https://doi.org/10.1111/cmi.12574> PMID: 26840427
138. Sugi T, Kawazu S-I, Horimoto T, Kato K. A single mutation in the gatekeeper residue in TgMAPKL-1 restores the inhibitory effect of a bumped kinase inhibitor on the cell cycle. *Int J Parasitol Drugs Drug Resist*. 2015;5: 1–8. <https://doi.org/10.1016/j.ijpddr.2014.12.001> PMID: 25941623
139. Pasquarelli RR, Back PS, Sha J, Wohlschlegel JA, Bradley PJ. Identification of IMC43, a novel IMC protein that collaborates with IMC32 to form an essential daughter bud assembly complex in *Toxoplasma gondii*. *PLoS Pathog*. 2023;19: e1011707. <https://doi.org/10.1371/journal.ppat.1011707> PMID: 37782662

## **Chapter 2:**

Identification of IMC43, a novel IMC protein that collaborates with IMC32 to form an essential daughter bud assembly complex in *Toxoplasma gondii*

RESEARCH ARTICLE

# Identification of IMC43, a novel IMC protein that collaborates with IMC32 to form an essential daughter bud assembly complex in *Toxoplasma gondii*

Rebecca R. Pasquarelli<sup>1</sup>, Peter S. Back<sup>1</sup>, Jihui Sha<sup>2</sup>, James A. Wohlschlegel<sup>2</sup>, Peter J. Bradley<sup>1,3\*</sup>

**1** Molecular Biology Institute, University of California, Los Angeles, California, United States of America, **2** Department of Biological Chemistry and Institute of Genomics and Proteomics, University of California, Los Angeles, California, United States of America, **3** Department of Microbiology, Immunology, and Molecular Genetics, University of California, Los Angeles, California, United States of America

\* [pbradley@ucla.edu](mailto:pbradley@ucla.edu)



**OPEN ACCESS**

**Citation:** Pasquarelli RR, Back PS, Sha J, Wohlschlegel JA, Bradley PJ (2023) Identification of IMC43, a novel IMC protein that collaborates with IMC32 to form an essential daughter bud assembly complex in *Toxoplasma gondii*. PLoS Pathog 19(10): e1011707. <https://doi.org/10.1371/journal.ppat.1011707>

**Editor:** Christopher J. Tonkin, The Walter and Eliza Hall Institute of Medical Research, AUSTRALIA

**Received:** July 26, 2023

**Accepted:** September 23, 2023

**Published:** October 2, 2023

**Peer Review History:** PLOS recognizes the benefits of transparency in the peer review process; therefore, we enable the publication of all of the content of peer review and author responses alongside final, published articles. The editorial history of this article is available here: <https://doi.org/10.1371/journal.ppat.1011707>

**Copyright:** © 2023 Pasquarelli et al. This is an open access article distributed under the terms of the [Creative Commons Attribution License](https://creativecommons.org/licenses/by/4.0/), which permits unrestricted use, distribution, and reproduction in any medium, provided the original author and source are credited.

**Data Availability Statement:** All relevant data are within the manuscript and its [Supporting Information](#) files.

## Abstract

The inner membrane complex (IMC) of *Toxoplasma gondii* is essential for all phases of the parasite's life cycle. One of its most critical roles is to act as a scaffold for the assembly of daughter buds during replication by endodyogeny. While many daughter IMC proteins have been identified, most are recruited after bud initiation and are not essential for parasite fitness. Here, we report the identification of IMC43, a novel daughter IMC protein that is recruited at the earliest stages of daughter bud initiation. Using an auxin-inducible degron system we show that depletion of IMC43 results in aberrant morphology, dysregulation of endodyogeny, and an extreme defect in replication. Deletion analyses reveal a region of IMC43 that plays a role in localization and a C-terminal domain that is essential for the protein's function. TurboID proximity labelling and a yeast two-hybrid screen using IMC43 as bait identify 30 candidate IMC43 binding partners. We investigate two of these: the essential daughter protein IMC32 and a novel daughter IMC protein we named IMC44. We show that IMC43 is responsible for regulating the localization of both IMC32 and IMC44 at specific stages of endodyogeny and that this regulation is dependent on the essential C-terminal domain of IMC43. Using pairwise yeast two-hybrid assays, we determine that this region is also sufficient for binding to both IMC32 and IMC44. As IMC43 and IMC32 are both essential proteins, this work reveals the existence of a bud assembly complex that forms the foundation of the daughter IMC during endodyogeny.

## Author summary

*Toxoplasma gondii* is an obligate intracellular parasite that causes disease in immunocompromised individuals and congenitally infected neonates. *Toxoplasma* replicates using a unique process of internal budding in which two daughter buds form inside a single

**Funding:** This work was supported by NIH grants AI123360 to P.J.B. and GM089778 to J.A.W. R.R.P. and P.S.B. were supported by the Ruth L. Kirschstein National Research Service Award GM007185 and UCLA Molecular Biology Institute (MBI) Whitcome Fellowship. R.R.P. was additionally supported by the Ruth L. Kirschstein National Research Service Award AI007323. The funders had no role in study design, data collection and analysis, decision to publish, or preparation of the manuscript.

**Competing interests:** The authors have declared that no competing interests exist.

maternal parasite. This process is facilitated by an organelle called the inner membrane complex (IMC) which is found in *Toxoplasma* and other parasites in the phylum Apicomplexa. Although the IMC is known to be required for parasite replication, only a few early-recruiting IMC proteins have been identified. In this study, we identify and functionally analyze a novel IMC protein which is one of the earliest components of daughter buds and plays an essential role in parasite replication. We also identify its binding partners and demonstrate how their interactions impact the construction of daughter cells. This work reveals the existence of an essential protein complex formed in the earliest stages of parasite replication, expands our understanding of the IMC's role in *Toxoplasma* replication, and identifies potential targets for therapeutic intervention.

## Introduction

The Apicomplexa are a phylum of obligate intracellular parasites which cause serious disease in both humans and animals worldwide, leading to significant morbidity and mortality as well as economic losses [1]. The phylum includes the human pathogens *Toxoplasma gondii* (toxoplasmosis), *Plasmodium spp.* (malaria), and *Cryptosporidium spp.* (diarrheal diseases) as well as the veterinary pathogens *Eimeria tenella* (chicken coccidiosis) and *Neospora caninum* (neosporosis) [2–6]. *T. gondii* infects roughly 30% of the global human population [7]. While infection is typically asymptomatic in healthy individuals, infection in immunocompromised individuals can lead to fatal encephalitis [8,9]. In addition, congenital toxoplasmosis derived from a primary maternal infection can cause severe fetal abnormalities and abortion [10]. Existing treatments are restricted to limiting acute disease and are poorly tolerated [9]. Thus, a deeper understanding of the biology of this important pathogen is critically needed for the development of therapies based on parasite-specific activities.

The life cycles of apicomplexan parasites depend on a specialized organelle named the inner membrane complex (IMC), which plays critical roles in motility, host cell invasion, and parasite replication [11]. In *T. gondii*, the IMC lies directly underneath the parasite's plasma membrane and is composed of two structures: a series of flattened vesicles called alveoli which are arranged in a quilt-like pattern and a supportive network of intermediate filament-like proteins called alveolins [12,13]. The IMC is further divided into distinct regions such as the cone-shaped apical cap at the apex of the parasite, a central body portion, and a ring-shaped basal complex at the basal end of the parasite. Detergent fractionation experiments have shown that IMC proteins can associate with the alveoli, the cytoskeletal network, or span between both layers [14–16]. Additionally, IMC proteins differ by their presence in the maternal IMC, daughter IMC, or both [14,16]. Underlying the IMC is an array of 22 subpellicular microtubules that provide additional structural support for the organelle.

One of the key functions of the IMC is to facilitate parasite replication. Apicomplexans replicate using a variety of different budding mechanisms, all of which rely on the IMC to act as a scaffold for the developing daughter buds [17,18]. *T. gondii* replicates asexually by endodyogeny, a process of internal budding in which two daughter buds develop within the cytoplasm of a single maternal parasite. Budding is initiated upon centrosome duplication, which is quickly followed by the sequential recruitment of IMC proteins to the daughter cell scaffold (DCS) [14,18–21]. As proteins are added to the DCS, polymerization of subpellicular microtubules underlying the daughter IMC drives elongation of the growing daughter buds [22,23]. In the final stages of bud maturation, the maternal IMC is degraded and the daughter cells adopt the maternal plasma membrane and emerge as two separate cells [11].

The synthesis and recruitment of IMC proteins to the DCS occurs in a “just in time” manner [24,25]. As such, IMC proteins can be categorized by their timing of recruitment. During bud initiation the daughter IMC proteins IMC29, IMC32, FBXO1, BCC0, and IMC15 are recruited to the DCS [14,26–29]. IMC32 and BCC0 have been shown to be essential for parasite replication and survival, as their loss leads to an inability to stably assemble the IMC [27,28]. IMC29 and FBXO1, while not essential, also play critical roles in supporting the organization and maturation of the daughter IMC during endodyogeny [26,29]. The essential apical cap proteins AC9 and AC10 also localize to the daughter IMC during bud initiation, but these proteins are maintained in the maternal IMC and are involved in host cell invasion, rather than replication [30,31]. After bud initiation is completed, additional proteins such as ISP1 and the alveolins are added sequentially to the growing buds [14,32]. Though many protein components of the DCS have recently been identified, the organization, regulation, and precise function of most of these proteins remain poorly understood.

In this study, we identified and functionally analyzed a novel IMC protein, IMC43. We determined that IMC43 localizes to the body of the daughter IMC and is recruited during bud initiation. Using an auxin-inducible degron (AID) approach, we conditionally depleted IMC43 and showed that loss of the protein results in severe morphological defects, dysregulation of endodyogeny, and loss of overall lytic ability. We then performed deletion analyses which established that the function of IMC43 is dependent on a small region towards the C-terminus of the protein. Next, we used IMC43 as bait in both a TurboID proximity labelling experiment and a yeast two-hybrid (Y2H) screen to identify candidate IMC43 binding partners and provide insight into the precise function of the protein. Two of these proteins, the essential daughter protein IMC32 and a hypothetical protein we named IMC44, were functionally analyzed in relation to IMC43. These experiments showed that IMC43 is required for the proper localization of both of its partners and that binding at the essential C-terminal region of IMC43 is responsible for these interactions. Overall, our work identifies IMC43 as a foundational component of the early daughter IMC and reveals the existence of an IMC43-IMC32 daughter bud assembly complex which is essential for parasite replication and survival.

## Results

### IMC43 is a component of the early daughter cell scaffold

We have previously conducted proximity labelling to identify novel IMC proteins. In one of these experiments in which we used IMC29 as bait, we identified the uncharacterized protein TGGT1\_238895 [29]. TGGT1\_238895 encodes a 1,653 amino acid hypothetical protein which contains no identifiable functional domains (Figs 1A and S1A) [33,34]. We selected TGGT1\_238895 for further analysis because of its extremely low phenotype score of -5.41 in a genome-wide CRISPR/Cas9 screen for fitness-conferring genes and its cyclical expression profile, which is similar to IMC29 (Fig 1B) [24,35].

To determine the localization of TGGT1\_238895, we endogenously tagged it with a C-terminal 3xHA epitope tag. The protein was undetectable by immunofluorescence assay (IFA) in mature parasites, but colocalized with the IMC body-localizing alveolin IMC6 in developing daughter buds (Fig 1C and 1D). To determine whether TGGT1\_238895 localized to the daughter apical cap, we co-stained with the apical cap marker ISP1. TGGT1\_238895 was found to be absent from the apical cap, indicating that it is exclusively an IMC body protein (Fig 1E). Based on its localization, we named the protein IMC43. To determine how early IMC43 is incorporated into developing daughter buds, we co-stained for other early daughter markers that have been previously studied. These experiments showed that IMC43 recruits to early

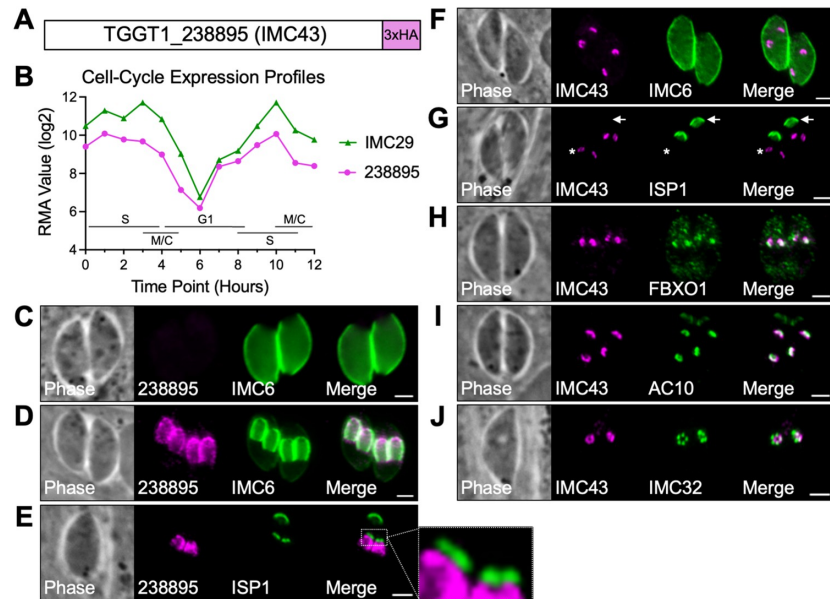


**Fig 1. TGGT1\_238895 localizes to the daughter IMC body and is recruited at the earliest stages of endodyogeny.** A) Gene model of TGGT1\_238895 (IMC43) showing the endogenous 3xHA tag fused to the C-terminus for localization studies. B) The cell-cycle expression profile for TGGT1\_238895 closely matches the cyclical pattern of the known daughter IMC protein IMC29. RMA = robust multi-array average [24]. C) IFA showing that TGGT1\_238895 is undetectable in mature parasites. Magenta = anti-HA detecting TGGT1\_238895<sup>3xHA</sup>, Green = anti-IMC6. D) IFA showing that TGGT1\_238895 localizes to daughter buds and colocalizes with IMC6. Magenta = anti-HA detecting TGGT1\_238895<sup>3xHA</sup>, Green = anti-IMC6. E) IFA of budding parasites showing that TGGT1\_238895 is excluded from the apical cap, marked by ISP1. Magenta = anti-HA detecting TGGT1\_238895<sup>3xHA</sup>, Green = anti-ISP1. F) IFA showing that IMC43 recruits to the daughter IMC before IMC6. Magenta = anti-HA detecting IMC43<sup>3xHA</sup>, Green = anti-IMC6. G) IFA showing that IMC43 recruits to the daughter IMC before ISP1. Arrow points to the mother cell apical cap. Asterisk indicates daughter buds. Magenta = anti-HA detecting IMC43<sup>3xHA</sup>, Green = anti-ISP1. H) IFA showing that IMC43 recruits to the daughter IMC at the same time as FBXO1. Magenta = anti-Ty detecting IMC43<sup>2xStrep3xTy</sup>, Green = anti-HA detecting FBXO1<sup>3xHA</sup>. I) IFA showing that IMC43 recruits to the daughter IMC at the same time as AC10. Magenta = anti-HA detecting IMC43<sup>3xHA</sup>, Green = anti-Ty detecting AC10<sup>2xStrep3xTy</sup>. J) IFA showing that IMC43 recruits to the daughter IMC at the same time as IMC32. Magenta = anti-HA detecting IMC43<sup>3xHA</sup>, Green = anti-V5 detecting IMC32<sup>3xV5</sup>. Scale bars = 2  $\mu$ m.

<https://doi.org/10.1371/journal.ppat.1011707.g001>

daughters before IMC6 and ISP1 and around the same time as FBXO1, AC10, and IMC32 (Fig 1F–J). From these data we concluded that IMC43 is a daughter-specific IMC body protein that is recruited to the DCS at the earliest stages of endodyogeny.

### IMC43 is an essential protein involved in endodyogeny

Because IMC43 has a low phenotype score and is a component of the early daughter cell scaffold, we hypothesized that it was likely to play a critical role in parasite survival and replication [35]. We were unable to genetically disrupt *IMC43*, despite successful CRISPR/Cas9 targeting to its endogenous locus, indicating that *IMC43* is likely essential as suggested by its phenotype score (S2 Fig). Thus, we used an auxin-inducible degron (AID) conditional knockdown system to study its function (Fig 2A) [36,37]. The degron-tagged protein (IMC43<sup>AID</sup>) localized correctly to the daughter IMC and was rapidly degraded upon treatment with indoleacetic acid (IAA) (Fig 2B). Western blot analysis confirmed efficient knockdown of the target protein (S3A Fig).

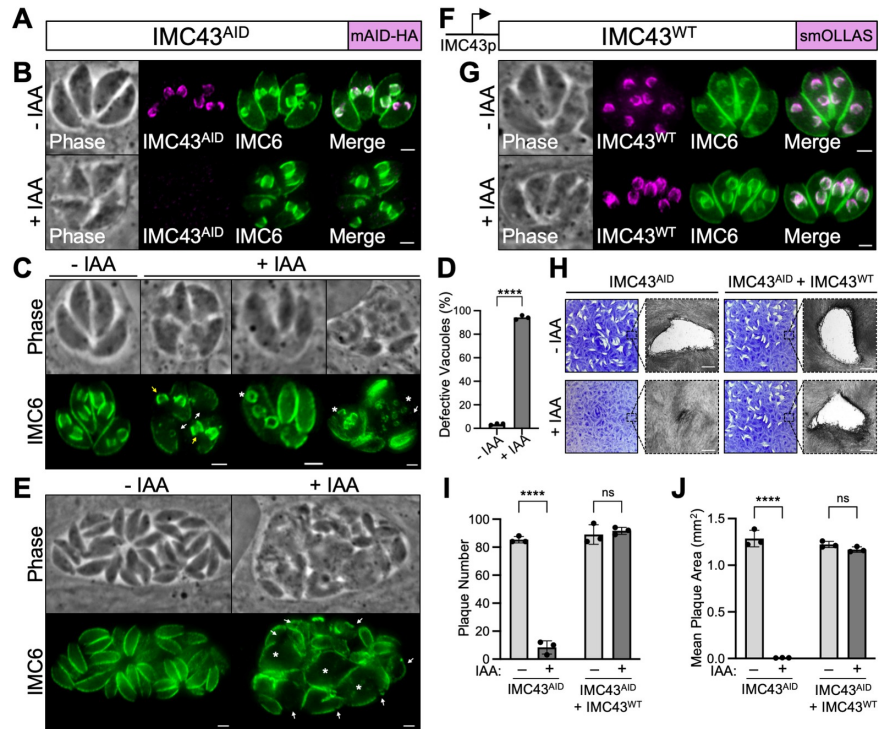


**Fig 2. IMC43 is essential for parasite replication and survival.** A) Diagram showing the mAID-3xHA degen tag fused to the C-terminus of IMC43 in a TIR1-expressing strain to facilitate proteasomal degradation upon treatment with IAA. B) IFA showing that the IMC43<sup>AID</sup> protein localizes normally to the daughter IMC and is depleted when the parasites are treated with IAA. Magenta = anti-HA detecting IMC43<sup>AID</sup>, Green = anti-IMC6. C) IFA showing the broad range of morphological and replication defects observed after treating IMC43<sup>AID</sup> parasites with IAA for 24 hours. White arrows point to large gaps in the IMC marked by IMC6. Yellow arrows point to daughter buds present outside of the maternal parasite. Asterisks mark parasites producing more than two daughter buds. All three +IAA vacuoles also display desynchronized endodyogeny, where parasites in the same vacuole are at different stages of replication. Green = anti-IMC6. D) Quantification of vacuoles displaying morphological and/or replication defects after 24 hours of IMC43 depletion. Statistical significance was determined using a two-tailed t test (\*\*\*\*,  $P < 0.0001$ ). E) IFA of IMC43<sup>AID</sup> parasites treated with IAA for 40 hours. White arrows point to large gaps in the IMC marked by IMC6. Asterisks indicate swollen parasites. Green = anti-IMC6. F) Diagram of the full-length smOLLAS-tagged IMC43 complementation construct driven by its endogenous promoter (IMC43<sup>WT</sup>) and integrated at the UPRT locus in IMC43<sup>AID</sup> parasites. G) IFA showing that IMC43<sup>WT</sup> localizes normally to the daughter IMC and rescues the morphological and replication defects observed upon treatment with IAA. Magenta = anti-OLLAS detecting IMC43<sup>WT</sup>, Green = anti-IMC6. H) Plaque assays for IMC43<sup>AID</sup> and IMC43<sup>AID</sup> + IMC43<sup>WT</sup> parasites grown for seven days +/- IAA. Depletion of IMC43 results in a severe defect in overall lytic ability, which is fully rescued by complementation with the wild-type protein. Scale bars = 0.5 mm. I) Quantification of plaque number for plaque assays shown in panel H. IMC43-depleted parasites form fewer than 10% as many plaques compared to control. Statistical significance was determined using multiple two-tailed t tests (\*\*\*\*,  $P < 0.0001$ ; ns = not significant). J) Quantification of plaque size for plaque assays shown in panel H. Plaques formed by IMC43-depleted parasites are <1% the usual size. Statistical significance was determined using multiple two-tailed t tests (\*\*\*\*,  $P < 0.0001$ ; ns = not significant). Scale bars for all IFAs = 2  $\mu$ m.

<https://doi.org/10.1371/journal.ppat.1011707.g002>

To assess the effects of IMC43 knockdown on parasite morphology over the course of multiple replication cycles, parasites were treated with IAA for 24 hours and assessed by IFA (Fig 2C). IMC43-depleted parasites showed severe defects in IMC morphology, such as large gaps in the cytoskeleton marked by IMC6 and the presence of daughter buds that appeared to not be encased by the maternal IMC. IMC43-depleted parasites also exhibited a variety of

replication defects, including asynchronous division and formation of more than two daughter buds per cell, indicating a severe dysregulation of endodyogeny. Quantification showed that 94.2% of vacuoles exhibited one or more of these issues after only 24 hours of IAA treatment (Fig 2D), with most vacuoles exhibiting multiple defects simultaneously. When we extended the IAA treatment to 40 hours, we saw continued growth despite these defects, which appeared to accumulate over time (Fig 2E). To confirm that these defects were due to the loss of IMC43, we generated a full-length IMC43 complementation construct driven by its endogenous promoter and integrated it at the UPRT locus (IMC43<sup>WT</sup>) (Figs 2F and S3B). Complementation with IMC43<sup>WT</sup> fully rescued the observed morphological and replication defects (Fig 2G).

To determine how loss of IMC43 affects the parasite's overall lytic ability on a longer time course, we performed plaque assays (Fig 2H). IMC43-depleted parasites exhibited a severe defect in plaque efficiency, forming <10% as many plaques compared to vehicle-treated IMC43<sup>AID</sup> parasites (Fig 2I). The few plaques that they did form were also drastically smaller than normal: <1% the size of plaques formed by vehicle-treated parasites (Fig 2J). The defects in both plaque efficiency and plaque size were fully rescued by complementation with the wild-type protein. Since we were unable to generate a stable knockout line, it's likely that these few small plaques are formed by a small percentage of parasites that experience incomplete knockdown.

To dissect the phenotype of IMC43-depleted parasites further, we co-stained for markers of key structures involved in endodyogeny. First, we stained for the daughter IMC body protein IMC29, which localized normally despite the gross morphological defects (Fig 3A). Next, we stained for the apical cap marker AC10, the basal complex marker MORN1, and tubulin. These experiments showed that the apical cap, basal complex, conoid, and subpellicular microtubules appear to assemble on nascent daughter buds in the absence of IMC43 (Fig 3B–3D). Finally, we stained for the centrosome marker Centrin1, as well as DNA marked by Hoechst staining. This showed that in the absence of IMC43, parasites continue nuclear division and centrosome duplication in an apparent attempt to continue replicating (Fig 3E and 3F). Together, these data indicate that IMC43 is an essential protein which is required for replication, structural integrity of the IMC, and parasite survival.

### IMC43 contains an essential functional domain near the C-terminus of the protein

Like many other IMC proteins, IMC43 lacks homology to known proteins and has no readily identifiable functional domains. To dissect which regions of the protein are important for localization and function, we developed a series of nine deletion constructs guided by predicted secondary structure and conservation with *N. caninum* (Figs 4A and S1B) [38]. Each deletion construct was integrated into the UPRT locus in the IMC43<sup>AID</sup> strain, as we did previously for IMC43<sup>WT</sup>. Western blot analysis confirmed that each of the deletion constructs was expressed at similar levels to IMC43<sup>WT</sup> and ran at approximately the expected size (S3C Fig). Eight of the nine deletion constructs colocalized completely with the wild-type protein (S4 Fig). The only deletion construct which did not was IMC43<sup>Δ402–494</sup>, which enriched at daughter buds but also partially mistargeted to the cytoplasm (Fig 4B). Surprisingly, almost all the deletion constructs were also able to rescue both the morphological and replication defects. The only exception was the Δ1441–1653 mutant, a C-terminal truncation of the protein (Fig 4C and 4D, S5). To narrow down the essential region of the C-terminus, we constructed two smaller sub-deletions: Δ1441–1561 and Δ1562–1653. The Δ1562–1653 mutant fully rescued the phenotype of the knockdown, while the Δ1441–1561 mutant did not, indicating that residues 1441–1561 are essential for the function of IMC43 (Figs 4E–4G and S3D).

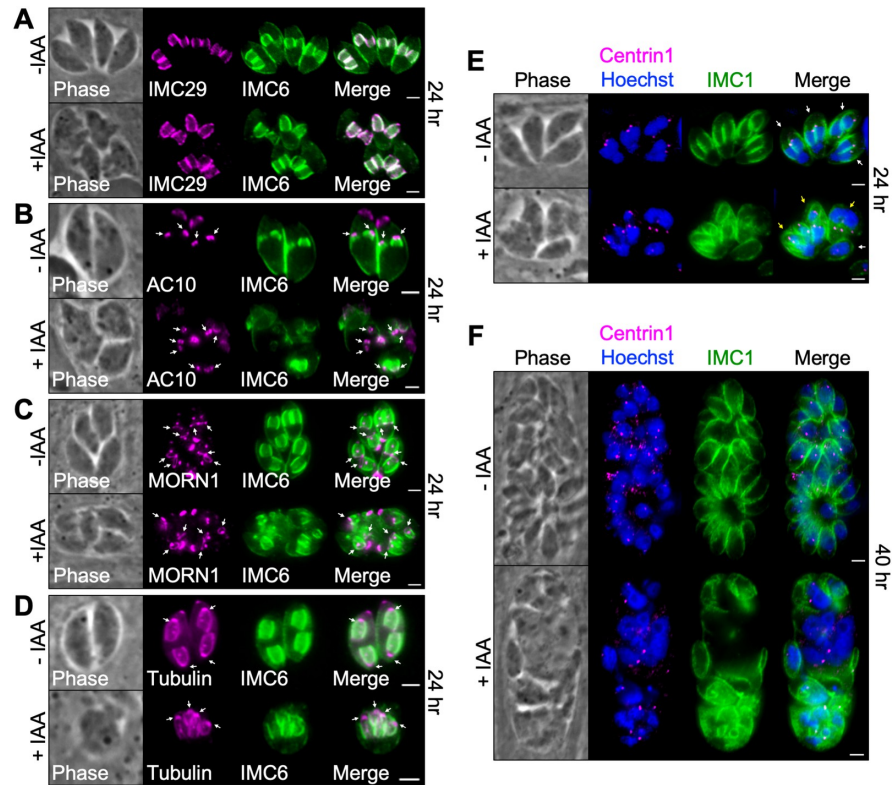


**Fig 3. Assessment of key structures involved in endodyogeny.** A) IFA showing that the daughter IMC protein IMC29 is unaffected by depletion of IMC43. Magenta = anti-V5 detecting IMC29<sup>3xV5</sup>, Green = anti-IMC6. B) IFA showing that the apical cap marker AC10 is unaffected by depletion of IMC43. Arrows point to the apical cap of daughter buds. Magenta = anti-V5 detecting AC10<sup>3xV5</sup>, Green = anti-IMC6. C) IFA showing that the basal complex marker MORN1 is unaffected by depletion of IMC43. Arrows point to the basal complex of daughter buds. Magenta = anti-V5 detecting MORN1<sup>3xV5</sup>, Green = anti-IMC6. D) IFA showing that the conoid and subpellicular microtubules still assemble on nascent daughter buds when IMC43 is depleted. Arrows point to daughter bud conoids. Magenta = transiently expressed Tubulin1-GFP, Green anti-IMC6. E) IFA showing that centrosome duplication continues when IMC43 is depleted. Centrosomes, marked by Centrin1, appear to duplicate and associate with daughter buds and dividing nuclei. Parasites forming more than two daughter buds also form more than two centrosomes. White arrow points to a single parasite containing two centrosomes (normal). Yellow arrows point to single parasites containing three or more centrosomes (abnormal). Magenta = anti-Centrin1, Green = anti-IMC1, Blue = Hoechst. F) IFA showing that nuclear division and centrosome duplication continue after 40 hours of IAA treatment. Magenta = anti-Centrin1, Green = anti-IMC1, Blue = Hoechst. Scale bars = 2 μm.

<https://doi.org/10.1371/journal.ppat.1011707.g003>

### Identification of IMC43 binding partners using TurboID and Y2H screening

To further investigate IMC43, we used both TurboID proximity labelling and a yeast two-hybrid (Y2H) screen to identify candidate binding partners [39–41]. For the TurboID experiment, we fused the TurboID biotin ligase plus a 3xHA tag to the C-terminus of IMC43 (Fig 5A). IMC43<sup>TurboID</sup> localized normally and robustly biotinylated the daughter IMC when treated with biotin, confirming that the TurboID biotin ligase is enzymatically active (Fig 5B). Therefore, we continued with a large-scale TurboID experiment and analyzed the results by mass spectrometry. The results were filtered to include only genes that were at least two-fold

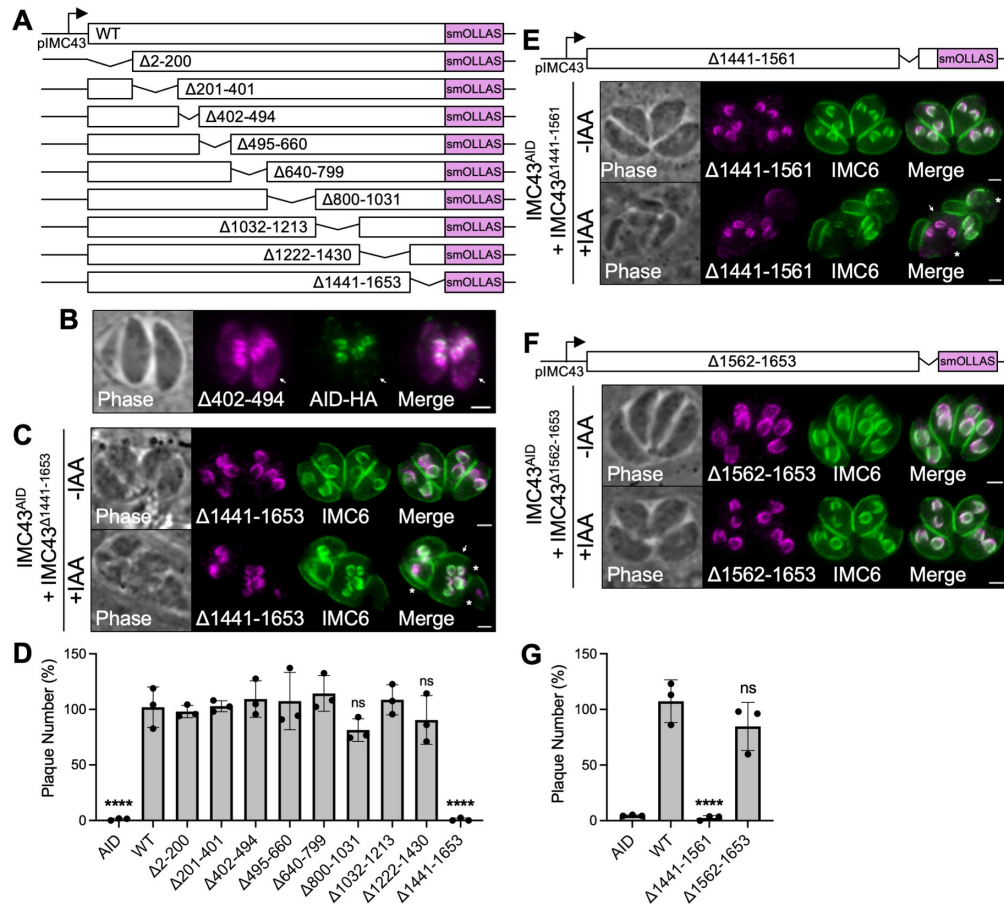


**Fig 4. Deletion analyses reveal regions involved in IMC43 localization and function.** A) Diagram of the nine deletion constructs generated for domain analysis of IMC43. B) IFA showing the localization of IMC43<sup>Δ402-494</sup> compared to IMC43<sup>AID</sup>. IMC43<sup>Δ402-494</sup> partially mislocalizes to the cytoplasm of parasites (arrow). Magenta = anti-OLLAS detecting IMC43<sup>Δ402-494</sup>, Green = anti-HA detecting IMC43<sup>AID</sup>. C) IFA showing that IMC43<sup>Δ1441-1653</sup> fails to rescue the morphological and replication defects caused by depletion of endogenous IMC43. Arrow points to a single maternal parasite producing five daughter buds, indicating dysregulation of endodyogeny. Asterisks indicate disruption of the cytoskeleton. Magenta = anti-OLLAS detecting IMC43<sup>Δ1441-1653</sup>, Green = anti-IMC6. D) Quantification of plaque number for IMC43<sup>AID</sup>, IMC43<sup>AID</sup> + IMC43<sup>WT</sup>, and all nine IMC43 deletion strains shown in panel A after seven days of growth +/- IAA. Y axis represents the number of plaques formed in +IAA conditions divided by the number of plaques formed in -IAA conditions for each strain. Statistical significance was determined by one-way ANOVA (\*\*\*\*, P < 0.0001; ns = not significant). E) IFA showing that IMC43<sup>Δ1441-1561</sup> fails to rescue the morphological and replication defects caused by depletion of endogenous IMC43. Arrow points to a single maternal parasite producing three daughter buds, indicating dysregulation of endodyogeny. Asterisks indicate disruption of the cytoskeleton. Magenta = anti-OLLAS detecting IMC43<sup>Δ1441-1561</sup>, Green = anti-IMC6. F) IFA showing that IMC43<sup>Δ1562-1653</sup> rescues the morphological and replication defects caused by depletion of endogenous IMC43. Magenta = anti-OLLAS detecting IMC43<sup>Δ1562-1653</sup>, Green = anti-IMC6. G) Quantification of plaque number for IMC43<sup>AID</sup>, IMC43<sup>AID</sup> + IMC43<sup>WT</sup>, IMC43<sup>AID</sup> + IMC43<sup>Δ1441-1561</sup>, and IMC43<sup>AID</sup> + IMC43<sup>Δ1562-1653</sup> parasites after seven days of growth +/- IAA. Y axis represents the number of plaques formed in +IAA conditions divided by the number of plaques formed in -IAA conditions for each strain. Statistical significance was determined by one-way ANOVA (\*\*\*\*, P < 0.0001; ns = not significant). Scale bars = 2 μm.

<https://doi.org/10.1371/journal.ppat.1011707.g004>

enriched with a difference of >5 spectral counts when comparing the IMC43<sup>TurboID</sup> sample to the control sample (S1 Table). For the Y2H screen, we used Hybrigenics Services to screen against the *T. gondii* RH strain cDNA library using the full-length IMC43 protein as the bait.

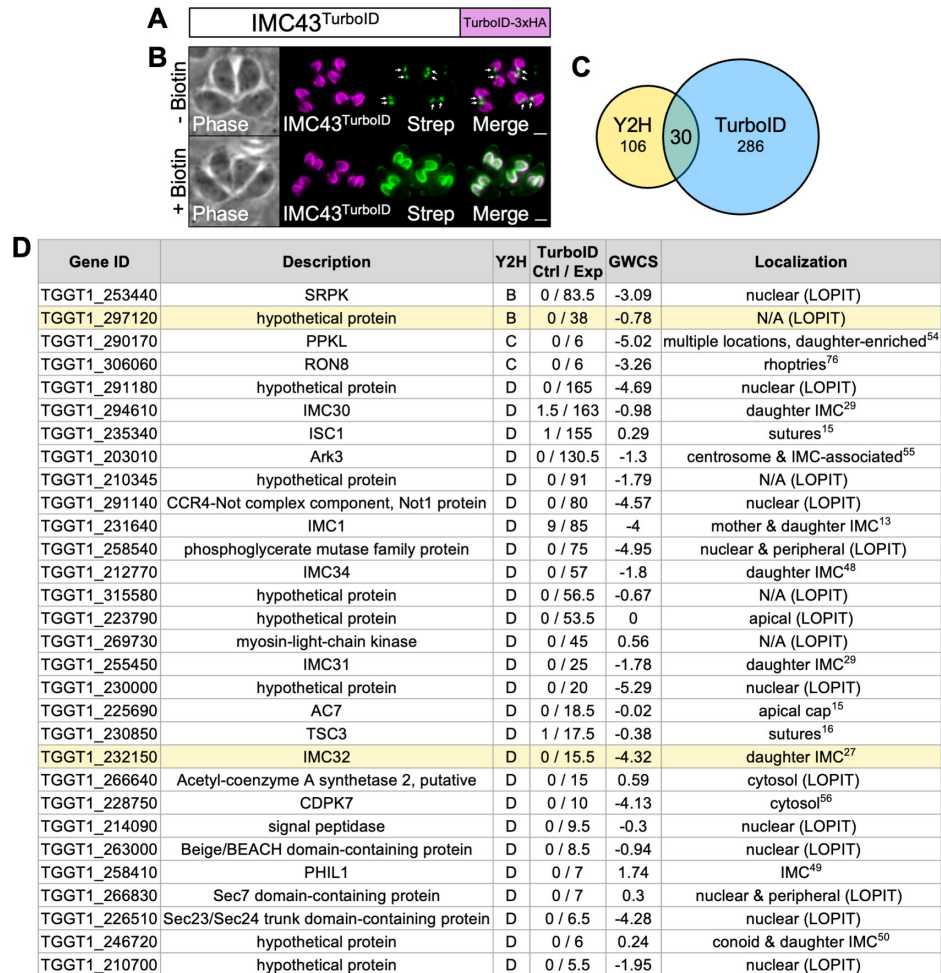


**Fig 5. TurboID and Y2H screens yield 30 candidate IMC43 binding partners.** A) Diagram of IMC43<sup>TurboID</sup>. B) IFA showing that IMC43<sup>TurboID</sup> localizes normally to the daughter IMC and biotinylates proximal proteins in a biotin-dependent manner. Arrows point to endogenously biotinylated apicoplasts. Magenta = anti-HA detecting IMC43<sup>TurboID</sup>, Green = streptavidin. Scale bars = 2  $\mu$ m. C) Venn diagram comparing genes identified in the Y2H screen and TurboID experiments. All Y2H hits that were ranked as “D” (moderate confidence) or higher were included. TurboID results were filtered to include only genes that were at least two-fold enriched with a difference of >5 spectral counts when comparing IMC43<sup>TurboID</sup> to control. 30 genes were identified in both experiments after filtering results as described. D) Table showing the 30 genes identified in both the TurboID and Y2H screens. The two candidate binding partners analyzed in this study are highlighted in yellow. “Y2H” column indicates the confidence score assigned in the Y2H screen (B = high confidence, C = good confidence, D = moderate confidence). “TurboID Ctrl / Exp” column indicates the average spectral count for each gene in the control and IMC43<sup>TurboID</sup> mass spectrometry results. “GWCS” refers to the phenotype score assigned to each gene in a genome-wide CRISPR/Cas9 screen [35]. “Localization” column reports the known localization of each protein [13,15,16,27,29,48–50,54–56,76]. Localizations followed by “(LOPIT)” indicate predicted localizations based on hyperplexed localization of organelle proteins by isotope tagging (hyperLOPIT) [42].

<https://doi.org/10.1371/journal.ppat.1011707.g005>

We included any hits that were assigned a confidence score of “A” (very high), “B” (high), “C” (good), or “D” (moderate) in our analysis (S2 Table). A total of 30 proteins were identified using both approaches (Fig 5C and 5D). To prioritize proteins for further analysis, we

considered their enrichment in the TurboID experiment, confidence score in the Y2H screen, transcriptional profile throughout the cell cycle, and known or predicted association with the daughter IMC [24,42]. Based on these criteria we selected two candidate IMC43 binding partners to explore further: the essential daughter protein IMC32 and the hypothetical protein encoded by TGGT1\_297120.

### **TGGT1\_297120 encodes a novel IMC protein with a dynamic localization that is dependent on IMC43**

TGGT1\_297120 was designated as a “B” hit in our Y2H screen and was highly enriched in our IMC43<sup>TurboID</sup> results (Figs 5D and 6A). It also exhibits a cyclical transcriptional profile throughout the cell cycle, closely mirroring that of IMC43 (Fig 6B) [24]. Endogenous tagging of the gene in our IMC43<sup>AID</sup> parasites revealed that the protein is absent from mature parasites and exhibits a dynamic localization pattern in the IMC of daughter buds. At bud initiation, TGGT1\_297120 appears in a small ring shape, similar to IMC43. During early budding, the protein appears to be restricted to the body of the daughter IMC. As the daughter buds expand, TGGT1\_297120 maintains its localization in the body of the IMC and additionally becomes enriched in the basal complex. Finally, during late endodyogeny and bud maturation, the protein shifts completely to the basal complex, where it localizes just adjacent to MORN1, and finally disappears once the buds emerge as mature cells (Fig 6C and 6D). Given the dynamic localization of TGGT1\_297120 within the daughter IMC, we named the protein IMC44.

To explore the function of IMC44, we used CRISPR/Cas9 to disrupt its gene, which was confirmed by IFA and PCR (S6A and S6B Fig). The  $\Delta imc44$  parasites did not have any gross morphological defects (S6A Fig). Plaque assays showed that loss of IMC44 had no effect on overall lytic ability, as expected based on its modest phenotype score (S6C and S6D Fig). We next endogenously tagged IMC43 in the  $\Delta imc44$  parasite line. IFA showed that the localization of IMC43 was unaffected in the  $\Delta imc44$  parasites, indicating that IMC43 localizes independently of its partner IMC44 (S6E Fig). Together, these data indicate that IMC44 is dispensable for parasite fitness and does not play a role in IMC43 localization.

We next wanted to assess how depletion of IMC43 affects the localization of IMC44. When IMC43 was depleted, IMC44 failed to localize to the body of the IMC during the early stages of endodyogeny and instead localized to the basal complex (Fig 6E). Normal IMC44 localization was restored when we complemented with IMC43<sup>WT</sup>, confirming that this change in localization was due to the loss of IMC43 (Fig 6F). To determine if this mislocalization could be linked to a specific region of IMC43, we endogenously tagged IMC44 in each of our ten IMC43 deletion constructs and used IFA to assess whether each deletion could rescue the mislocalization of IMC44 in the presence of IAA. Only the  $\Delta 1441-1561$  mutant failed to rescue the mislocalization of IMC44, indicating that the essential region of IMC43 plays a role in the localization of IMC44 (Figs 6G and S7). To determine whether this region is directly involved in binding to IMC44, we used pairwise Y2H assays. Fragments of IMC43 and IMC44 were cloned into Y2H bait and prey vectors, co-transformed into yeast, and spotted on permissive (-L/W) and restrictive (-L/W/H) media to assess binding. These experiments demonstrated that the C-terminus of IMC43, which contains the essential domain, is sufficient for binding to IMC44 at either its N-terminus or its C-terminus (Fig 6H and 6I). Together these data indicate that the essential C-terminal domain of IMC43 binds to IMC44 and regulates its localization during endodyogeny.

### **IMC43 regulates the organization of IMC32 in the daughter cell scaffold**

The second candidate IMC43 binding partner we explored was IMC32, a daughter-enriched IMC body protein that we previously showed is essential for parasite replication and survival

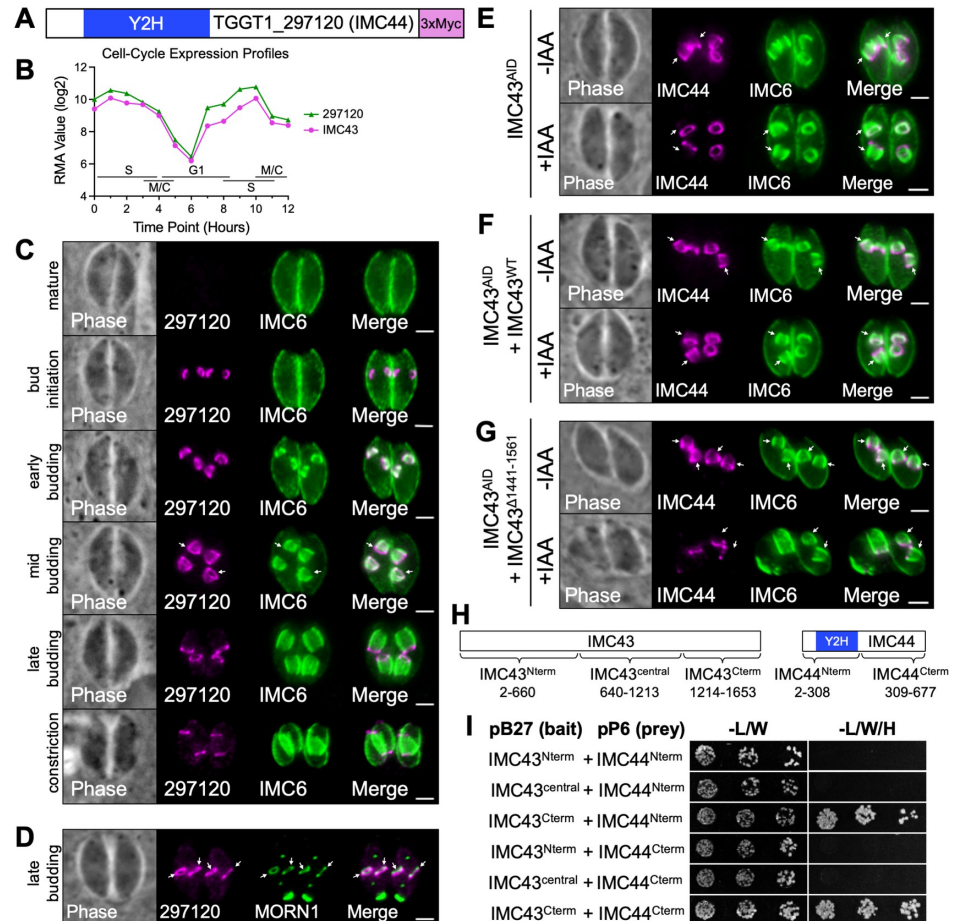


**Fig 6. IMC44 is a novel IMC protein which depends on IMC43 binding for regulation of its dynamic localization.** A) Gene model of TGGT1\_297120 (IMC44) showing the region determined to interact with IMC43 by the Y2H screen. B) The cell-cycle expression profile for TGGT1\_297120 closely mirrors the cyclical pattern of IMC43. RMA = robust multi-array average [24]. C) IFAs showing the localization of TGGT1\_297120 at different stages of endodyogeny. Arrows indicate the point at which TGGT1\_297120 can be first seen localizing to the basal complex of daughter buds. Magenta = anti-Myc detecting TGGT1\_297120<sup>3xMyc</sup>, Green = anti-IMC6. D) IFAs comparing the localization of TGGT1\_297120 with the basal complex marker MORN1. Arrows point to the basal complex of daughter buds. Magenta = anti-Myc detecting TGGT1\_297120<sup>3xMyc</sup>, Green = anti-V5 detecting MORN1<sup>3xV5</sup>. E) IFA showing the localization of IMC44 in IMC43<sup>AID</sup> parasites -/+ IAA. Depletion of IMC43 causes IMC44 to fail to localize to the body of the IMC. Arrows point to the body of the IMC in daughter buds. Magenta = anti-Myc detecting IMC44<sup>3xMyc</sup>, Green = anti-IMC6. F) IFA showing the localization of IMC44 in IMC43<sup>AID</sup> + IMC43<sup>WT</sup> parasites -/+ IAA. IMC43<sup>WT</sup> rescues the mislocalization of IMC44 observed in IMC43-depleted parasites. Arrows point to the body of the IMC in daughter buds. Magenta = anti-Myc detecting IMC44<sup>3xMyc</sup>, Green = anti-IMC6. G) IFA showing the localization of IMC44 in IMC43<sup>AID</sup> + IMC43<sup>Δ1441-1561</sup> parasites -/+ IAA. IMC43<sup>Δ1441-1561</sup> fails to rescue the mislocalization of IMC44 observed in IMC43-depleted parasites. Arrows point to the body of the IMC in daughter buds. Magenta = anti-Myc detecting IMC44<sup>3xMyc</sup>, Green = anti-IMC6. Scale bars = 2 μm. H) Diagrams showing the fragments of IMC43 and IMC44 that were fused to LexA/GAL4<sup>AD</sup> for pairwise Y2H assays. I) Pairwise Y2H assays assessing the interaction of IMC43 and IMC44. Growth on restrictive (-L/W/H) media indicates binding between the indicated fragments of each protein.

<https://doi.org/10.1371/journal.ppat.1011707.g006>

[27]. IMC32 contains five coiled-coil (CC) domains at its C-terminus, which we previously determined to be necessary for both its localization and function [27]. We also recently discovered a domain in the center of the protein which has structural homology to the fused Ig-PH

domain from the plant actin-binding protein SCAB1 (Fig 7A). IMC32 was identified as a “D” hit in our Y2H screen and was also relatively low abundance in our TurboID mass spectrometry results (Fig 5D). However, its localization, timing of recruitment, and function are all very similar to IMC43. Additionally, our Y2H screen data determined that three of the essential CC domains of IMC32 are involved in binding to IMC43, further supporting that IMC32 may be a true binding partner of IMC43 (Fig 7A).

To investigate the relationship between IMC32 and IMC43, we endogenously tagged IMC32 in our IMC43<sup>AID</sup> line. As we previously reported, IMC32 localizes to five distinct puncta arranged in a pentagon during bud initiation. As the buds elongate, IMC32 extends into a series of five longitudinal stripes that stretch along the body of the daughter IMC (Fig 7B) [27]. When we examined IMC32 localization in IMC43-depleted parasites, we found that IMC32 exhibited normal localization during the bud initiation and early budding stages (Fig 7C). However, during mid- and late-budding, IMC32 became disorganized. The usual pattern of stripes along the body of the IMC was frequently missing, and instead, IMC32 had a diffuse staining pattern in the body of the daughter IMC and in the cytoplasm (Fig 7D). Accumulation of these defects during a longer IAA treatment led to increased cytoplasmic mislocalization (Fig 7E). Quantification showed that IMC32 was mislocalized in approximately 78% of vacuoles containing parasites at the mid- and late-budding stages when IMC43 was depleted. This defect was fully rescued by complementation with IMC43<sup>WT</sup> (Fig 7F and 7G). This indicates that while IMC32 initially recruits to the DCS independently of IMC43, its organization during later stages of endodyogeny is dependent on IMC43.

To determine whether IMC43 relies on IMC32 for its localization as well, we generated an IMC32<sup>AID</sup> line in which IMC43 is endogenously tagged (S8A Fig). IFA showed efficient depletion of IMC32 resulting in severe morphological and replication defects as we have previously reported using an anhydrotetracycline transactivator-based regulation system (S8B Fig) [27]. IMC32 depletion had no effect on the localization of IMC43, indicating that IMC43 localizes independently of IMC32 (S8C Fig).

Next, we wanted to determine which region of IMC43 is required for the proper organization of IMC32 in the DCS. To assess this, we endogenously tagged IMC32 in each of our ten IMC43 deletion lines and used IFA to determine whether each deletion could rescue the mislocalization of IMC32. The  $\Delta 1441-1561$  mutant was the only one that failed to rescue the mislocalization of IMC32, indicating that the essential region of IMC43 is involved in regulating the localization of IMC32 (Figs 7H and S9). To directly assess the binding interaction between IMC43 and IMC32, we once again used pairwise Y2H assays. These experiments demonstrated that the C-terminus of IMC43 is sufficient for binding to IMC32's CC domains (Fig 7I and 7J). Together, these data indicate that the essential C-terminal domain of IMC43 binds to IMC32's CC domains and controls its localization during the middle and late stages of endodyogeny.

## Discussion

In this study, we identified and characterized IMC43 as a novel daughter-specific IMC protein which plays an essential role in endodyogeny. We also used proximity labelling and Y2H approaches to identify and explore its binding partners. Our data demonstrates that depletion of IMC43 results in severe morphological and replication defects, resulting in a loss of overall lytic ability. The phenotype of IMC43-depleted parasites closely resembles that of IMC32-depleted parasites [27]. Loss of both proteins results in cytoskeletal instability, swelling, asynchronous division, formation of more than two daughter buds per cell, and excessive rounds of nuclear division and centrosome duplication (Fig 8A) [27]. The observed morphological defects are also similar to that observed for BCC0 [28]. One key difference between IMC43

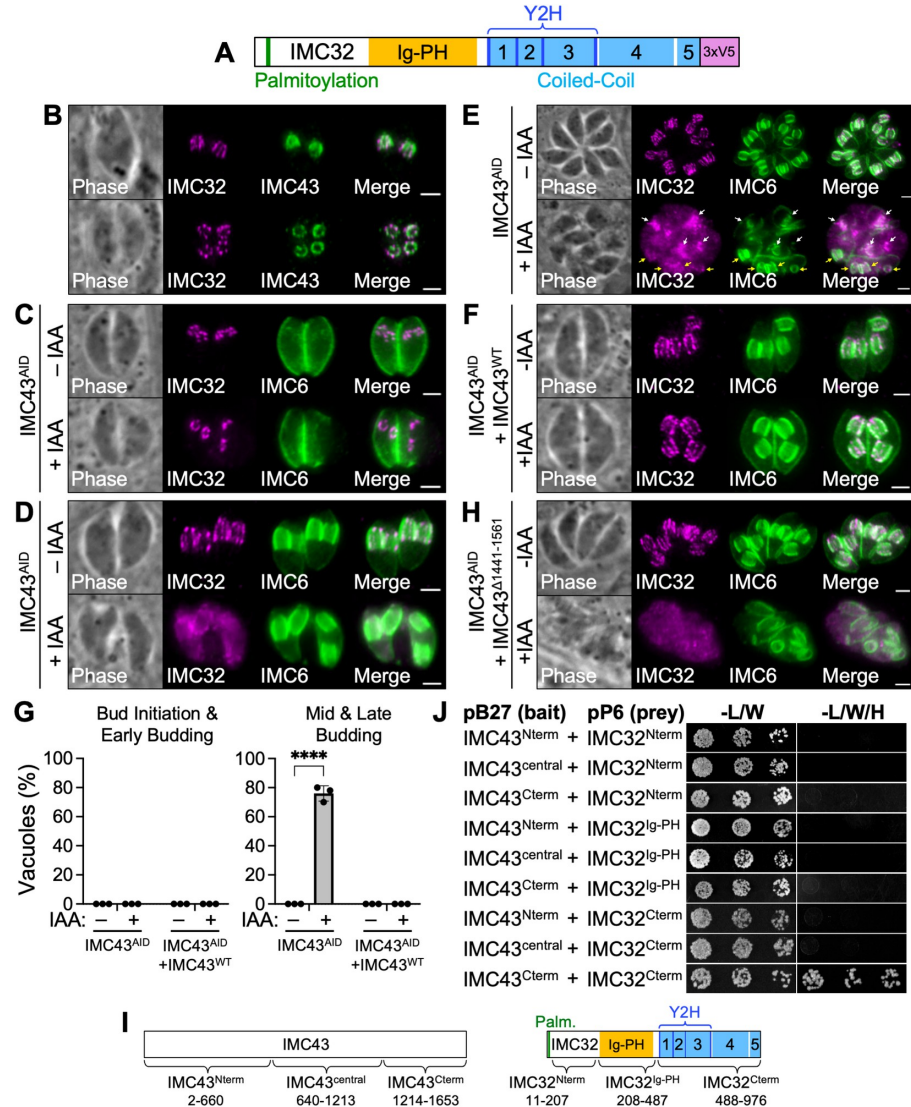


**Fig 7. IMC43 binding is required for maintenance of IMC32 during later stages of endodyogeny.** A) Gene model of IMC32 showing its predicted N-terminal palmitoylation site, Ig-PH domain, 5 predicted CC domains, and IMC43-interacting region identified by the Y2H screen. B) IFA comparing the localization of IMC43 and IMC32 at the mid/late budding stages of endodyogeny. Top: Daughter buds viewed from the side. Bottom: Daughter buds viewed from below. Magenta = anti-V5 detecting IMC32<sup>3xV5</sup>, Green = anti-HA detecting IMC43<sup>AID</sup>. C) IFA showing the localization of IMC32 during bud initiation in IMC43<sup>AID</sup> parasites after 18 hours of growth -/+ IAA. Depletion of IMC43 has no effect on IMC32 localization during bud initiation. Magenta = anti-V5 detecting IMC32<sup>3xV5</sup>, Green = anti-IMC6. D) IFA showing the localization of IMC32 during the late-budding stage in IMC43<sup>AID</sup> parasites after 18 hours of growth -/+ IAA. Depletion of IMC43 causes IMC32 to lose its characteristic striped localization pattern at this stage of endodyogeny. Magenta = anti-V5 detecting IMC32<sup>3xV5</sup>, Green = anti-IMC6. E) IFA showing the localization of IMC32 in IMC43<sup>AID</sup> parasites after 30 hours of growth -/+ IAA. Depletion of IMC43 over a longer time course results in an accumulation of mislocalized IMC32 in the cytoplasm. White arrows point to IMC32 enriching at early daughter buds. Yellow arrows point to daughter buds at the mid/late-budding stage with diffuse and disorganized IMC32 staining. Magenta = anti-V5 detecting IMC32<sup>3xV5</sup>, Green = anti-IMC6. F) IFA showing the localization of IMC32 in IMC43<sup>AID</sup> + IMC43<sup>WT</sup> parasites after 18 hours of growth -/+ IAA. IMC43<sup>WT</sup> rescues the mislocalization of IMC32 caused by depletion of IMC43. Magenta = anti-V5 detecting

IMC32<sup>3xV5</sup>, Green = anti-IMC6. G) Quantification of vacuoles with mislocalized IMC32 at different stages of endodyogeny after 18 hours of growth +/- IAA. Approximately 76% of vacuoles at the mid and late budding stages exhibited mislocalization of IMC32 when IMC43 was depleted. This phenotype was fully rescued by complementation with IMC43<sup>WT</sup>. Statistical significance was determined using multiple two-tailed t tests (\*\*\*\*, P < 0.0001; ns = not significant). H) IFA showing the localization of IMC32 in IMC43<sup>ΔID</sup> + IMC43<sup>Δ1441-1561</sup> parasites after 24 hours of growth +/- IAA. IMC43<sup>Δ1441-1561</sup> fails to rescue the mislocalization of IMC32 caused by depletion of IMC43. Magenta = anti-V5 detecting IMC32<sup>3xV5</sup>, Green = anti-IMC6. Scale bars = 2 μm. I) Diagrams showing the fragments of IMC43 and IMC32 that were fused to LexA/GAL4<sup>ΔD</sup> for pairwise Y2H assays. J) Pairwise Y2H assays assessing the interaction of IMC43 and IMC32. Growth on restrictive (-L/W/H) media indicates binding between the indicated fragments of each protein.

<https://doi.org/10.1371/journal.ppat.1011707.g007>

and BCC0 is that loss of BCC0 was reported to cause a partial disruption of the basal complex in daughter buds, whereas we demonstrated that the basal complex is unaffected by loss of IMC43. Finally, the severe replication defects are also similar to *Δimc29* parasites, although these defects are observed at a higher frequency in IMC43-depleted parasites [29].

While IMC43 does not contain any functional domains identifiable by sequence or structural homology, our deletion analyses identified two important regions. We first identified a small region towards the N-terminus (residues 402–494) which plays a minor role in localization of the protein. Deletion of this region led to a partial mislocalization of the protein to the cytoplasm. While this partial mislocalization could be due to protein misfolding, the fact that the *Δ402–494* mutant rescues the phenotype of the knockdown makes this less likely.

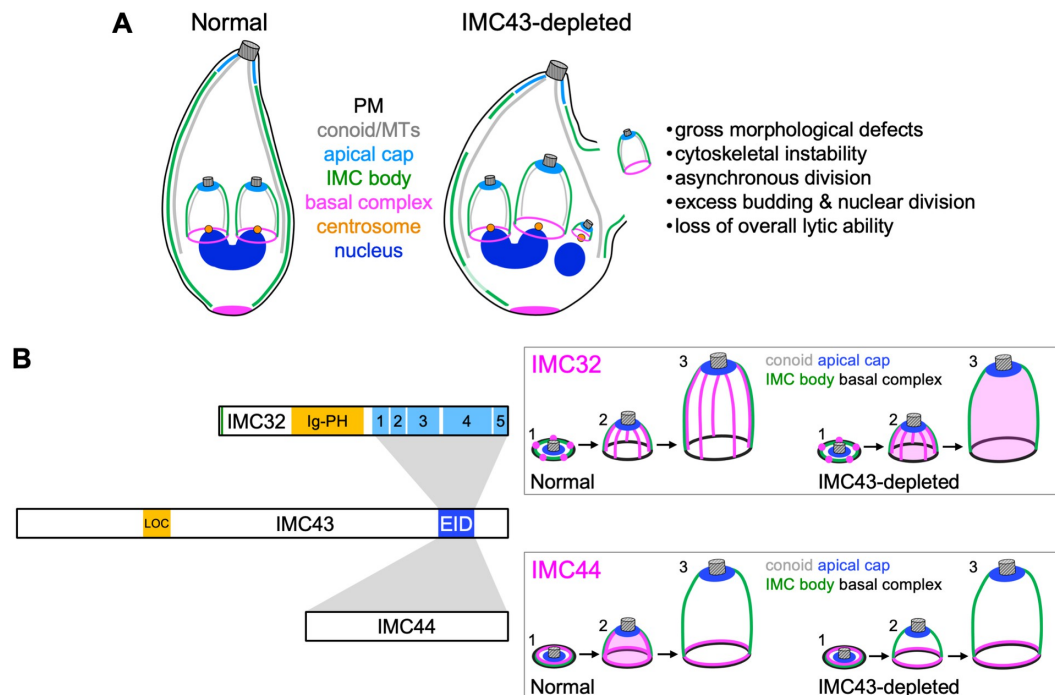


**Fig 8. Summary.** A) Diagram summarizing the effects of IMC43 depletion. Depletion of IMC43 causes gross morphological defects such as swelling, cytoskeletal instability, asynchronous division, excess budding & nuclear division, and loss of overall lytic ability. Assembly of the basal complex and apical cap remain unaffected. B) Diagram summarizing the relationship between IMC43 and its binding partners IMC32 and IMC44. The newly identified Localization domain (LOC) and Essential Interaction Domain (EID) of IMC43 are shown. Grey boxes indicate interactions between the Essential Interaction Domain of IMC43 and IMC32/IMC44. Boxed panels include a diagram showing how depletion of IMC43 affects the localization of IMC32 and IMC44 throughout bud initiation (1), early/mid-budding (2), and late budding (3).

<https://doi.org/10.1371/journal.ppat.1011707.g008>

Furthermore, this region of the protein is more conserved than nearby regions, supporting the hypothesis that this region may contain a domain involved in localization. Given these data, we tentatively assign the region encompassed by residues 402–494 as the Localization Domain (LOC) (Fig 8B). However, since none of the deletions fully abolished targeting to the IMC, other regions of the protein must play a role in localization. We also identified a domain near the C-terminus of the protein which is essential for the function of IMC43. This region is highly conserved and is one of the few regions of the protein that is not predicted to be intrinsically disordered [43]. AlphaFold predicts a four-helix bundle in this region, although the confidence is relatively weak [33,44,45]. Four-helix bundles are structurally similar to coiled-coils which often play roles in protein-protein interactions [46,47]. Based on its essential function in facilitating interaction between IMC43 and its partners, we named this region the Essential Interaction Domain (EID) (Fig 8B).

By combining the results of TurboID proximity labelling and a Y2H screen, we identified 30 candidate IMC43 binding partners and investigated two of them in relation to IMC43. This led us to two key findings: the identification of IMC44 as a novel daughter IMC protein with a dynamic localization which is dependent on IMC43, and the discovery of an essential IMC43-IMC32 daughter bud assembly complex that is critical for endodyogeny. IMC44 was found to have a dynamic localization pattern in which it localizes to the body of the IMC during the early stages of endodyogeny and then transitions to the basal complex during the middle and late stages. A similar dynamic localization has previously been reported for the alveolins IMC5, -8, -9, and -13, and also for the recently discovered BCC3 [14,28]. IMC44's localization within the IMC body is similar to the alveolins, whereas BCC3 appears to be present in the sutures of the daughter bud. However, the timing of IMC44's shift to the basal complex is more like that of BCC3, which also begins to transition to the basal complex during mid-budding, rather than just prior to bud constriction like the alveolins. Interestingly, all five of these proteins, as well as IMC44, have moderate fitness scores, and we showed here that IMC44 is dispensable [35]. Given their shared localization patterns, it's possible that there may be some functional redundancy among these proteins that explains their dispensability. For IMC44, we found that localization to the IMC body is dependent on IMC43, while localization to the basal complex occurs independent of IMC43. It's possible that IMC44's localization to the basal complex relies instead on binding to another basal complex-localizing protein. Since IMC5, -8, -9, and -13 shift to the basal complex later than IMC44, it will be interesting to see whether disruption of IMC44 affects any of their localizations.

The identification of IMC32 as an IMC43 binding partner was exciting due to their similar essential functions in endodyogeny. Intriguingly, we found that while IMC32 can localize to the early DCS during bud initiation independently, the maintenance of its striped localization pattern during mid and late budding requires IMC43. We also demonstrated that the C-terminus of IMC43 is sufficient for binding to IMC32's C-terminal CC domains (Fig 8B). In our previous study, we showed that the localization of IMC32 requires both its predicted N-terminal palmitoylation site and at least one of its C-terminal CC domains [27]. This suggests a model in which IMC32 initially recruits to the DCS via palmitoylation and is maintained in the later stages of endodyogeny by binding to IMC43. Together, our data indicates that IMC43 and IMC32 make up an essential protein complex in the DCS and are required for proper progression of endodyogeny. However, it is somewhat puzzling that IMC32 appears to be conserved throughout the Apicomplexa, whereas clear orthologs of IMC43 are only found in *N. caninum*, *Hammondia hammondi*, and *Besnoitia besnoiti* [27]. One possibility is that an ortholog of IMC43 is present in other apicomplexans but has diverged so much that it's no longer recognizable by sequence homology. This hypothesis is supported by the fact that the 43 kDa *Sarcocystis neurona* protein encoded by SN3\_03500255 and the 62 kDa *Cystoisospora suis*

protein encoded by CSUI\_009138 have significant homology to the essential C-terminus of IMC43. Alternatively, it is possible that IMC32 evolved to localize independently of other proteins in other apicomplexan parasites or relies on a different binding partner. Investigating the function of IMC32 in *Plasmodium spp.* would provide more insight into this question.

Of the remaining 28 candidate IMC43 binding partners, 25 were identified as “D” hits in the Y2H screen. “D” hits indicate moderate confidence in the interaction and represent a mix of false-positives and genuine interactions that are difficult to detect by Y2H due to low mRNA abundance in the *T. gondii* library, difficulty folding in yeast, or toxicity when expressed in yeast [40,41]. Given this caveat, it’s important to directly interrogate each candidate to determine whether it’s likely to be a bona fide binding partner. One example of this is IMC32, which was scored as a D hit and was validated in this study as a true partner of IMC43. It’s likely that IMC32 had a moderate confidence score due to low mRNA abundance in the *T. gondii* library, which was produced using extracellular (non-budding) parasites. Other D hits include several proteins which are known to localize to daughter buds, including IMC30, IMC31, IMC34, PHIL1, IMC1, and TGGT1\_246720 [13,29,48–50]. Given their shared localization with IMC43, these proteins represent interesting targets for future studies.

Another interesting finding from our interaction screening experiments was the identification of three kinases and one phosphatase as candidate IMC43 binding partners. Phosphoproteomics studies have identified several phosphorylation sites in IMC43, raising the possibility that phosphorylation could be important for the regulation of IMC43 localization or function. The putative cell-cycle-associated protein kinase SRPK was identified as a B hit and was found to bind via its kinase domain to IMC43 [51]. Similarly, the kelch repeat domain-containing serine/threonine protein phosphatase protein PPKL was identified as a “C” hit and was found to bind to IMC43 at two locations: its phosphatase domain and a region just N-terminal to the kelch repeat domain [52]. The fact that IMC43 binds to these proteins at their active sites suggests that IMC43 could be a substrate of SRPK and/or PPKL. SRPK has not been studied in *T. gondii*, but its low phenotype score suggests an essential function [35]. In *P. falciparum*, PPKL has been shown to be crucial for ookinete development and microtubule tethering to the IMC, and a recent pre-print by Yang et al. demonstrated that it plays an essential role in regulating daughter bud formation in *T. gondii* [53,54]. Additionally, both the aurora kinase Ark3 and the calcium-dependent protein kinase CDPK7 were identified as “D” hits and were previously shown to be involved in parasite replication [55,56]. Neither protein was found to bind to IMC43 at their kinase domain, so they are less likely to phosphorylate IMC43. However, IMC43 could still bind to these proteins to regulate their localization or activity. Exploring these candidate interactors and determining how their activity affects the function of IMC43 will be a fascinating topic of future studies.

Together, the data presented in this study identifies IMC43 as a foundational protein involved in *T. gondii* endodyogeny and reveals the existence of an essential IMC43-IMC32 daughter bud assembly complex. The protein-protein interaction data presented in this study yields ample opportunities for future studies that will inform our knowledge of how daughter IMC assembly is regulated. Furthering our understanding of this process will be vital for the identification of novel drug and vaccine targets for diseases caused by apicomplexan parasites.

## Materials and methods

### *T. gondii* and host cell culture

Parental *T. gondii* RH $\Delta$ hxgprt $\Delta$ ku80 (wild-type) and subsequent strains were grown on confluent monolayers of human foreskin fibroblasts (BJ, ATCC, Manassas, VA) at 37°C and 5% CO<sub>2</sub> in Dulbecco’s Modified Eagle Medium (DMEM) supplemented with 5% fetal bovine serum (Gibco), 5% Cosmic calf serum (Hyclone), and 1x penicillin-streptomycin-L-glutamine

(Gibco). Constructs containing selectable markers were selected using 1  $\mu$ M pyrimethamine (dihydrofolate reductase-thymidylate synthase [DHFR-TS]), 50  $\mu$ g/mL mycophenolic acid-xanthine (HXGPRT), or 40  $\mu$ M chloramphenicol (CAT) [57–59]. Homologous recombination to the UPRT locus was negatively selected using 5  $\mu$ M 5-fluorodeoxyuridine (FUdR) [60].

### Antibodies

The HA epitope was detected with mouse monoclonal antibody (mAb) HA.11 (BioLegend; 901515) and rabbit polyclonal antibody (pAb) anti-HA (Invitrogen; PI715500). The Ty1 epitope was detected with mouse mAb BB2 [61]. The c-Myc epitope was detected with mouse mAb 9E10 [62]. The V5 epitope was detected with mouse mAb anti-V5 (Invitrogen; R96025) and rabbit mAb anti-V5 (Cell Signaling Technology; 13202S). The OLLAS epitope was detected with rat mAb anti-OLLAS [63]. *Toxoplasma*-specific antibodies include rabbit pAb anti-IMC6 [64], mouse mAb anti-IMC1 [65], mouse mAb anti-ISP1 [32], rabbit pAb anti-Centrin1 (Kerafast; EBC004) [66], and rabbit anti-Catalase [67].

### Endogenous epitope tagging and knockout

For C-terminal endogenous tagging, a pU6-Universal plasmid containing a protospacer against the 3' untranslated region (UTR) of the target protein approximately 100 bp downstream of the stop codon was generated, as described previously [68]. A homology-directed repair (HDR) template was PCR amplified using the  $\Delta ku80$ -dependent LIC vector pmAID3xHA.LIC-HXGPRT, pmAID3xTy.LIC-HXGPRT, p3xHA.LIC-DHFR, p3xMyc.LIC-DHFR, p2xStrep3xTy.LIC-CAT, p2xStrep3xTy.LIC-HXGPRT, p3xV5.LIC-DHFR, p3xV5.LIC-HXGPRT, psmOLLAS.LIC-DHFR, or pTurboID3xHA.LIC-DHFR, all of which include the epitope tag, 3' UTR, and a selection cassette [69]. The 60-bp primers include 40 bp of homology immediately upstream of the stop codon or 40 bp of homology within the 3' UTR downstream of the CRISPR/Cas9 cut site. Primers that were used for the pU6-Universal plasmid as well as the HDR template are listed in S3 Table.

For N-terminal endogenous tagging of MORN1, a synthetic gene containing 146 bp of homology upstream of the start codon, a 3xV5 tag, and 219 bp of homology downstream of the start codon (primer P55) was ligated into a pJet vector (MORN1.3xV5.pJet). A homology-directed repair (HDR) template was PCR amplified from the MORN1.3xV5.pJet vector using primers P58 and P59. The protospacer was designed to target the sequence just downstream of the MORN1 start codon and was ligated into the pU6-Universal plasmid.

For knockout of IMC43 and IMC44, the protospacer was designed to target the coding region of the gene of interest, ligated into the pU6-Universal plasmid and prepared similarly to the endogenous tagging constructs. The HDR template was PCR amplified from a pJET vector containing the HXGPRT drug marker driven by the NcGRA7 promoter using primers that included 40 bp of homology immediately upstream of the start codon or 40 bp of homology downstream of the region used for homologous recombination for endogenous tagging.

For all tagging and knockout constructs, approximately 50  $\mu$ g of the sequence-verified pU6-Universal plasmid and the PCR-amplified HDR template were electroporated into the appropriate parasite strain. Transfected cells were allowed to invade a confluent monolayer of HFFs overnight, and appropriate selection was applied. Successful tagging was confirmed by IFA, and clonal lines of tagged parasites were obtained through limiting dilution.

### Complementation of IMC43<sup>AID</sup> parasites

The IMC43 coding region was PCR amplified from cDNA using primers P9 and P10. This was cloned into pUPRTKO-IMC32HA [27] using BglII/NotI to make pUPRTKO-IMC32p-

IMC43-3xHA. Next, the endogenous promoter (EP) was amplified from genomic DNA using primers P11 and P12 and the entire pUPRKO-IMC32p-IMC43-3xHA plasmid except for the IMC32 promoter was amplified using primer P13 and P14. The two fragments were then ligated using Gibson Assembly to make pUPRKO-EP-IMC43-3xHA (E2611, NEB). Finally, an smOLLAS tag was amplified from the p-smOLLAS-DHFR-LIC vector using primers P15 and P16 and the entire pUPRKO-EP-IMC43-3xHA plasmid except for the 3xHA tag was amplified using primers P17 and P18. The two fragments were then ligated using Gibson assembly to make pUPRKO-EP-IMC43<sup>WT</sup>-smOLLAS (IMC43<sup>WT</sup>). This complement vector was then linearized with PstI-HFv2 and transfected into IMC43<sup>AID</sup> parasites along with a pU6 that targets the UPRT coding region. Selection was performed with 5 µg/mL 5-fluorodeoxyuridine (FUDR) for replacement of UPRT. Clones were screened by IFA, and an smOLLAS-positive clone was designated IMC43<sup>WT</sup>. IMC43<sup>WT</sup> was used as the template to generate deletion constructs using Q5 site-directed mutagenesis with primers P19-P38 (E0552S, NEB). The same processes for linearization, transfection, and selection were followed for all deletion and mutant constructs. All restriction enzymes were purchased from NEB.

### Immunofluorescence assay

Confluent HFF cells were grown on glass coverslips and infected with *T. gondii*. After 18–40 hours, the coverslips were fixed with 3.7% formaldehyde in PBS and processed for immunofluorescence as described [70]. Primary antibodies were detected by species-specific secondary antibodies conjugated to Alexa Fluor 594/488/405 (ThermoFisher). Coverslips were mounted in Vectashield (Vector Labs), viewed with an Axio Imager.Z1 fluorescent microscope and processed with ZEN 2.3 software (Zeiss).

### Western blot

Parasites were lysed in 1x Laemmli sample buffer with 100 mM DTT and boiled at 100°C for 5 minutes. Lysates were resolved by SDS-PAGE and transferred to nitrocellulose membranes, and proteins were detected with the appropriate primary antibody and corresponding secondary antibody conjugated to horseradish peroxidase. Chemiluminescence was induced using the SuperSignal West Pico substrate (Pierce) and imaged on a ChemiDoc XRS+ (Bio-Rad).

### Plaque assay

HFF monolayers were infected with 200 parasites/well of individual strains and allowed to form plaques for 7 days. Cells were then fixed with ice-cold methanol and stained with crystal violet. All plaque assays were performed in triplicate. To quantify plaque size, the areas of 50 plaques per condition were measured using ZEN software (Zeiss). To quantify plaque number, the total number of plaques in each condition was counted manually. Graphical and statistical analyses were performed using Prism GraphPad 8.0.

### Quantification of defective vacuoles and mislocalized IMC32

For quantification of morphological and replication defects, HFF monolayers grown on glass coverslips were infected with IMC43<sup>AID</sup> parasites at low MOI +/- IAA. 24 hours post-infection, coverslips were fixed with 3.7% PFA, processed for immunofluorescence, and labeled with anti-HA and anti-IMC6. For both the -IAA and +IAA conditions, >100 vacuoles spread across at least 10 fields were scored as defective or normal. Vacuoles were scored as defective if they exhibited any of the following defects: desynchronized endodyogeny, >2 daughter buds per cell, immature daughter cells present outside of a maternal cell, gaps in the cytoskeleton

marked by IMC6, or severe swelling. The experiment was performed in triplicate. Significance was determined using a two-tailed t-test.

For quantification of mislocalized IMC32, HFF monolayers grown on glass coverslips were infected with IMC32<sup>3xV5</sup>IMC43<sup>AID</sup> parasites at low MOI +/- IAA. 18 hours post-infection, coverslips were fixed with 3.7% PFA, processed for immunofluorescence, and labeled with anti-V5 and anti-IMC6. For both the -IAA and +IAA conditions, >100 vacuoles containing parasites at the bud initiation and early budding stages of endodyogeny spread across at least 10 fields were scored as either normal or mislocalized. Vacuoles were scored as mislocalized at these stages if IMC32 signal was not observed in 5 distinct puncta/short stripes arranged in a ring-shape on nascent daughter buds. Then, >100 different vacuoles containing parasites at the mid and late budding stages of endodyogeny were scored as either normal or mislocalized. Vacuoles were scored as mislocalized at these stages if IMC32 signal was not observed in a series of longitudinal stripes along the body of the IMC. The experiment was performed in triplicate. Significance was determined using a two-tailed t-test.

### Affinity capture of biotinylated proteins

For affinity capture of proteins from whole cell lysates, HFF monolayers infected with IMC43<sup>TurboID</sup> or control parasites (RHΔ*hxgprt*Δ*ku80*, WT) were grown in medium containing 150 μM biotin for 30 hours. Intracellular parasites in large vacuoles were collected by manual scraping, washed in PBS, and lysed in radioimmunoprecipitation assay (RIPA) buffer (50 mM Tris [pH 7.5], 150 mM NaCl, 0.1% SDS, 0.5% sodium deoxycholate, 1% NP-40) supplemented with Complete Protease Inhibitor Cocktail (Roche) for 30 min on ice. Lysates were centrifuged for 15 min at 14,000 x g to pellet insoluble material, and the supernatant was incubated with Streptavidin Plus UltraLink resin (Pierce) overnight at 4°C under gentle agitation. Beads were collected and washed five times in RIPA buffer, followed by three washes in 8 M urea buffer (50 mM Tris-HCl [pH 7.4], 150 mM NaCl) [71]. Samples were submitted for on-bead digests and subsequently analyzed by mass spectrometry. The experiment was performed in duplicate.

### Mass spectrometry of biotinylated proteins

Purified proteins bound to streptavidin beads were reduced, alkylated, and digested by sequential addition of Lys-C and trypsin proteases. Samples were then desalted using C18 tips (Pierce) and fractionated online using a 75-μm inner-diameter fritted fused silica capillary column with a 5-μm pulled electrospray tip and packed in-house with 25 cm of C18 (Dr. Maisch GmbH) 1.9-μm reversed-phase particles. The gradient was delivered by a 140-minute gradient of increasing acetonitrile and eluted directly into a Thermo Orbitrap Fusion Lumos instrument where MS/MS spectra were acquired by Data Dependent Acquisition (DDA). Data analysis was performed using ProLuCID and DTASelect2 implemented in Integrated Proteomics Pipeline IP2 (Integrated Proteomics Applications) [72–74]. Database searching was performed using a FASTA protein database containing *T. gondii* GT1-translated open reading frames downloaded from ToxoDB. Protein and peptide identifications were filtered using DTASelect and required a minimum of two unique peptides per protein and a peptide-level false positive rate of less than 5% as estimated by a decoy database strategy. Candidates were ranked by spectral count comparing IMC43<sup>TurboID</sup> versus control samples [75].

### Yeast two-hybrid

Y2H screening was performed by Hybrigenics Services as previously described [40,41]. Briefly, the full-length coding sequence of IMC43 was cloned into the pB35 vector (N-GAL4-bait-C fusion, inducible) and transformed in yeast. This construct was screened for interactions

against the *T. gondii* RH strain cDNA library with 37 million interactions tested. Confidence for each interaction was assessed algorithmically (Predicted Biological Score, PBS).

For pairwise Y2H assays, fragments of IMC43, IMC44, and IMC32 were cloned into the pB27 (N-LexA-bait-C fusion) or pP6 (N-GAL4<sup>AD</sup>-prey-C fusion) vectors (Hybrigenics Services) as N-terminal fusions with the LexA DNA binding domain or GAL4 activation domain, respectively. All pB27 and pP6 constructs were cloned by Gibson Assembly using primers P68-P101. Pairs of pB27 and pP6 constructs were co-transformed into the L40 strain of *S. cerevisiae* [MATa his3D200trp1-901 leu2-3112 ade2 LYS2::(4lexAop-HIS3) URA3::(8lexAop-lacZ) GAL4]. Strains were grown overnight in permissive (-Leu/-Trp) medium, normalized to OD<sub>600</sub> = 2, then spotted in six serial dilutions onto permissive (-Leu/-Trp) and restrictive (-Leu/-Trp/-His) media. Growth was assessed after 3–5 days.

## Supporting information

**S1 Fig. Conservation and secondary structure predictions for TGGT1\_238895.** A) ToxoDB reports TGGT1\_238895 as a 1,654 amino acid protein, with the first two residues being methionine. Alignment of TGGT1\_238895 with its *N. caninum* homolog NCLIV\_015750 show that the first methionine (lowercase, bold) in TGGT1\_238895 is not conserved. The second methionine (uppercase, bold) and much of the N-terminus is highly conserved. The second methionine is also a more favorable start codon based on the *T. gondii* consensus translation initiation sequence (A at position -3, G at position +4) [77]. We therefore determined that the protein is likely to start at the second methionine, resulting in TGGT1\_238895 encoding a 1,653 amino acid protein. Residues are numbered accordingly in this study. B) The amino acid sequence of IMC43 (TGGT1\_238895) was aligned to its *N. caninum* ortholog NCLIV\_015750 using ClustalO 1.2.4. Alpha-helices predicted by PSIPRED are shown above their corresponding sequences. Regions chosen for the deletion series are highlighted.  
(TIF)

**S2 Fig. IFA showing successful targeting of the IMC43 locus using CRISPR/Cas9.** A) Diagram showing the strategy used to genetically disrupt IMC43 in an IMC43<sup>3xHA</sup> parental line. B) IFA showing that FLAG-positive/HA-negative parasites with severe morphological defects were observed 30 hours after transfection, indicating successful ablation of the target gene. The  $\Delta imc43$  parasites were rapidly lost from the population and could not be recovered. Arrows point to daughter buds lacking HA staining. Magenta = anti-HA, Green = anti-FLAG detecting Cas9<sup>3xFLAG</sup>, Blue = anti-IMC6. Scale bar = 2  $\mu$ m.  
(TIF)

**S3 Fig. Western blots showing depletion and complementation of IMC43<sup>AID</sup>.** A) Western blot showing efficient depletion of IMC43<sup>AID</sup> after four hours of IAA treatment. Parasites were grown intracellularly for 24 hours prior to adding IAA. Catalase is used as a loading control. B) Western blot of IMC43<sup>AID</sup> + IMC43<sup>WT</sup> parasites after four hours of IAA treatment. IMC43<sup>WT</sup> expresses at equal levels +/- IAA. Catalase is used as a loading control. C) Western blots comparing expression levels of IMC43<sup>WT</sup> with the IMC43 deletion constructs shown in Fig 4A. Catalase was used as a loading control. D) Western blots comparing expression levels of IMC43<sup>WT</sup> with IMC43 <sup>$\Delta$ 1441-1561</sup> and IMC43 <sup>$\Delta$ 1562-1653</sup>. Catalase was used as a loading control.  
(TIF)

**S4 Fig. Most IMC43 deletion constructs localize normally to the daughter IMC.** IFAs showing that eight of the IMC43 deletion constructs colocalize with IMC43<sup>AID</sup>. Magenta = anti-OLLAS detecting IMC43 deletion constructs, Green = anti-HA detecting IMC43<sup>AID</sup>. Scale bars = 2  $\mu$ m.  
(TIF)

**S5 Fig. Most IMC43 deletion constructs rescue the morphological and replication defects observed upon depletion of IMC43.** IFAs showing that eight of the IMC43 deletion constructs fully rescue the morphological and replication defects caused by depletion of IMC43. Magenta = anti-OLLAS detecting IMC43 deletion constructs, Green = anti-IMC6. Scale bars = 2  $\mu$ m.

(TIF)

**S6 Fig. IMC44 is dispensable for the *T. gondii* lytic cycle and does not impact IMC43 localization.** A) The endogenous locus for IMC44 was disrupted in the IMC44<sup>3xMyc</sup> parent strain. IFA of  $\Delta imc44$  parasites confirms loss of IMC44<sup>3xMyc</sup> signal. Magenta = anti-Myc, Green = anti-IMC6. B) PCR verification for genomic DNA of WT and  $\Delta imc44$  parasites. Diagram indicates the binding location of primers used to amplify the IMC44 coding sequencing (blue arrows) and the site of recombination for the knockout (red arrows). C) Plaque assays of WT and  $\Delta imc44$  parasites. D) Quantification of plaque size for plaque assays shown in panel C. Statistical significance was determined using a two-tailed t test (ns = not significant). E) IFA showing normal localization of IMC43 in  $\Delta imc44$  parasites. Magenta = anti-Ty detecting IMC43<sup>2xStrep3xTy</sup>, Green = anti-IMC6. Scale bars = 2  $\mu$ m.

(TIF)

**S7 Fig. Most IMC43 deletion constructs rescue the mislocalization of IMC44 caused by depletion of IMC43.** IFAs showing the localization of IMC44 in nine of the IMC43 deletion lines. All nine shown in this figure rescue the mislocalization of IMC44. Magenta = anti-Myc detecting IMC44<sup>3xMyc</sup>, Green = anti-IMC6. Scale bars = 2  $\mu$ m.

(TIF)

**S8 Fig. Depletion of IMC32 has no effect on IMC43 localization.** A) An mAID-3xTy degen tag was fused to the C-terminus of IMC32 in a TIR1-expressing strain to facilitate proteasomal degradation upon treatment with IAA. B) IFA of IMC32<sup>AID</sup> parasites after 24 hours of growth +/- IAA. Depletion of IMC32 results in morphological and replication defects as previously described [27]. Magenta = anti-Ty detecting IMC32<sup>AID</sup>, Green = anti-IMC6. C) IFA showing the localization of IMC43 in IMC32<sup>AID</sup> parasites after 24 hours of growth +/- IAA. IMC43 is unaffected by depletion of IMC32. Magenta = anti-HA detecting IMC43<sup>3xHA</sup>, Green = anti-IMC6. Scale bars = 2  $\mu$ m.

(TIF)

**S9 Fig. Most IMC43 deletion constructs rescue the mislocalization of IMC32 caused by depletion of IMC43.** IFAs showing the localization of IMC32 in nine of the IMC43 deletion lines. All nine shown in this figure rescue the mislocalization of IMC32. Magenta = anti-V5 detecting IMC32<sup>3xV5</sup>, Green = anti-IMC6. Scale bars = 2  $\mu$ m.

(TIF)

**S1 Table. Full IMC43<sup>TurboID</sup> mass spectrometry results.** Full list of genes identified by mass spectrometry in the IMC43<sup>TurboID</sup> experiment. Spectral counts are shown for each gene. “Enrichment Diff” refers to the difference between the average spectral count in IMC43<sup>TurboID</sup> and control parasites. “Enrichment Fold” refers to the average spectral count for IMC43<sup>TurboID</sup> samples divided by the average spectral count for control samples.

(XLSX)

**S2 Table. Full IMC43 Y2H screen results.** Full list of genes identified by the Hybrigenics Y2H screen. All clones identified for a specific gene are grouped. Clones that were found to be out-of-frame are greyed out. Global PBS indicates the confidence score assigned to each clone

[40,41].  
(XLSX)

**S3 Table. Oligonucleotides used in this study.**  
(XLSX)

## Acknowledgments

We thank Dominique Soldati-Favre for the catalase antibody, Gary Ward for the IMC1 antibody, and Michael Reese for the pP6 and pB27 plasmids, L40 strain of yeast, and protocols for pairwise Y2H assays. We thank members of the Bradley lab for helpful reading of the manuscript.

## Author Contributions

**Conceptualization:** Rebecca R. Pasquarelli, Peter J. Bradley.

**Data curation:** Jihui Sha, James A. Wohlschlegel.

**Formal analysis:** Rebecca R. Pasquarelli.

**Funding acquisition:** James A. Wohlschlegel, Peter J. Bradley.

**Investigation:** Rebecca R. Pasquarelli, Peter S. Back, Jihui Sha.

**Project administration:** James A. Wohlschlegel, Peter J. Bradley.

**Resources:** James A. Wohlschlegel, Peter J. Bradley.

**Supervision:** James A. Wohlschlegel, Peter J. Bradley.

**Validation:** Rebecca R. Pasquarelli.

**Visualization:** Rebecca R. Pasquarelli.

**Writing – original draft:** Rebecca R. Pasquarelli, Jihui Sha, Peter J. Bradley.

**Writing – review & editing:** Rebecca R. Pasquarelli, Peter J. Bradley.

## References

1. Hill DE, Chirukandoth S, Dubey JP. Biology and epidemiology of *Toxoplasma gondii* in man and animals. *Anim Health Res Rev*. 2005 Jun; 6(1):41–61. <https://doi.org/10.1079/ahr2005100> PMID: 16164008
2. Mackintosh CL, Beeson JG, Marsh K. Clinical features and pathogenesis of severe malaria. *Trends Parasitol*. 2004 Dec; 20(12):597–603. <https://doi.org/10.1016/j.pt.2004.09.006> PMID: 15522670
3. Sow SO, Muhsen K, Nasrin D, Blackwelder WC, Wu Y, Farag TH, et al. The Burden of Cryptosporidium Diarrheal Disease among Children < 24 Months of Age in Moderate/High Mortality Regions of Sub-Saharan Africa and South Asia, Utilizing Data from the Global Enteric Multicenter Study (GEMS). *PLoS Negl Trop Dis*. 2016 May; 10(5):e0004729.
4. Sharman PA, Smith NC, Wallach MG, Katrib M. Chasing the golden egg: vaccination against poultry coccidiosis. *Parasite Immunol*. 2010 Aug; 32(8):590–8. <https://doi.org/10.1111/j.1365-3024.2010.01209.x> PMID: 20626814
5. Kivaria FM. Estimated direct economic costs associated with tick-borne diseases on cattle in Tanzania. *Trop Anim Health Prod*. 2006 May; 38(4):291–9. <https://doi.org/10.1007/s11250-006-4181-2> PMID: 17137131
6. Dubey JP. Review of *Neospora caninum* and neosporosis in animals. *Korean J Parasitol*. 2003 Mar; 41(1):1–16. <https://doi.org/10.3347/kjp.2003.41.1.1> PMID: 12666725
7. Pappas G, Roussos N, Falagas ME. Toxoplasmosis snapshots: global status of *Toxoplasma gondii* seroprevalence and implications for pregnancy and congenital toxoplasmosis. *Int J Parasitol*. 2009 Oct; 39(12):1385–94. <https://doi.org/10.1016/j.ijpara.2009.04.003> PMID: 19433092

8. Tenter AM, Heckerth AR, Weiss LM. *Toxoplasma gondii*: from animals to humans. *Int J Parasitol*. 2000 Nov; 30(12–13):1217–58. [https://doi.org/10.1016/s0020-7519\(00\)00124-7](https://doi.org/10.1016/s0020-7519(00)00124-7) PMID: 11113252
9. Luft BJ, Remington JS. Toxoplasmic Encephalitis in AIDS. *Clin Infect Dis*. 1992 Aug 1; 15(2):211–22. <https://doi.org/10.1093/clinids/15.2.211> PMID: 1520757
10. Martin S. Congenital Toxoplasmosis. *Neonatal Netw*. 2001 Jun; 20(4):23–30. <https://doi.org/10.1891/0730-0832.20.4.23> PMID: 12143899
11. Blader IJ, Coleman BI, Chen CT, Gubbels MJ. Lytic Cycle of *Toxoplasma gondii*: 15 Years Later. *Annu Rev Microbiol*. 2015; 69:463–85. <https://doi.org/10.1146/annurev-micro-091014-104100> PMID: 26332089
12. D'Haese J, Mehlhorn H, Peters W. Comparative electron microscope study of pellicular structures in coccidia (*Sarcocystis*, *Besnoitia* and *Eimeria*). *Int J Parasitol*. 1977 Dec; 7(6):505–18. [https://doi.org/10.1016/0020-7519\(77\)90014-5](https://doi.org/10.1016/0020-7519(77)90014-5) PMID: 413801
13. Mann T, Beckers C. Characterization of the subpellicular network, a filamentous membrane skeletal component in the parasite *Toxoplasma gondii*. *Mol Biochem Parasitol*. 2001 Jul; 115(2):257–68. [https://doi.org/10.1016/s0166-6851\(01\)00289-4](https://doi.org/10.1016/s0166-6851(01)00289-4) PMID: 11420112
14. Anderson-White BR, Ivey FD, Cheng K, Szatanek T, Lorestani A, Beckers CJ, et al. A family of intermediate filament-like proteins is sequentially assembled into the cytoskeleton of *Toxoplasma gondii*: IMC proteins in *Toxoplasma* cell division. *Cell Microbiol*. 2011 Jan; 13(1):18–31.
15. Chen AL, Kim EW, Toh JY, Vashisht AA, Rashoff AQ, Van C, et al. Novel components of the *Toxoplasma* inner membrane complex revealed by BioID. *mBio*. 2015; 6(1):e02357–14. <https://doi.org/10.1128/mBio.02357-14> PMID: 25691595
16. Chen AL, Moon AS, Bell HN, Huang AS, Vashisht AA, Toh JY, et al. Novel insights into the composition and function of the *Toxoplasma* IMC sutures. *Cell Microbiol*. 2016; 19(4):e12678. <https://doi.org/10.1111/cmi.12678> PMID: 27696623
17. Gubbels MJ, Keroack CD, Dangoudoubyam S, Worliczek HL, Paul AS, Bauwens C, et al. Fussing About Fission: Defining Variety Among Mainstream and Exotic Apicomplexan Cell Division Modes. *Front Cell Infect Microbiol*. 2020 Jun 5; 10:269. <https://doi.org/10.3389/fcimb.2020.00269> PMID: 32582569
18. Francia ME, Striepen B. Cell division in apicomplexan parasites. *Nat Rev Microbiol*. 2014 Feb; 12(2):125–36. <https://doi.org/10.1038/nrmicro3184> PMID: 24384598
19. Chen CT, Gubbels MJ. The *Toxoplasma gondii* centrosome is the platform for internal daughter budding as revealed by a Nek1 kinase mutant. *J Cell Sci*. 2013 Aug 1; 126(15):3344–55. <https://doi.org/10.1242/jcs.123364> PMID: 23729737
20. Anderson-White B, Beck JR, Chen CT, Meissner M, Bradley PJ, Gubbels MJ. Cytoskeleton assembly in *Toxoplasma gondii* cell division. *Int Rev Cell Mol Biol*. 2012; 298:1–31. <https://doi.org/10.1016/B978-0-12-394309-5.00001-8> PMID: 22878103
21. Suvorova ES, Francia M, Striepen B, White MW. A Novel Bipartite Centrosome Coordinates the Apicomplexan Cell Cycle. Pellman D, editor. *PLOS Biol*. 2015 Mar 3; 13(3):e1002093.
22. Morrisette NS, Sibley LD. Disruption of microtubules uncouples budding and nuclear division in *Toxoplasma gondii*. *J Cell Sci*. 2002 Mar 1; 115(Pt 5):1017–25. <https://doi.org/10.1242/jcs.115.5.1017> PMID: 11870220
23. Shaw MK, Compton HL, Roos DS, Tilney LG. Microtubules, but not actin filaments, drive daughter cell budding and cell division in *Toxoplasma gondii*. *J Cell Sci*. 2000 Apr 1; 113(7):1241–54.
24. Behnke MS, Wootton JC, Lehmann MM, Radke JB, Lucas O, Nawas J, et al. Coordinated progression through two subtranscriptomes underlies the tachyzoite cycle of *Toxoplasma gondii*. *PLoS One*. 2010 Aug 26; 5(8):e12354. <https://doi.org/10.1371/journal.pone.0012354> PMID: 20865045
25. Ouologuem DT, Roos DS. Dynamics of the *Toxoplasma gondii* inner membrane complex. *J Cell Sci*. 2014 Jan 1; jcs.147736. <https://doi.org/10.1242/jcs.147736> PMID: 24928899
26. Baptista CG, Lis A, Deng B, Gas-Pascual E, Dittmar A, Sigurdson W, et al. *Toxoplasma* F-box protein 1 is required for daughter cell scaffold function during parasite replication. Gubbels MJ, editor. *PLOS Pathog*. 2019 Jul 26; 15(7):e1007946. <https://doi.org/10.1371/journal.ppat.1007946> PMID: 31348812
27. Torres JA, Pasquarelli RR, Back PS, Moon AS, Bradley PJ. Identification and Molecular Dissection of IMC32, a Conserved *Toxoplasma* Inner Membrane Complex Protein That Is Essential for Parasite Replication. *mBio*. 2021 Feb 23; 12(1):e03622–20. <https://doi.org/10.1128/mBio.03622-20> PMID: 33593973
28. Engelberg K, Bechtel T, Michaud C, Weerapana E, Gubbels MJ. Proteomic characterization of the *Toxoplasma gondii* cytokinesis machinery portrays an expanded hierarchy of its assembly and function. *Nat Commun*. 2022 Aug 8; 13(1):4644. <https://doi.org/10.1038/s41467-022-32151-0> PMID: 35941170

29. Back PS, Moon AS, Pasquarelli RR, Bell HN, Torres JA, Chen AL, et al. IMC29 Plays an Important Role in Toxoplasma Endodyogeny and Reveals New Components of the Daughter-Enriched IMC Proteome. *mBio*. 2023 Jan 9;e0304222. <https://doi.org/10.1128/mbio.03042-22> PMID: 36622147
30. Back PS, O'Shaughnessy WJ, Moon AS, Dewangan PS, Hu X, Sha J, et al. Ancient MAPK ERK7 is regulated by an unusual inhibitory scaffold required for Toxoplasma apical complex biogenesis. *Proc Natl Acad Sci*. 2020 Jun 2; 117(22):12164–73. <https://doi.org/10.1073/pnas.1921245117> PMID: 32409604
31. Tosetti N, Dos Santos Pacheco N, Bertiaux E, Maco B, Bournonville L, Hamel V, et al. Essential function of the alveolin network in the subpellicular microtubules and conoid assembly in Toxoplasma gondii. *eLife*. 2020 May 7; 9:e56635. <https://doi.org/10.7554/eLife.56635> PMID: 32379047
32. Beck JR, Rodriguez-Fernandez IA, Cruz de Leon J, Huynh MH, Carruthers VB, Morrissette NS, et al. A Novel Family of Toxoplasma IMC Proteins Displays a Hierarchical Organization and Functions in Coordinating Parasite Division. Soldati-Favre D, editor. *PLoS Pathog*. 2010 Sep 9; 6(9):e1001094. <https://doi.org/10.1371/journal.ppat.1001094> PMID: 20844581
33. Ludwiczak J, Winski A, Szczepaniak K, Alva V, Dunin-Horkawicz S. DeepCoil—a fast and accurate prediction of coiled-coil domains in protein sequences. *Bioinforma Oxf Engl*. 2019 Aug 15; 35(16):2790–5. <https://doi.org/10.1093/bioinformatics/bty1062> PMID: 30601942
34. Lupas A, Van Dyke M, Stock J. Predicting coiled coils from protein sequences. *Science*. 1991 May 24; 252(5009):1162–4. <https://doi.org/10.1126/science.252.5009.1162> PMID: 2031185
35. Sidik SM, Huet D, Ganesan SM, Huynh MH, Wang T, Nasamu AS, et al. A Genome-wide CRISPR Screen in Toxoplasma Identifies Essential Apicomplexan Genes. *Cell*. 2016; 166(6):1423–1435.e12. <https://doi.org/10.1016/j.cell.2016.08.019> PMID: 27594426
36. Nishimura K, Fukagawa T, Takisawa H, Kakimoto T, Kanemaki M. An auxin-based degron system for the rapid depletion of proteins in nonplant cells. *Nat Methods*. 2009 Dec; 6(12):917–22. <https://doi.org/10.1038/nmeth.1401> PMID: 19915560
37. Brown KM, Long S, Sibley LD. Plasma Membrane Association by N-Acylation Governs PKG Function in Toxoplasma gondii. *mBio*. 2017; 8(3):e00375–17. <https://doi.org/10.1128/mBio.00375-17> PMID: 28465425
38. Buchan DWA, Jones DT. The PSIPRED Protein Analysis Workbench: 20 years on. *Nucleic Acids Res*. 2019 Jul 2; 47(W1):W402–7. <https://doi.org/10.1093/nar/gkz297> PMID: 31251384
39. Branon TC, Bosch JA, Sanchez AD, Udeshi ND, Svinkina T, Carr SA, et al. Efficient proximity labeling in living cells and organisms with TurboID. *Nat Biotechnol*. 2018; 36(9):880–7. <https://doi.org/10.1038/nbt.4201> PMID: 30125270
40. Rain JC, Selig L, De Reuse H, Battaglia V, Reverdy C, Simon S, et al. The protein-protein interaction map of Helicobacter pylori. *Nature*. 2001 Jan 11; 409(6817):211–5. <https://doi.org/10.1038/35051615> PMID: 11196647
41. Formstecher E, Aresta S, Collura V, Hamburger A, Meil A, Trehin A, et al. Protein interaction mapping: a Drosophila case study. *Genome Res*. 2005 Mar; 15(3):376–84. <https://doi.org/10.1101/gr.2659105> PMID: 15710747
42. Barylyuk K, Koreny L, Ke H, Butterworth S, Crook OM, Lassadi I, et al. A Comprehensive Subcellular Atlas of the Toxoplasma Proteome via hyperLOPIT Provides Spatial Context for Protein Functions. *Cell Host Microbe*. 2020 Nov; 28(5):752–766.e9. <https://doi.org/10.1016/j.chom.2020.09.011> PMID: 33053376
43. He B, Wang K, Liu Y, Xue B, Uversky VN, Dunker AK. Predicting intrinsic disorder in proteins: an overview. *Cell Res*. 2009 Aug; 19(8):929–49. <https://doi.org/10.1038/cr.2009.87> PMID: 19597536
44. Jumper J, Evans R, Pritzel A, Green T, Figurnov M, Ronneberger O, et al. Highly accurate protein structure prediction with AlphaFold. *Nature*. 2021 Aug; 596(7873):583–9. <https://doi.org/10.1038/s41586-021-03819-2> PMID: 34265844
45. Varadi M, Anyango S, Deshpande M, Nair S, Natassia C, Yordanova G, et al. AlphaFold Protein Structure Database: massively expanding the structural coverage of protein-sequence space with high-accuracy models. *Nucleic Acids Res*. 2022 Jan 7; 50(D1):D439–44. <https://doi.org/10.1093/nar/gkab1061> PMID: 34791371
46. Kamtekar S, Hecht MH. Protein Motifs. 7. The four-helix bundle: what determines a fold? *FASEB J Off Publ Fed Am Soc Exp Biol*. 1995 Aug; 9(11):1013–22. <https://doi.org/10.1096/fasebj.9.11.7649401> PMID: 7649401
47. Lupas AN, Bassler J. Coiled Coils—A Model System for the 21st Century. *Trends Biochem Sci*. 2017 Feb; 42(2):130–40. <https://doi.org/10.1016/j.tibs.2016.10.007> PMID: 27884598
48. Dos Santos Pacheco N, Tosetti N, Krishnan A, Haase R, Maco B, Suarez C, et al. Revisiting the Role of Toxoplasma gondii ERK7 in the Maintenance and Stability of the Apical Complex. *mBio*. 2021 Oct 26; 12(5):e0205721. <https://doi.org/10.1128/mBio.02057-21> PMID: 34607461

49. Gilk SD, Raviv Y, Hu K, Murray JM, Beckers CJM, Ward GE. Identification of PhIL1, a novel cytoskeletal protein of the *Toxoplasma gondii* pellicle, through photosensitized labeling with 5-[125I]iodonaphthalene-1-azide. *Eukaryot Cell*. 2006 Oct; 5(10):1622–34. <https://doi.org/10.1128/EC.00114-06> PMID: 17030994
50. Oliveira Souza RO, Jacobs KN, Back PS, Bradley PJ, Arrizabalaga G. IMC10 and LMF1 mediate mitochondrial morphology through mitochondrion-pellicle contact sites in *Toxoplasma gondii*. *J Cell Sci*. 2022 Nov 15; 135(22):jcs260083. <https://doi.org/10.1242/jcs.260083> PMID: 36314270
51. Talevich E, Mirza A, Kannan N. Structural and evolutionary divergence of eukaryotic protein kinases in Apicomplexa. *BMC Evol Biol*. 2011; 11(1):321. <https://doi.org/10.1186/1471-2148-11-321> PMID: 22047078
52. Yang C, Arrizabalaga G. The serine/threonine phosphatases of apicomplexan parasites. *Mol Microbiol*. 2017 Oct; 106(1):1–21. <https://doi.org/10.1111/mmi.13715> PMID: 28556455
53. Guttery DS, Poulin B, Ferguson DJP, Szöör B, Wickstead B, Carroll PL, et al. A unique protein phosphatase with kelch-like domains (PPKL) in *Plasmodium* modulates ookinete differentiation, motility and invasion. *PLoS Pathog*. 2012 Sep; 8(9):e1002948. <https://doi.org/10.1371/journal.ppat.1002948> PMID: 23028336
54. Yang C, Doud EH, Sampson E, Arrizabalaga G. The protein phosphatase PPKL is a key regulator of daughter parasite development in *Toxoplasma gondii*. *BioRxiv* [Preprint]; 2023 Jun [cited 2023 Jun 21]. Available from: <http://biorxiv.org/lookup/doi/10.1101/2023.06.13.544803>
55. Berry L, Chen CT, Reininger L, Carvalho TG, El Hajj H, Morlon-Guyot J, et al. The conserved apicomplexan Aurora kinase TgArk3 is involved in endodyogeny, duplication rate and parasite virulence. *Cell Microbiol*. 2016 Aug; 18(8):1106–20. <https://doi.org/10.1111/cmi.12571> PMID: 26833682
56. Morlon-Guyot J, Berry L, Chen CT, Gubbels MJ, Lebrun M, Daher W. The *Toxoplasma gondii* calcium-dependent protein kinase 7 is involved in early steps of parasite division and is crucial for parasite survival. *Cell Microbiol*. 2014 Jan; 16(1):95–114. <https://doi.org/10.1111/cmi.12186> PMID: 24011186
57. Donald RG, Roos DS. Stable molecular transformation of *Toxoplasma gondii*: a selectable dihydrofolate reductase-thymidylate synthase marker based on drug-resistance mutations in malaria. *Proc Natl Acad Sci U S A*. 1993 Dec 15; 90(24):11703–7. <https://doi.org/10.1073/pnas.90.24.11703> PMID: 8265612
58. Kim K, Soldati D, Boothroyd JC. Gene replacement in *Toxoplasma gondii* with chloramphenicol acetyltransferase as selectable marker. *Science*. 1993 Nov 5; 262(5135):911–4. <https://doi.org/10.1126/science.8235614> PMID: 8235614
59. Donald RG, Carter D, Ullman B, Roos DS. Insertional tagging, cloning, and expression of the *Toxoplasma gondii* hypoxanthine-xanthine-guanine phosphoribosyltransferase gene: Use as a selectable marker for stable transformation. *J Biol Chem*. 1996 Jun 14; 271(24):14010–9.
60. Donald RG, Roos DS. Insertional mutagenesis and marker rescue in a protozoan parasite: cloning of the uracil phosphoribosyltransferase locus from *Toxoplasma gondii*. *Proc Natl Acad Sci U S A*. 1995 Jun 6; 92(12):5749–53. <https://doi.org/10.1073/pnas.92.12.5749> PMID: 7777580
61. Bastin P, Bagherzadeh Z, Matthews KR, Gull K. A novel epitope tag system to study protein targeting and organelle biogenesis in *Trypanosoma brucei*. *Mol Biochem Parasitol*. 1996 May; 77(2):235–9. [https://doi.org/10.1016/0166-6851\(96\)02598-4](https://doi.org/10.1016/0166-6851(96)02598-4) PMID: 8813669
62. Evan GI, Lewis GK, Ramsay G, Bishop JM. Isolation of monoclonal antibodies specific for human c-myc proto-oncogene product. *Mol Cell Biol*. 1985 Dec; 5(12):3610–6. <https://doi.org/10.1128/mcb.5.12.3610-3616.1985> PMID: 3915782
63. Viswanathan S, Williams ME, Bloss EB, Stasevich TJ, Speer CM, Nern A, et al. High-performance probes for light and electron microscopy. *Nat Methods*. 2015 Jun; 12(6):568–76. <https://doi.org/10.1038/nmeth.3365> PMID: 25915120
64. Choi CP, Moon AS, Back PS, Jami-Alahmadi Y, Vashisht AA, Wohlschlegel JA, et al. A photoactivatable crosslinking system reveals protein interactions in the *Toxoplasma gondii* inner membrane complex. *PLOS Biol*. 2019 Oct 4; 17(10):e3000475. <https://doi.org/10.1371/journal.pbio.3000475> PMID: 31584943
65. Wichroski MJ, Melton JA, Donahue CG, Tweten RK, Ward GE. Clostridium septicum alpha-toxin is active against the parasitic protozoan *Toxoplasma gondii* and targets members of the SAG family of glycosylphosphatidylinositol-anchored surface proteins. *Infect Immun*. 2002 Aug; 70(8):4353–61. <https://doi.org/10.1128/IAI.70.8.4353-4361.2002> PMID: 12117945
66. Fung C, Beck JR, Robertson SD, Gubbels MJ, Bradley PJ. *Toxoplasma* ISP4 is a central IMC sub-compartment protein whose localization depends on palmitoylation but not myristoylation. *Mol Biochem Parasitol*. 2012 Aug; 184(2):99–108. <https://doi.org/10.1016/j.molbiopara.2012.05.002> PMID: 22659420

67. Bullen HE, Jia Y, Yamaryo-Botté Y, Bisio H, Zhang O, Jemelin NK, et al. Phosphatidic Acid-Mediated Signaling Regulates Microneme Secretion in *Toxoplasma*. *Cell Host Microbe*. 2016 Mar 9; 19(3):349–60. <https://doi.org/10.1016/j.chom.2016.02.006> PMID: 26962945
68. Sidik SM, Hackett CG, Tran F, Westwood NJ, Lourido S. Efficient Genome Engineering of *Toxoplasma gondii* Using CRISPR/Cas9. Blader IJ, editor. *PLoS ONE*. 2014 Jun 27; 9(6):e100450. <https://doi.org/10.1371/journal.pone.0100450> PMID: 24971596
69. Huynh MH, Carruthers VB. Tagging of endogenous genes in a *Toxoplasma gondii* strain lacking Ku80. *Eukaryot Cell*. 2009 Apr; 8(4):530–9. <https://doi.org/10.1128/EC.00358-08> PMID: 19218426
70. Bradley PJ, Ward C, Cheng SJ, Alexander DL, Collier S, Coombs GH, et al. Proteomic Analysis of Rhoptry Organelles Reveals Many Novel Constituents for Host-Parasite Interactions in *Toxoplasma gondii*. *J Biol Chem*. 2005 Oct; 280(40):34245–58. <https://doi.org/10.1074/jbc.M504158200> PMID: 16002398
71. Bradley PJ, Rayatpisheh S, Wohlschlegel JA, Nadipuram SM. Using BioID for the Identification of Interacting and Proximal Proteins in Subcellular Compartments in *Toxoplasma gondii*. *Methods Mol Biol Clifton NJ*. 2020; 2071:323–46. [https://doi.org/10.1007/978-1-4939-9857-9\\_18](https://doi.org/10.1007/978-1-4939-9857-9_18) PMID: 31758461
72. Xu T, Park SK, Venable JD, Wohlschlegel JA, Diedrich JK, Cociorva D, et al. ProLuCID: An improved SEQUEST-like algorithm with enhanced sensitivity and specificity. *J Proteomics*. 2015 Nov 3; 129:16–24. <https://doi.org/10.1016/j.jprot.2015.07.001> PMID: 26171723
73. Tabb DL, McDonald WH, Yates JR. DTASelect and Contrast: Tools for Assembling and Comparing Protein Identifications from Shotgun Proteomics. *J Proteome Res*. 2002 Feb 1; 1(1):21–6. <https://doi.org/10.1021/pr015504q> PMID: 12643522
74. Cociorva D, L. Tabb D, Yates JR. Validation of Tandem Mass Spectrometry Database Search Results Using DTASelect. *Curr Protoc Bioinforma*. 2006; 16(1):13.4.1–13.4.14.
75. Florens L, Carozza MJ, Swanson SK, Fournier M, Coleman MK, Workman JL, et al. Analyzing chromatin remodeling complexes using shotgun proteomics and normalized spectral abundance factors. *Methods*. 2006 Dec 1; 40(4):303–11. <https://doi.org/10.1016/j.ymeth.2006.07.028> PMID: 17101441
76. Straub KW, Cheng SJ, Sohn CS, Bradley PJ. Novel components of the Apicomplexan moving junction reveal conserved and coccidia-restricted elements. *Cell Microbiol*. 2009 Apr; 11(4):590–603. <https://doi.org/10.1111/j.1462-5822.2008.01276.x> PMID: 19134112
77. Seeber F. Consensus sequence of translational initiation sites from *Toxoplasma gondii* genes. *Parasitol Res*. 1997; 83(3):309–11. <https://doi.org/10.1007/s004360050254> PMID: 9089733

## 2.8 Supplemental Material

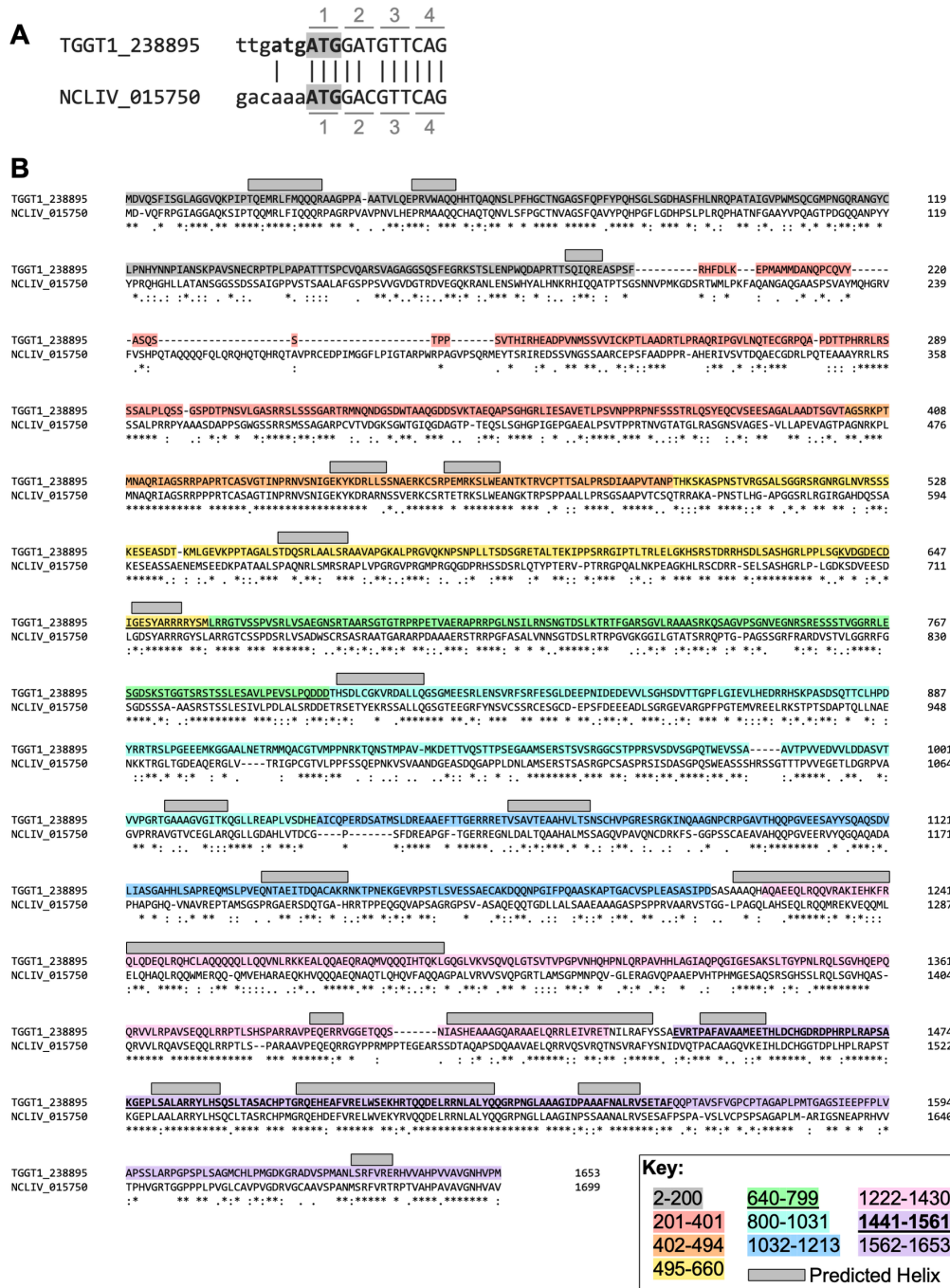


**Figure 2-S1. Conservation and secondary structure predictions for TGGT1\_238895.**

A) ToxoDB reports TGGT1\_238895 as a 1,654 amino acid protein, with the first two residues being methionine. Alignment of TGGT1\_238895 with its *N. caninum* homolog NCLIV\_015750 show that the first methionine (lowercase, bold) in TGGT1\_238895 is not conserved. The

second methionine (uppercase, bold) and much of the N-terminus is highly conserved. The second methionine is also a more favorable start codon based on the *T. gondii* consensus translation initiation sequence (A at position -3, G at position +4) [77]. We therefore determined that the protein is likely to start at the second methionine, resulting in TGGT1\_238895 encoding a 1,653 amino acid protein. Residues are numbered accordingly in this study. B) The amino acid sequence of IMC43 (TGGT1\_238895) was aligned to its *N. caninum* ortholog NCLIV\_015750 using ClustalO 1.2.4. Alpha-helices predicted by PSIPRED are shown above their corresponding sequences. Regions chosen for the deletion series are highlighted.

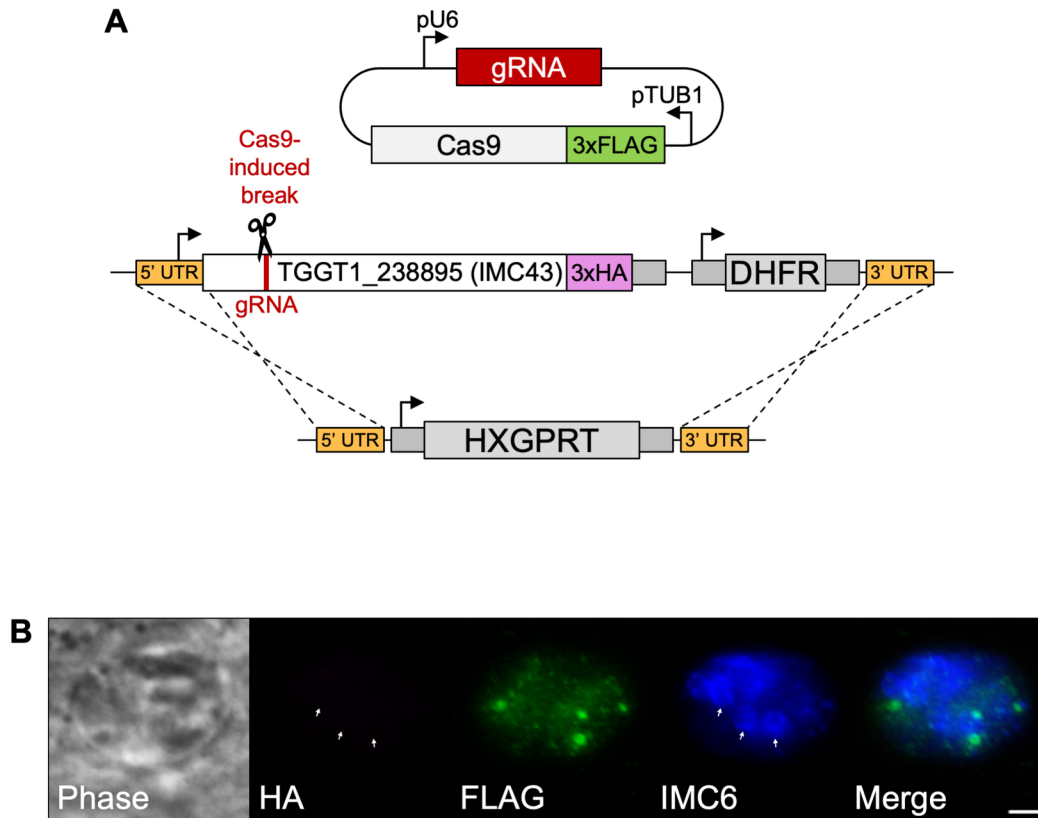


**Figure 2-S2. IFA showing successful targeting of the IMC43 locus using CRISPR/Cas9.** A) Diagram showing the strategy used to genetically disrupt IMC43 in an IMC43<sup>3xHA</sup> parental line. . B) IFA showing that FLAG-positive/HA-negative parasites with severe morphological defects were observed 30 hours after transfection, indicating successful ablation of the target gene. The  $\Delta imc43$  parasites were rapidly lost from the population and could not be recovered. Arrows point to daughter buds lacking HA staining. Magenta = anti-HA, Green = anti-FLAG detecting Cas9<sup>3xFLAG</sup>, Blue = anti-IMC6. Scale bar = 2  $\mu$ m.

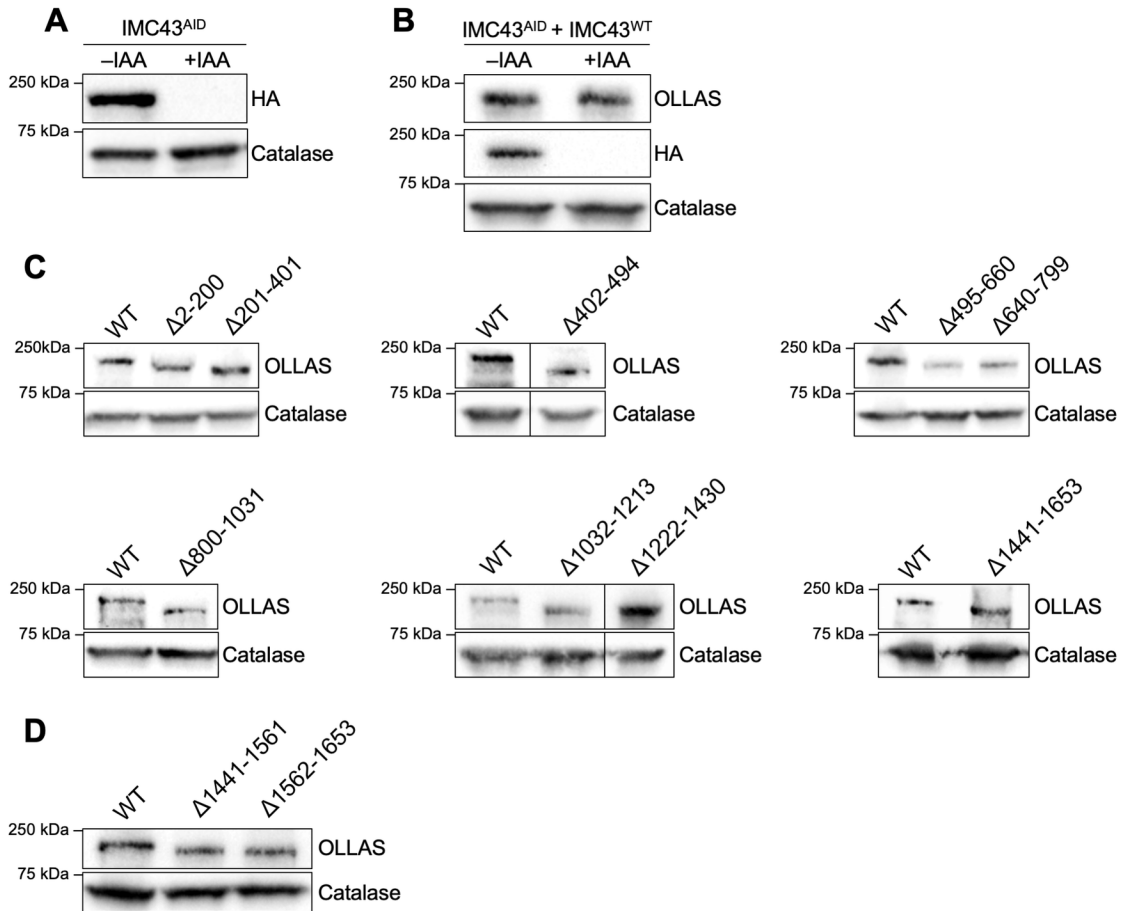


**Figure 2-S3. Western blots showing depletion and complementation of IMC43<sup>AID</sup>.**

A) Western blot showing efficient depletion of IMC43<sup>AID</sup> after four hours of IAA treatment. Parasites were grown intracellularly for 24 hours prior to adding IAA. Catalase is used as a loading control. B) Western blot of IMC43<sup>AID</sup> + IMC43<sup>WT</sup> parasites after four hours of IAA treatment. IMC43<sup>WT</sup> expresses at equal levels -/+ IAA. Catalase is used as a loading control. C) Western blots comparing expression levels of IMC43<sup>WT</sup> with the IMC43 deletion constructs shown in Figure 4A. Catalase was used as a loading control. D) Western blots comparing expression levels of IMC43<sup>WT</sup> with IMC43<sup>Δ1441-1561</sup> and IMC43<sup>Δ1562-1653</sup>. Catalase was used as a loading control.

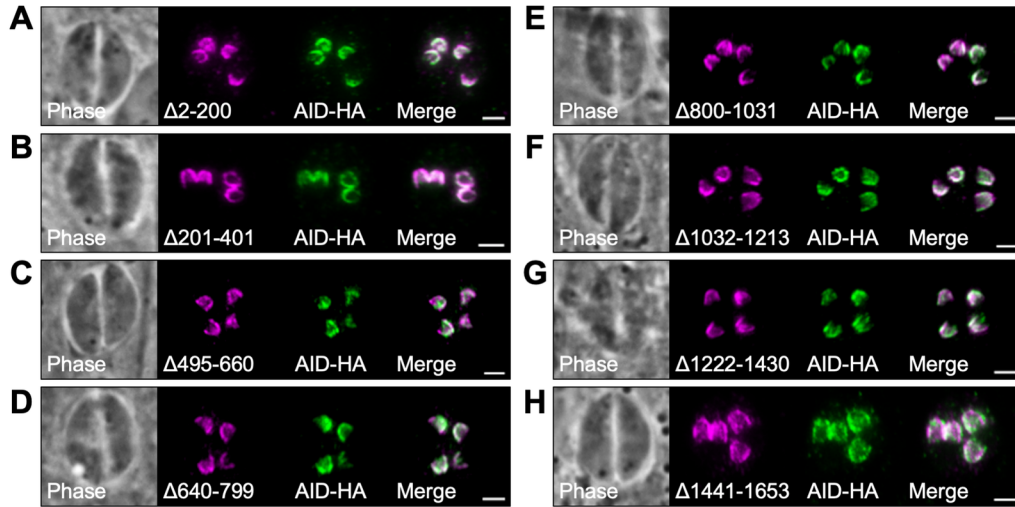


**Figure 2-S4. Most IMC43 deletion constructs localize normally to the daughter IMC.**

IFAs showing that eight of the IMC43 deletion constructs colocalize with IMC43<sup>AID</sup>. Magenta = anti-OLLAS detecting IMC43 deletion constructs, Green = anti-HA detecting IMC43<sup>AID</sup>. Scale bars = 2  $\mu$ m.

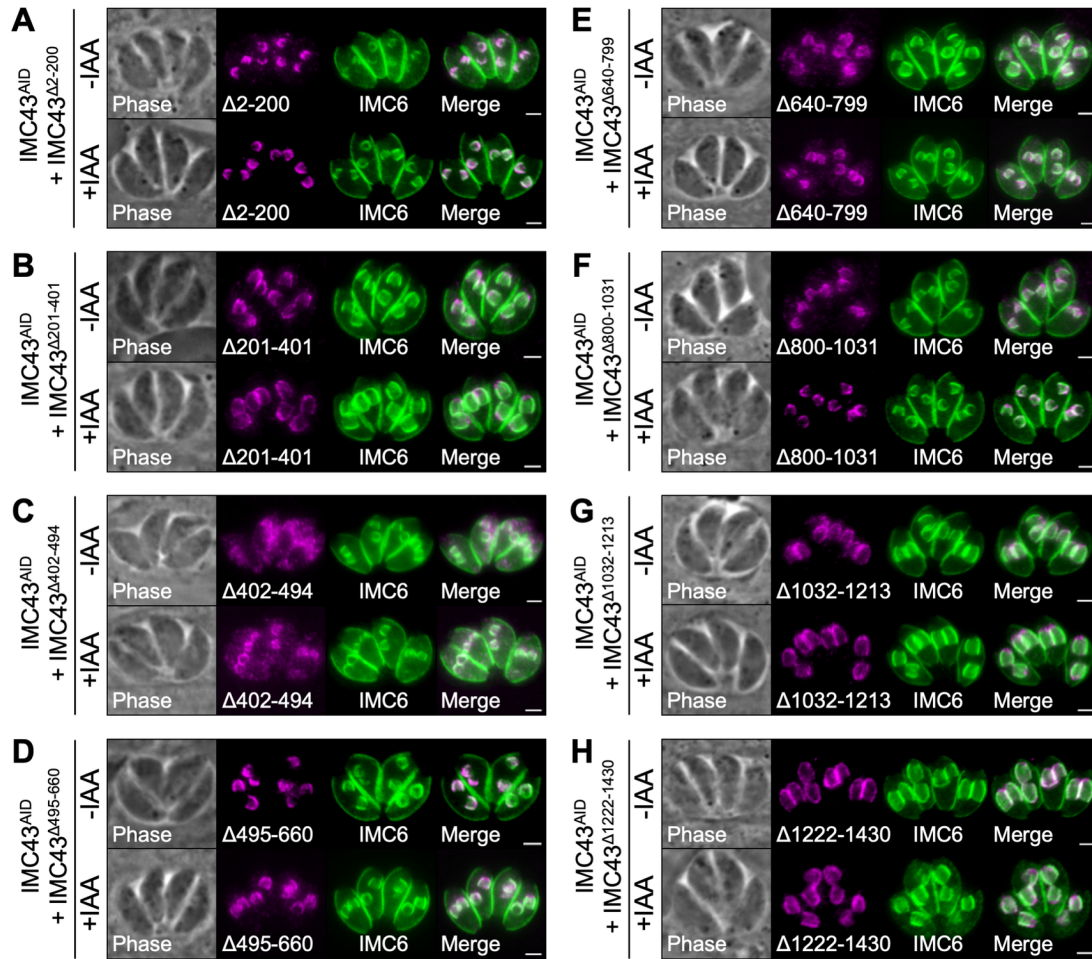


**Figure 2-S5. Most IMC43 deletion constructs rescue the morphological and replication defects observed upon depletion of IMC43.** IFAs showing that eight of the IMC43 deletion constructs fully rescue the morphological and replication defects caused by depletion of IMC43. Magenta = anti-OLLAS detecting IMC43 deletion constructs, Green = anti-IMC6. Scale bars = 2  $\mu\text{m}$ .

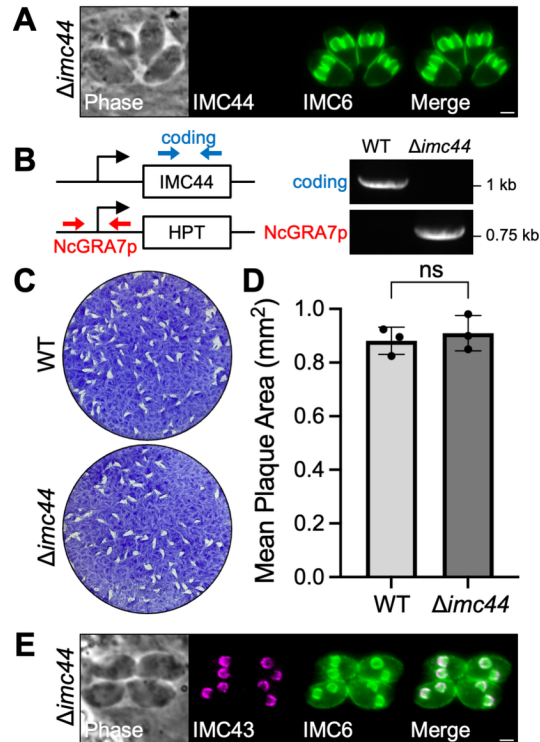


**Figure 2-S6. IMC44 is dispensable for the *T. gondii* lytic cycle and does not impact IMC43 localization.** A) The endogenous locus for IMC44 was disrupted in the IMC44<sup>3xMyc</sup> parent strain. IFA of  $\Delta imc44$  parasites confirms loss of IMC44<sup>3xMyc</sup> signal. Magenta = anti-Myc, Green = anti-IMC6. B) PCR verification for genomic DNA of WT and  $\Delta imc44$  parasites. Diagram indicates the binding location of primers used to amplify the IMC44 coding sequencing (blue arrows) and the site of recombination for the knockout (red arrows). C) Plaque assays of WT and  $\Delta imc44$  parasites. D) Quantification of plaque size for plaque assays shown in panel D. Statistical significance was determined using a two-tailed t test (ns = not significant). E) IFA showing normal localization of IMC43 in  $\Delta imc44$  parasites. Magenta = anti-Ty detecting IMC43<sup>2xStrep3xTy</sup>, Green = anti-IMC6. Scale bars = 2  $\mu$ m.

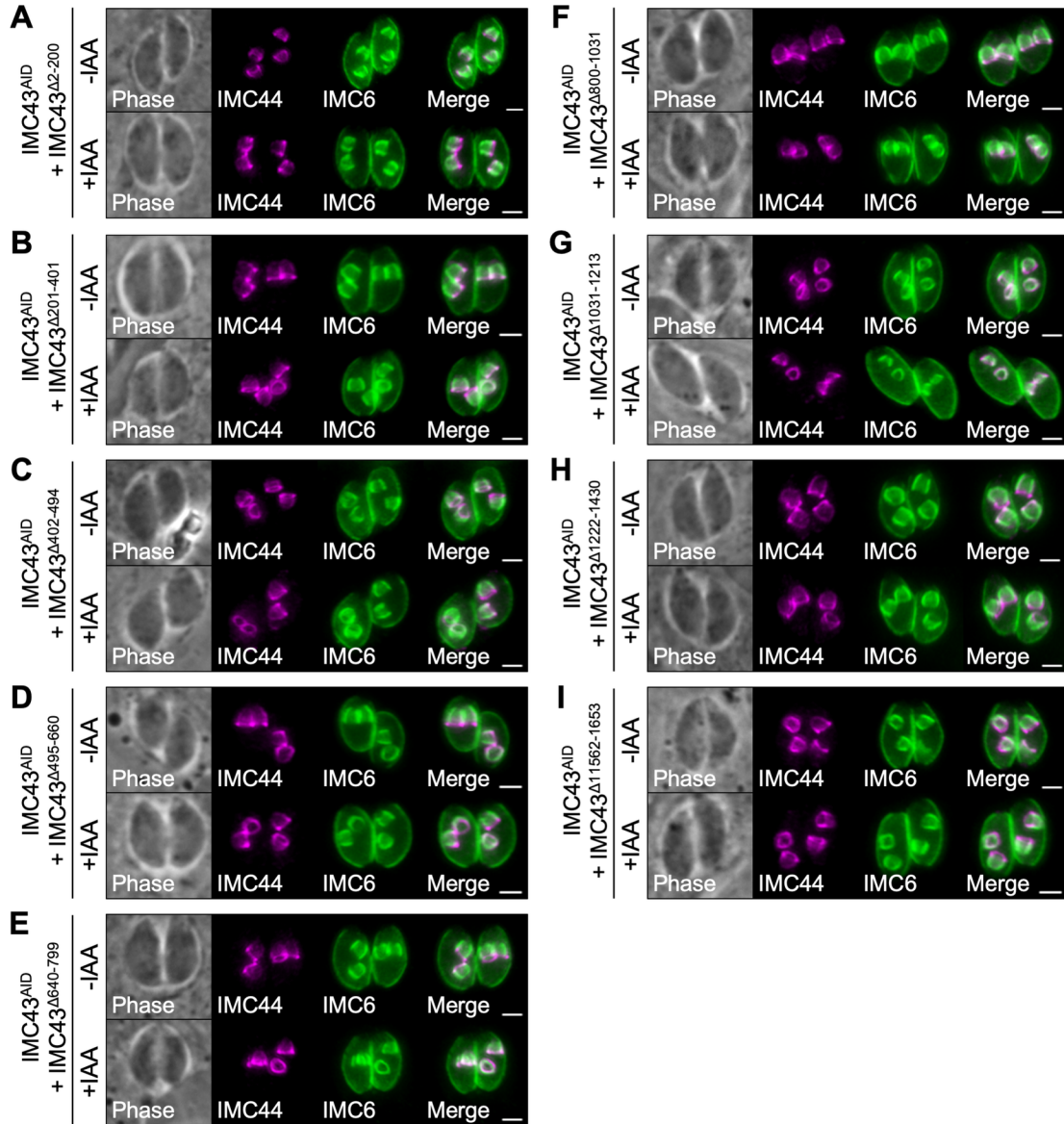


**Figure 2-S7. Most IMC43 deletion constructs rescue the mislocalization of IMC44 caused by depletion of IMC43.** IFAs showing the localization of IMC44 in nine of the IMC43 deletion lines. All nine shown in this figure rescue the mislocalization of IMC44. Magenta = anti-Myc detecting IMC44<sup>3xMyc</sup>, Green = anti-IMC6. Scale bars = 2  $\mu$ m.

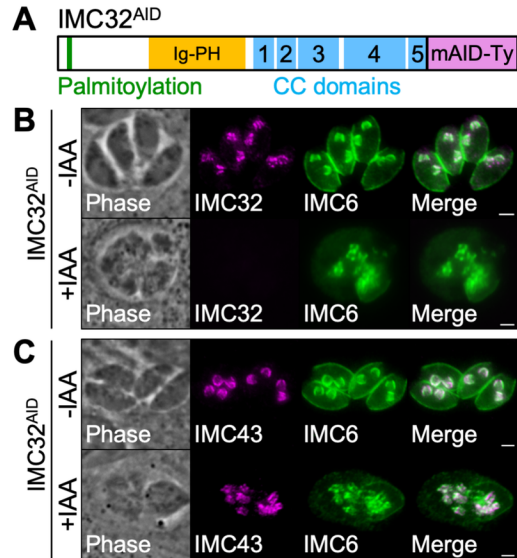


**Figure 2-S8. Depletion of IMC32 has no effect on IMC43 localization.** A) An mAID-3xTy degon tag was fused to the C-terminus of IMC32 in a TIR1-expressing strain to facilitate proteasomal degradation upon treatment with IAA. B) IFA of IMC32<sup>AID</sup> parasites after 24 hours of growth +/- IAA. Depletion of IMC32 results in morphological and replication defects as previously described [27]. Magenta = anti-Ty detecting IMC32<sup>AID</sup>, Green = anti-IMC6. C) IFA showing the localization of IMC43 in IMC32<sup>AID</sup> parasites after 24 hours of growth +/- IAA. IMC43 is unaffected by depletion of IMC32. Magenta = anti-HA detecting IMC43<sup>3xHA</sup>, Green = anti-IMC6. Scale bars = 2  $\mu$ m.

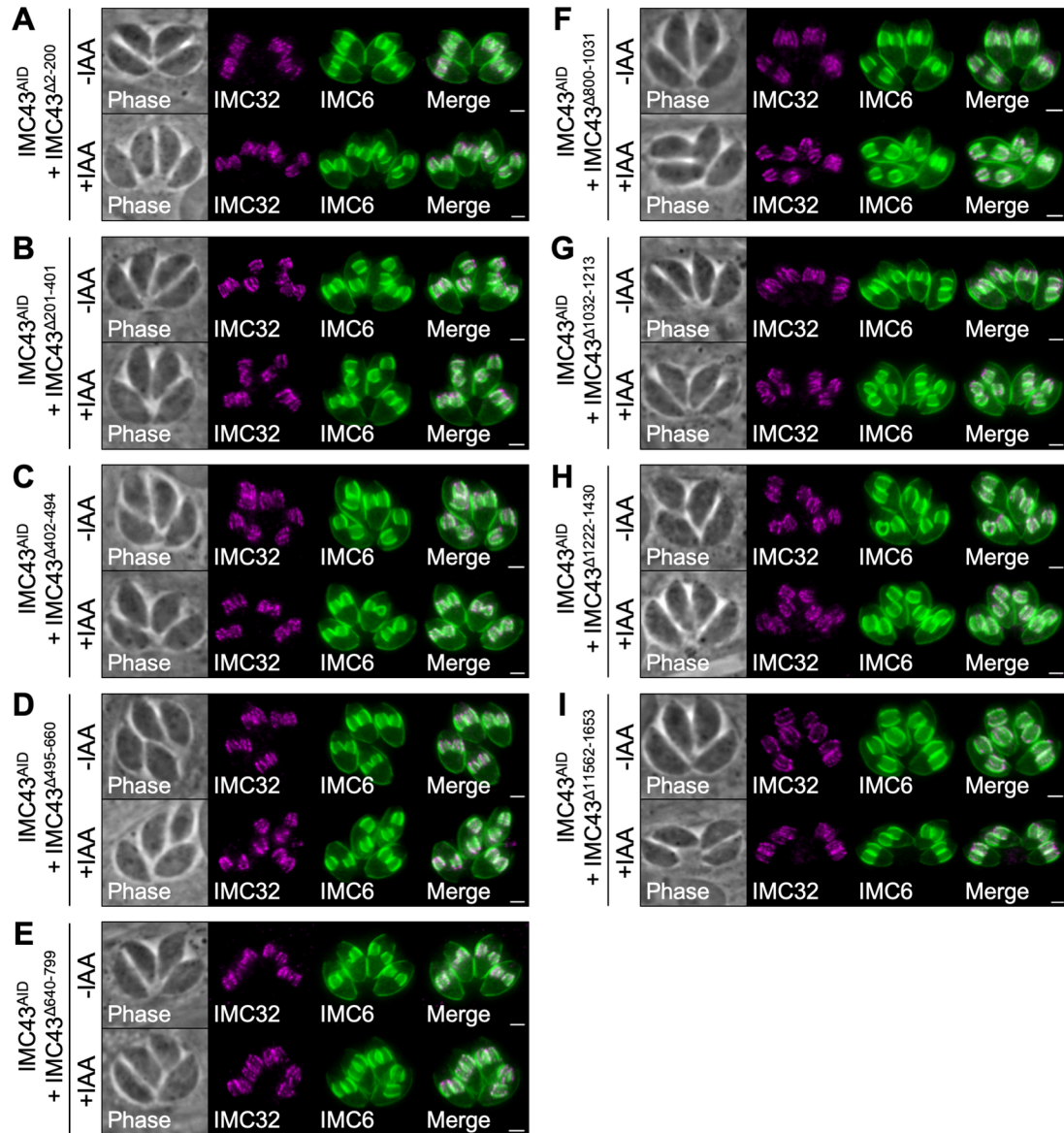


**Figure 2-S9. Most IMC43 deletion constructs rescue the mislocalization of IMC32 caused by depletion of IMC43.** IFAs showing the localization of IMC32 in nine of the IMC43 deletion lines. All nine shown in this figure rescue the mislocalization of IMC32. Magenta = anti-V5 detecting IMC32<sup>3xV5</sup>, Green = anti-IMC6. Scale bars = 2  $\mu$ m.

**Table 2-S1. Full IMC43<sup>TurboID</sup> mass spectrometry results.** Full list of genes identified by mass spectrometry in the IMC43<sup>TurboID</sup> experiment. Spectral counts are shown for each gene.

“Enrichment Diff” refers to the difference between the average spectral count in IMC43<sup>TurboID</sup> and control parasites. “Enrichment Fold” refers to the average spectral count for IMC43<sup>TurboID</sup> samples divided by the average spectral count for control samples.

<https://doi.org/10.1371/journal.ppat.1011707.s010>

**Table 2-S2. Full IMC43 Y2H screen results.** Full list of genes identified by the Hybrigenics Y2H screen. All clones identified for a specific gene are grouped. Clones that were found to be out-of-frame are greyed out. Global PBS indicates the confidence score assigned to each clone [40, 41].

<https://doi.org/10.1371/journal.ppat.1011707.s011>

**Table 2-S3. Oligonucleotides used in this study.**

<https://doi.org/10.1371/journal.ppat.1011707.s012>

### **Chapter 3:**

BCC0 collaborates with IMC32 and IMC43 to form the *Toxoplasma gondii* essential daughter bud assembly complex

RESEARCH ARTICLE

# BCC0 collaborates with IMC32 and IMC43 to form the *Toxoplasma gondii* essential daughter bud assembly complex

Rebecca R. Pasquarelli<sup>1</sup>, Jihui Sha<sup>2</sup>, James A. Wohlschlegel<sup>2</sup>, Peter J. Bradley<sup>1,3\*</sup>

**1** Molecular Biology Institute, University of California, Los Angeles, California, United States of America, **2** Department of Biological Chemistry and Institute of Genomics and Proteomics, University of California, Los Angeles, California, United States of America, **3** Department of Microbiology, Immunology, and Molecular Genetics, University of California, Los Angeles, California, United States of America

\* [pbradley@ucla.edu](mailto:pbradley@ucla.edu)



**OPEN ACCESS**

**Citation:** Pasquarelli RR, Sha J, Wohlschlegel JA, Bradley PJ (2024) BCC0 collaborates with IMC32 and IMC43 to form the *Toxoplasma gondii* essential daughter bud assembly complex. PLoS Pathog 20(7): e1012411. <https://doi.org/10.1371/journal.ppat.1012411>

**Editor:** Sébastien Besteiro, University of Montpellier: Université de Montpellier, FRANCE

**Received:** May 29, 2024

**Accepted:** July 10, 2024

**Published:** July 18, 2024

**Peer Review History:** PLOS recognizes the benefits of transparency in the peer review process; therefore, we enable the publication of all of the content of peer review and author responses alongside final, published articles. The editorial history of this article is available here: <https://doi.org/10.1371/journal.ppat.1012411>

**Copyright:** © 2024 Pasquarelli et al. This is an open access article distributed under the terms of the [Creative Commons Attribution License](https://creativecommons.org/licenses/by/4.0/), which permits unrestricted use, distribution, and reproduction in any medium, provided the original author and source are credited.

**Data Availability Statement:** All relevant data are within the manuscript and its [Supporting Information](#) files.

## Abstract

*Toxoplasma gondii* divides by endodyogeny, in which two daughter buds are formed within the cytoplasm of the maternal cell using the inner membrane complex (IMC) as a scaffold. During endodyogeny, components of the IMC are synthesized and added sequentially to the nascent daughter buds in a tightly regulated manner. We previously showed that the early recruiting proteins IMC32 and IMC43 form an essential daughter bud assembly complex which lays the foundation of the daughter cell scaffold in *T. gondii*. In this study, we identify the essential, early recruiting IMC protein BCC0 as a third member of this complex by using IMC32 as bait in both proximity labeling and yeast two-hybrid screens. We demonstrate that BCC0's localization to daughter buds depends on the presence of both IMC32 and IMC43. Deletion analyses and functional complementation studies reveal that residues 701–877 of BCC0 are essential for both its localization and function and that residues 1–899 are sufficient for function despite minor mislocalization. Pairwise yeast two-hybrid assays additionally demonstrate that BCC0's essential domain binds to the coiled-coil region of IMC32 and that BCC0 and IMC43 do not directly interact. This data supports a model for complex assembly in which an IMC32-BCC0 subcomplex initially recruits to nascent buds via palmitoylation of IMC32 and is locked into the scaffold once bud elongation begins by IMC32 binding to IMC43. Together, this study dissects the organization and function of a complex of three early recruiting daughter proteins which are essential for the proper assembly of the IMC during endodyogeny.

## Author summary

*Toxoplasma gondii* is an obligate intracellular parasite that causes severe and even fatal disease in congenitally infected neonates and the immunocompromised. The parasite replicates using an internal budding mechanism called endodyogeny, in which two daughter buds form within the cytoplasm of a maternal parasite. Nascent daughter buds are scaffolded by the inner membrane complex (IMC), a unique organelle found in *T. gondii* and

**Funding:** This work was supported by NIH grants AI123360 to P.J.B. and GM153408 to J.A.W. R.R.P. was supported by the Ruth L. Kirschstein National Research Service Awards GM007185 and AI007323, as well as the UCLA Molecular Biology Institute Whitcome Fellowship. The funders had no role in study design, data collection and analysis, decision to publish, or preparation of the manuscript.

**Competing interests:** The authors have declared that no competing interests exist.

other parasites such as *Plasmodium spp.*, the causative agent of malaria. Many proteins that localize to the IMC of daughter buds have been identified, but only three of these proteins are essential for parasite replication and survival: IMC43, IMC32, and BCC0. In this study, we demonstrate that these three proteins exist in a complex, explore which features of BCC0 are critical for its localization and function, and develop a model for how the complex is assembled. This work expands our understanding of how the foundation of the early daughter buds is established during endodyogeny.

## Introduction

*Toxoplasma gondii* is a protozoan pathogen that can infect any warm-blooded animal worldwide [1]. *T. gondii* belongs to the Apicomplexa, a phylum of obligate intracellular parasites that cause significant human morbidity and mortality including *Plasmodium spp.* (malaria) and *Cryptosporidium spp.* (diarrheal disease) [2,3]. The phylum also includes important veterinary pathogens such as *Eimeria spp.* (chicken coccidiosis) and *Neospora caninum* (neosporosis) which cause economic loss in the livestock industry [4–6]. Approximately 30% of the global human population is chronically infected with *T. gondii* [7]. Healthy individuals typically remain asymptomatic, but infection can result in severe or even fatal disease in immunocompromised individuals or congenitally-infected neonates [8–10]. Current treatments can limit the acute disease but cannot clear the parasite from the host, resulting in lifelong chronic infection [9]. To identify targets for the development of new therapeutics, a deeper understanding of the parasite's unique biology is needed.

One unique feature of apicomplexan parasites is the inner membrane complex (IMC), a specialized organelle that plays critical roles throughout the *T. gondii* lytic cycle [11]. The *T. gondii* IMC underlies the parasite's plasma membrane and has both membrane and cytoskeletal components. The first layer is a series of flattened vesicles called alveoli which are sutured together in a quilt-like pattern [12]. Many IMC-localizing proteins associate with the membranes of the alveoli using either transmembrane domains or acylation [13–17]. The second layer of the IMC is composed of intermediate filament-like proteins called alveolins which form a supportive mesh-like network [18,19]. Additional IMC proteins associate with the network by binding to the alveolins [20,21]. Within the IMC, there are three distinct subdomains that have different protein components and functions. At the apex of the parasite, a single cone-shaped vesicle defines the apical cap. Proteins that localize specifically to this region of the organelle such as AC9 and AC10 are required for host cell invasion [21,22]. The central portion of the organelle is referred to as the IMC body. This portion of the organelle contains proteins with a wide variety of functions such as maintaining parasite structure and hosting the actin-myosin motor that facilitates parasite gliding motility [23,24]. Finally, the base of the IMC contains a ring-shaped structure called the basal complex, which mediates bud constriction at the conclusion of cell division [25]. Directly underneath the IMC there is an array of 22 subpellicular microtubules (SPMTs) which originate in the apical complex of the parasite and extend approximately two-thirds of the way down the parasite body, providing further structural support [26].

One of the critical functions of the IMC is to act as a scaffold for developing daughter cells during parasite replication. While the exact mechanism varies across the phylum, many apicomplexan parasites replicate using a unique process of internal budding in which two or more daughter buds are formed within the cytoplasm of a maternal parasite [27,28]. The human-infecting form of *T. gondii* replicates asexually using a form of internal budding called

endodyogeny, in which two daughter buds are formed. Endodyogeny occurs in a series of tightly regulated steps, and parasites within a single vacuole typically replicate synchronously [27,29]. The first step of endodyogeny, bud initiation, occurs immediately after centrosome duplication. During bud initiation, the daughter cell scaffold assembles on top of the centrosome as early IMC proteins are recruited and the tubulin-based conoid and SPMTs are formed [19,30–33]. As endodyogeny continues, the daughter buds elongate, driven by polymerization of the SPMTs [34]. As buds approach maturation, the basal complex of the nascent daughter buds constricts and the maternal IMC is degraded [25,35]. Finally, the two daughter buds adopt the maternal plasma membrane and emerge as separate cells. Throughout this process, IMC proteins are synthesized and recruited to the daughter cell scaffold sequentially in a “just in time” manner, with some proteins appearing as early as bud initiation and others only appearing after bud maturation is complete [19,36,37]. Interestingly, some IMC proteins have been shown to localize only to the developing daughter buds and are removed during bud maturation and emergence [14,19,38–40].

Until recent years, it was unclear which IMC proteins served as the essential foundation of the organelle during endodyogeny. Several of the alveolins are thought to be essential, but most of these proteins recruit after budding has already been initiated [19]. They are also maintained in mature parasites where they play critical roles in maintaining cellular structure. Other proteins such as IMC15, IMC29, FBXO1, and MORN1 have been shown to recruit during bud initiation and play important roles in endodyogeny, but all four of these can be genetically disrupted [19,38,41,42]. We recently identified two proteins, IMC32 and IMC43, that form a complex in the early daughter cell scaffold and are essential for the stable assembly of the IMC during endodyogeny [39,40]. We demonstrated that a domain towards the C-terminus of IMC43 binds directly to the C-terminal coiled-coil (CC) domains of IMC32. While IMC32 initially recruits independently of IMC43 during bud initiation, IMC43 binding was found to be essential for the maintenance of IMC32's localization during the middle and late stages of endodyogeny. Since loss of either of these proteins results in a lethal inability to stably assemble the daughter IMC, we termed this the IMC43-IMC32 essential daughter bud assembly complex.

In this study, we set out to identify additional components of the IMC43-IMC32 essential daughter bud assembly complex. Using IMC32 as bait in both proximity labeling and yeast two-hybrid (Y2H) screens, we identify the essential early daughter IMC protein BCC0 as the third component of this complex and subsequently show that BCC0 localization is dependent on both IMC32 and IMC43. Deletion analyses and pairwise Y2H assays reveal that a domain towards the N-terminus of BCC0 is essential for both the protein's localization and function and for binding to its partner, IMC32. This work functionally connects the only three known essential early daughter IMC proteins and expands our understanding of how the early daughter IMC is assembled during endodyogeny.

## Results

### Identification of candidate IMC32 binding partners

To identify additional components of the IMC43-IMC32 essential daughter bud assembly complex, we used IMC32 as the bait in both a TurboID proximity labeling screen and a Y2H screen [43–45]. For the TurboID experiment, we fused sequences encoding a TurboID biotin ligase along with a 3xHA epitope tag to the C-terminus of the IMC32 endogenous locus (Fig 1A). Immunofluorescence assay (IFA) confirmed that the IMC32<sup>TurboID</sup> fusion protein localized normally to the daughter IMC (Fig 1B). After four hours of treatment with biotin, daughter buds were robustly biotinylated, confirming that the biotin ligase was enzymatically active.

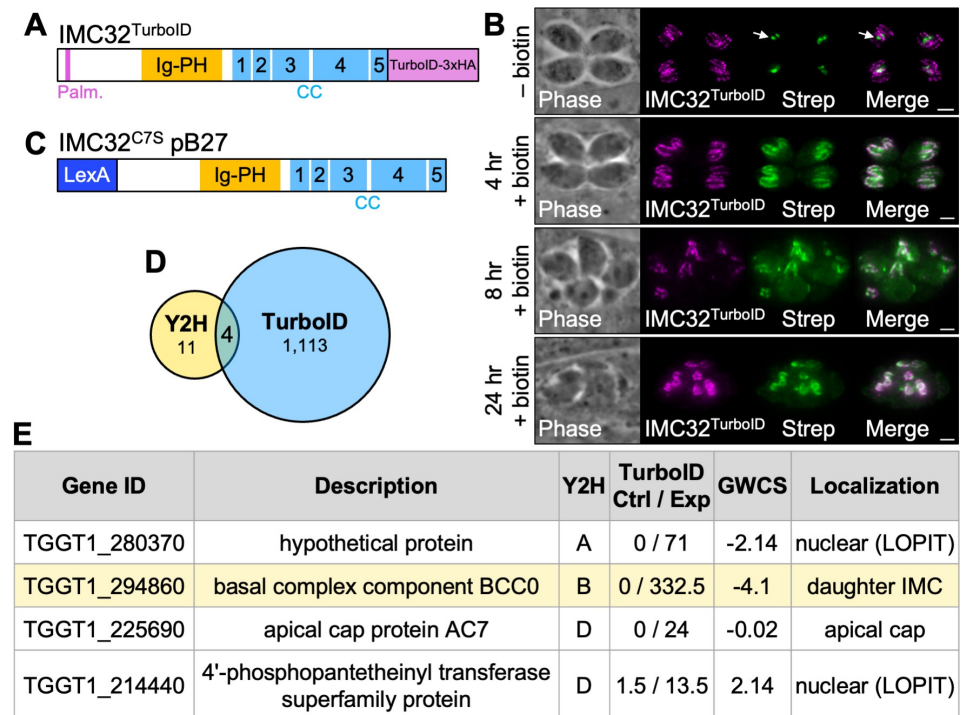


**Fig 1. TurboID and Y2H screens identify BCC0 as a candidate IMC32 binding partner.** A) Diagram of IMC32<sup>TurboID</sup> showing its predicted palmitoylation site (Palm.), Ig-PH domain, and five coiled-coil (CC) domains. A 3xHA-tagged TurboID biotin ligase was added to the C-terminus of the protein. B) IFAs of IMC32<sup>TurboID</sup> parasites after 0, 4, 8, or 24 hours of biotin treatment. Arrow points to the endogenously biotinylated apicoplast in the -biotin control. Morphological defects are visible at the 8 and 24-hour time points. Magenta = anti-HA detecting IMC32<sup>TurboID</sup>, Green = streptavidin. Scale bars = 2  $\mu$ m. C) Diagram of the IMC32<sup>C7S</sup> N-terminal LexA fusion protein used for Y2H screening. D) Venn diagram comparing the genes identified in the TurboID and Y2H screens. All Y2H hits that were not out-of-frame or antisense were included. TurboID results were filtered to include only genes that were at least two-fold enriched with a difference of >5 spectral counts when comparing IMC32<sup>TurboID</sup> to control. Four genes were identified in both experiments after filtering results as described. E) Table showing the four genes that were identified in both the TurboID and Y2H screens. "Y2H" column indicates the confidence score assigned in the Y2H screen (A = very high confidence, B = high confidence, D = moderate confidence). "TurboID Ctrl / Exp" column indicates the average spectral count for each gene in the control and IMC32<sup>TurboID</sup> mass spectrometry results. "GWCS" refers to the phenotype score assigned to each gene in a genome-wide CRISPR/Cas9 screen [65]. "Localization" column reports the known localization of each protein [14,38,46]. Localizations followed by "(LOPIT)" indicate predicted localizations based on hyperplexed localization of organelle proteins by isotope tagging (hyperLOPIT) [83].

<https://doi.org/10.1371/journal.ppat.1012411.g001>

However, after eight hours of treatment with biotin, IMC32<sup>TurboID</sup> parasites exhibited morphological defects which became more severe by 24 hours. To avoid issues with toxicity, we treated parasites with biotin for five hours before harvesting and performing streptavidin affinity chromatography and subsequent mass spectrometry analysis (S1 Table). Y2H screening was performed by Hybrigenics Services using full-length IMC32 with the predicted palmitoylation site at position 7 mutated to serine. This protein was cloned into the pB27 bait vector as a LexA N-terminal fusion (IMC32<sup>C7S</sup> pB27) and screened against the *T. gondii* RH strain cDNA library to identify direct protein-protein interactions (Fig 1C and S2 Table). The results of the IMC32 TurboID and Y2H screens were compared, resulting in the identification of four candidate binding partners that were found in both approaches: a hypothetical protein encoded by the gene ID TGGT1\_280370, the essential early daughter IMC protein BCC0, the

apical cap protein AC7, and a 4'-phosphopantetheinyl transferase superfamily protein (Fig 1D and 1E). BCC0 was a high confidence hit in the Y2H screen and the sixth most enriched protein in the TurboID screen. In addition, it has previously been shown to localize to daughter buds in a similar pattern to IMC32 and play an essential role in endodyogeny [38,46]. We therefore selected it for further study.

### BCC0 depends on IMC32 and IMC43 for its localization to the daughter IMC

BCC0 is a large protein composed of 2,457 amino acids (Fig 2A) [47]. The protein is predicted to contain a myristoylation site, three palmitoylation sites, and a coiled-coil domain at the N-terminus of the protein [48–51]. Our Y2H screen determined that residues 570–899 of BCC0 were involved in the interaction with the bait protein IMC32 (S2 Table). To determine the extent to which BCC0 and IMC32 colocalize, we endogenously tagged BCC0 with a spaghetti monster (sm) OLLAS epitope tag in an IMC32<sup>2xStrep3xTy</sup> parent strain. IFA showed that the two proteins exhibited near-perfect overlap during both bud initiation, when both proteins appear as five distinct puncta arranged symmetrically, and mid-budding, when both proteins appear as a series of five discontinuous longitudinal stripes along the body of the daughter IMC (Fig 2B and 2C). To determine whether BCC0's localization was dependent on either of the other two proteins in the essential daughter bud assembly complex (Fig 2D), we endogenously tagged BCC0 in both the IMC32<sup>AID</sup> and IMC43<sup>AID</sup> strains [40,52,53]. After 24 hours of indoleacetic acid (IAA) treatment, BCC0 became severely mislocalized in both IMC32-depleted and IMC43-depleted parasites (Fig 2E and 2F). Since IMC32's localization is dependent on binding to IMC43, this suggests that the complex assembles hierarchically.

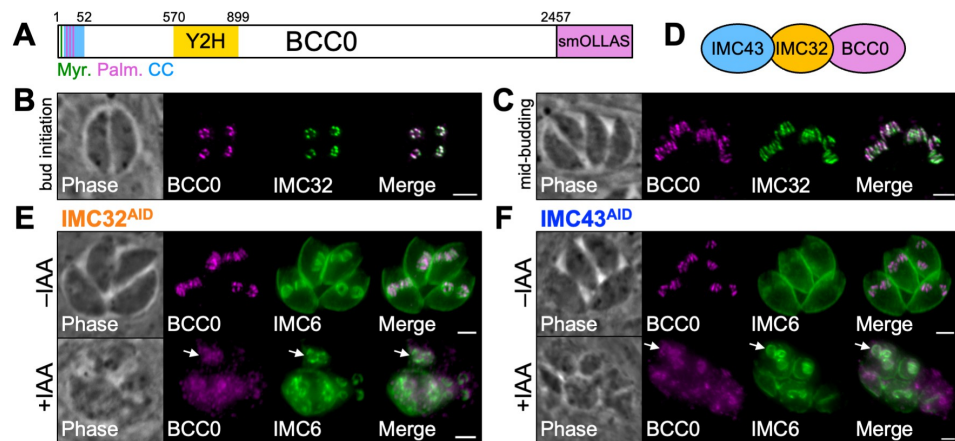


**Fig 2. BCC0 requires both IMC32 and IMC43 for its localization to the daughter IMC.** A) Diagram of BCC0 showing its predicted myristoylation site at residue 2 (Myr.), predicted palmitoylation sites at residues 10, 11, and 17 (Palm.), predicted coiled-coil domain at residues 9–52 (CC), and IMC32-binding region at residues 570–899 identified by Y2H screening (Y2H). An smOLLAS tag was added to the C-terminus of the protein. B–C) IFAs showing that BCC0 and IMC32 colocalize closely in the daughter IMC during both bud initiation and mid-budding. Magenta = anti-OLLAS detecting BCC0<sup>smOLLAS</sup>, Green = anti-Ty detecting IMC32<sup>2xStrep3xTy</sup>. D) Diagram of the essential daughter bud assembly complex composed of IMC43, IMC32, and BCC0. E) IFA of IMC32<sup>AID</sup> parasites grown  $-/+$  IAA for 24 hours showing that depletion of IMC32 causes BCC0 to mislocalize to the cytoplasm but remain slightly enriched at daughter buds (arrows). Magenta = anti-OLLAS detecting BCC0<sup>smOLLAS</sup>, Green = anti-IMC6. F) IFA of IMC43<sup>AID</sup> parasites grown  $-/+$  IAA for 24 hours showing that depletion of IMC43 causes BCC0 to mislocalize to the cytoplasm but remain slightly enriched at daughter buds (arrows). Magenta = anti-OLLAS detecting BCC0<sup>smOLLAS</sup>, Green = anti-IMC6. Scale bars = 2  $\mu$ m.

<https://doi.org/10.1371/journal.ppat.1012411.g002>

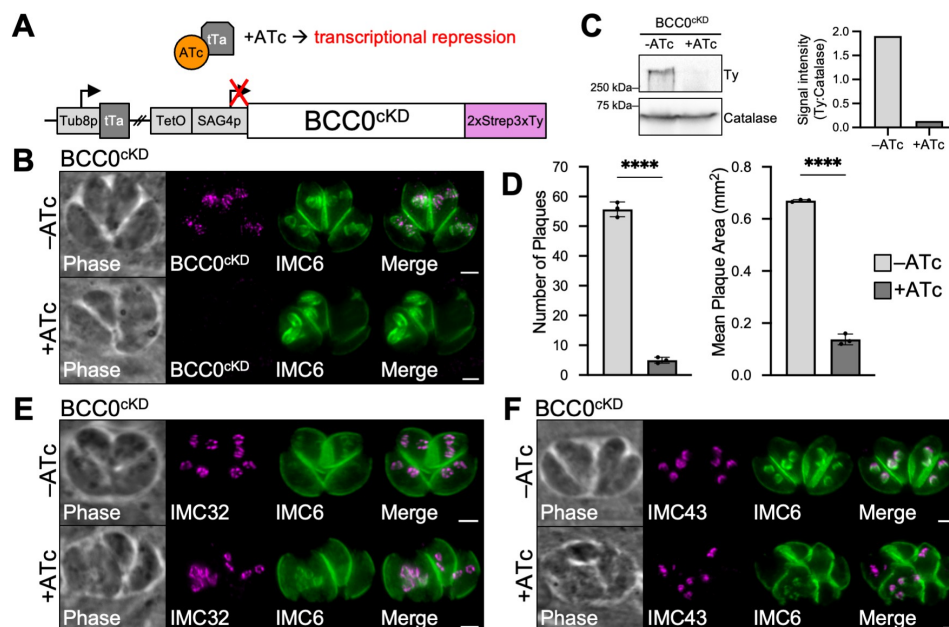


**Fig 3. BCC0 knockdown does not affect the localization of IMC32 or IMC43.** A) Diagram depicting the ATc-regulatable transcriptional repression system used for BCC0 knockdown. The endogenous promoter for BCC0 was replaced with a TetO7-SAG4p minimal promoter in a BCC0<sup>2xStrep3xTy</sup> strain expressing the Tati transactivator. B) IFA of BCC0<sup>cKD</sup> parasites grown +/- ATc for 24 hours showing that knockdown of BCC0 results in severe morphological defects. Magenta = anti-Ty detecting BCC0<sup>cKD</sup>, Green = anti-IMC6. C) Western blot and quantification showing that BCC0<sup>cKD</sup> is 93% depleted after 24 hours of ATc treatment. D) Plaque assays show that both plaque number and size are significantly reduced when BCC0 is knocked down. Statistical significance was determined using a two-tailed t-test (\*\*\*\*,  $P < 0.0001$ ). E) IFA of BCC0<sup>cKD</sup> parasites grown +/- ATc for 24 hours showing that knockdown of BCC0 does not affect IMC32 localization. Magenta = anti-Myc detecting IMC32<sup>3xMyc</sup>, Green = anti-IMC6. F) IFA of BCC0<sup>cKD</sup> parasites grown +/- ATc for 24 hours showing that knockdown of BCC0 does not affect IMC43 localization. Magenta = anti-HA detecting IMC43<sup>smHA</sup>, Green = anti-IMC6. Scale bars = 2 μm.

<https://doi.org/10.1371/journal.ppat.1012411.g003>

We next wanted to determine how loss of BCC0 would affect the localization of IMC32 and IMC43. We initially tried to use the auxin-inducible degron (AID) system, but endogenously tagging BCC0 with either the mAID<sup>3xHA</sup> or the mIAA7<sup>3xHA</sup> degron resulted in insufficient knockdown (S1 Fig) [54]. Thus, we utilized a transcriptional repression system to study BCC0 [55,56]. To do this, we endogenously tagged BCC0 with a 2xStrep3xTy epitope tag in an RHΔ*ku80*-Tati-HXGPRT parent strain, then replaced the endogenous promoter with a TetO7-SAG4 minimal promoter (BCC0<sup>cKD</sup>) (Fig 3A). Treatment with anhydrotetracycline (ATc) for 24 hours caused the protein to be knocked down to an undetectable level by IFA and resulted in severe morphological defects, as expected based on published data (Fig 3B) [46]. Western blot confirmed that 24 hours of ATc treatment resulted in a 93% reduction in the level of BCC0 expression (Fig 3C). Plaque assays demonstrated that knockdown of BCC0 led to a severe 92% reduction in plaque number and an 80% reduction in plaque size (Fig 3D). These few small plaques are likely formed due to the incomplete knockdown observed by western blot (Fig 3C). To determine the effect of BCC0 knockdown on IMC32 and IMC43, we endogenously tagged IMC32 with a 3xMyc tag and IMC43 with an smHA tag in the BCC0<sup>cKD</sup> strain. IFA demonstrated that despite the severe morphological defects observed in these parasites, IMC32 and IMC43 localization remained unaffected (Fig 3E and 3F).

### Residues 701–877 are essential for BCC0 localization and function

Since BCC0 is a large protein with no identifiable functional domains or homology to known proteins, we next wanted to determine which regions of the protein are important for its localization and function. To do this, we created a series of 12 smHA-tagged constructs for functional complementation studies (Fig 4A). These included the full-length protein (BCC0<sup>WTc</sup>) as a control and 11 mutant proteins each containing a deletion of approximately 150–300 amino acids. Regions for the deletions were chosen based on conservation with *N. caninum* and predicted secondary structure (S2 Fig) [57]. Each construct was driven by the endogenous promoter for BCC0 and contained flanking regions for integration at the UPRT locus in a BCC0<sup>smOLLAS</sup> strain (Fig 4B). Localization was assessed by co-staining for the smHA-tagged construct and wild-type BCC0<sup>smOLLAS</sup>. We then attempted to disrupt the endogenous BCC0 locus in each of these strains. Successful knockouts were assessed by IFA and plaque assay to determine whether each deletion could fully complement the function of wild-type BCC0.

BCC0<sup>WTc</sup> and 10 of the deletion constructs colocalized perfectly with endogenous BCC0<sup>smOLLAS</sup> (Figs 4C and S3). However, BCC0<sup>Δ701–877</sup> became severely mislocalized with most of the protein being mistargeted to the cytoplasm, although there was a slight enrichment at daughter buds (Fig 4D). Attempts to disrupt the endogenous BCC0 locus in the BCC0<sup>smOLLAS</sup> + BCC0<sup>Δ701–877</sup> strain were unsuccessful, indicating that this region of the protein is likely required for its function. We were able to successfully disrupt the BCC0 locus in the BCC0<sup>WTc</sup> strain and all other deletion strains, which was confirmed by both PCR verification and IFA showing loss of the BCC0<sup>smOLLAS</sup> signal (S4 Fig). No obvious morphological defects were observed for any of these strains, although the  $\Delta bcc0$  + BCC0<sup>Δ170–375</sup> strain often exhibited desynchronized endodyogeny, suggesting possible dysregulation (Fig 4E–4O). Plaque assays demonstrated that BCC0<sup>WTc</sup> and all deletions except for BCC0<sup>Δ170–375</sup> were sufficient to maintain normal growth (Fig 4P). The  $\Delta bcc0$  + BCC0<sup>Δ170–375</sup> strain exhibited a significant 32% reduction in plaque size, indicating this region likely plays a minor role in the function of BCC0. The  $\Delta 2–169$  and  $\Delta 376–569$  deletions, which flank this region, exhibited modest but nonsignificant reductions in plaque size (17% and 12%, respectively).

Since we were unable to disrupt the endogenous BCC0 locus in the BCC0<sup>smOLLAS</sup> + BCC0<sup>Δ701–877</sup> strain, we integrated the BCC0<sup>WTc</sup> and BCC0<sup>Δ701–877</sup> constructs at the UPRT locus in the BCC0<sup>cKD</sup> strain and used IFA and plaque assays to assess whether each construct could rescue the defects observed upon BCC0 knockdown (Fig 5A and 5B). While the BCC0<sup>WTc</sup> construct was able to fully rescue the morphological defects observed by IFA, the BCC0<sup>Δ701–877</sup> construct could not (Fig 5C and 5D). Knockdown of BCC0<sup>cKD</sup> resulted in an 83% reduction in plaque efficiency and a 62% reduction in plaque size (Fig 5E and 5F). Both of these defects were slightly more modest than what we previously observed, suggesting that the leaky expression of BCC0<sup>cKD</sup> may have increased over time (Fig 3C and 3D). The BCC0<sup>WTc</sup> construct restored plaque size to approximately 80% the size of plaques formed by untreated parasites, as expected based on ATc toxicity in wild-type parasites (Figs 5E and 5S) [40]. The BCC0<sup>Δ701–877</sup> construct completely failed to rescue the defect in both plaque efficiency and plaque size caused by knockdown of BCC0<sup>cKD</sup>, confirming that this region is essential for both the localization and function of BCC0 (Fig 5E and 5F).

### Residues 1–899 are sufficient for BCC0 function

Since only residues 701–877 are necessary for BCC0 function, we wondered how much of the protein was sufficient for its function. To determine this, we began by making C-terminal truncations of the protein at its endogenous locus. We found that BCC0 was able to be truncated at residue 1519 (BCC0<sup>1–1519</sup>) without having any effect on the protein's localization

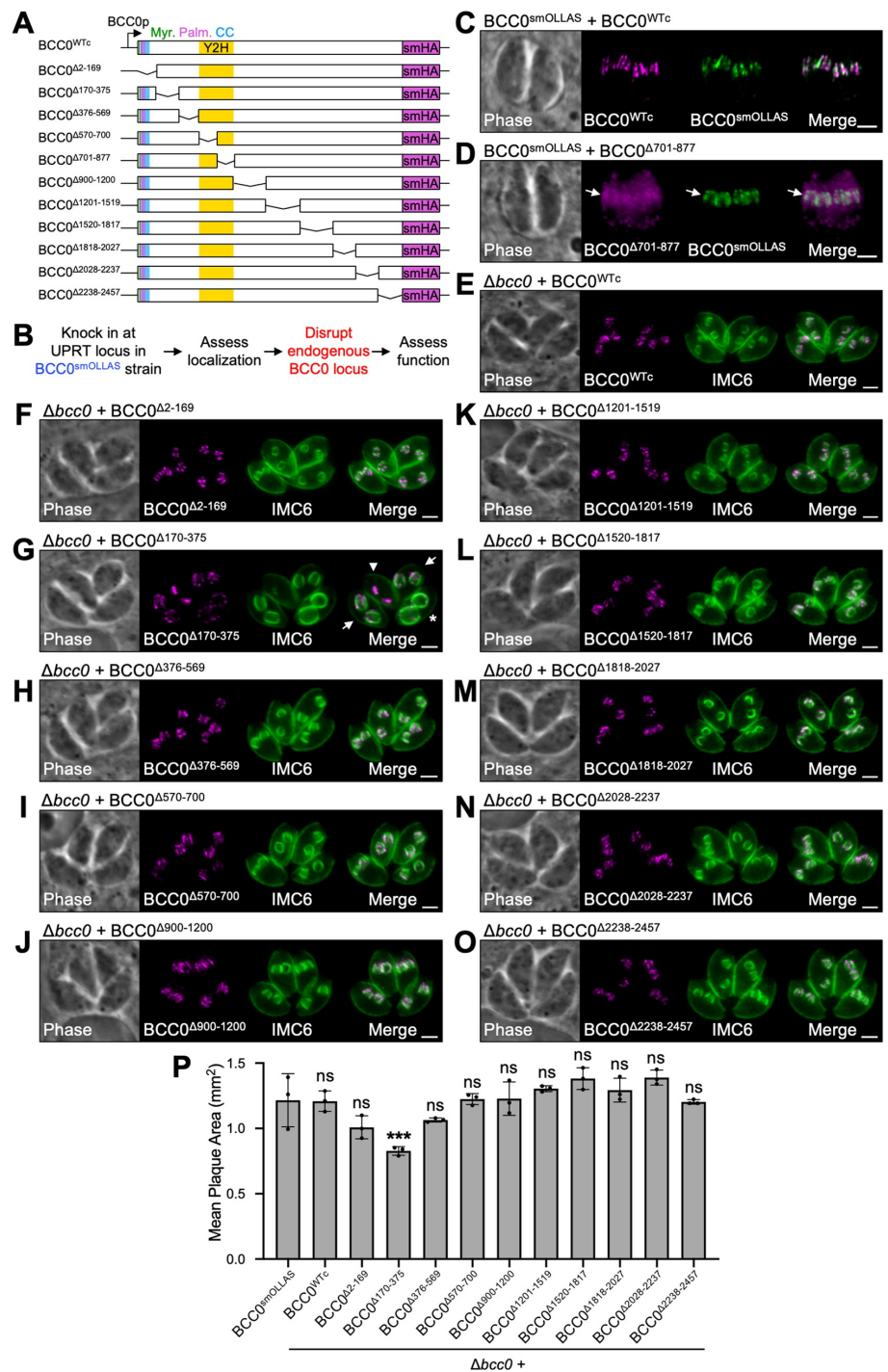


**Fig 4. BCC0 residues 701–877 are required for localization and residues 170–375 have a minor impact on function.** A) Diagram showing the 12 constructs used for functional complementation of BCC0. All 12 constructs were driven by the endogenous promoter for BCC0 and include a C-terminal smHA tag. “Myr.” = predicted myristoylation site. “Palm.” = predicted palmitoylation sites. “Y2H” = IMC32-binding region identified by Y2H screen. B) Workflow used to assess the effect of each region of BCC0 on the protein’s localization and function. C) IFA of BCC0<sup>smOLLAS</sup> + BCC0<sup>WTc</sup> parasites showing that BCC0<sup>WTc</sup> localizes normally. Magenta = anti-HA detecting BCC0<sup>WTc</sup>, Green = anti-OLLAS detecting BCC0<sup>smOLLAS</sup>. D) IFA of BCC0<sup>smOLLAS</sup> + BCC0<sup>A701–877</sup> parasites showing that BCC0<sup>A701–877</sup> severely mislocalizes to the cytoplasm and is slightly enriched at daughter buds (arrows). Magenta = anti-HA detecting BCC0<sup>A701–877</sup>, Green = anti-OLLAS detecting endogenous BCC0<sup>smOLLAS</sup>. E) IFA of  $\Delta bcc0$  + BCC0<sup>WTc</sup> parasites which exhibit no obvious morphological defects. Magenta = anti-HA detecting BCC0<sup>WTc</sup>, Green = anti-IMC6. F-O) IFAs for all deletion strains in which endogenous BCC0<sup>smOLLAS</sup> was successfully disrupted. BCC0<sup>A701–877</sup> is not shown because endogenous BCC0<sup>smOLLAS</sup> was unable to be disrupted in this background. Panel G shows  $\Delta bcc0$  + BCC0<sup>A170–375</sup> parasites undergoing desynchronized endodyogeny. An arrowhead indicates a parasite at the early budding stage, arrows indicate parasites at the mid-budding stage, and an asterisk indicates a parasite at the late budding stage. Magenta = anti-HA detecting BCC0 deletions, Green = anti-IMC6. P) Plaque assays for all deletion strains in which endogenous BCC0<sup>smOLLAS</sup> was successfully disrupted. BCC0<sup>A701–877</sup> is not shown because endogenous BCC0<sup>smOLLAS</sup> was unable to be disrupted in this background. Only the  $\Delta bcc0$  + BCC0<sup>A170–375</sup> strain exhibited a significant reduction in plaque size. Statistical significance was determined by one-way ANOVA comparing each strain to BCC0<sup>smOLLAS</sup> (\*\*\*,  $P < 0.001$ ; ns = not significant). Scale bars for all IFAs = 2  $\mu$ m.

<https://doi.org/10.1371/journal.ppat.1012411.g004>

(Fig 6A). Truncation at residue 899 (BCC0<sup>1–899</sup>) resulted in partial mislocalization of the protein, which was most apparent in the later stages of endodyogeny (Fig 6B). Despite this partial mislocalization, this truncated protein did not exhibit a fitness defect (Fig 6C). Since any further truncation would disrupt the essential domain within residues 701–877, we next asked whether additional deletions could be made at the N-terminus of the protein. To determine this, we designed four constructs containing residues 170–899, 376–899, 570–899, and 701–899 and integrated them at the UPRT locus in a wild-type BCC0<sup>smOLLAS</sup> strain (Fig 6D). As we had done previously for our initial deletion series, we assessed the localization of each of these mutant proteins and then disrupted the endogenous BCC0 locus to assess its function (Fig 6E). All four mutant proteins severely mislocalized to the cytoplasm (S6A–S6D Fig). Surprisingly, despite this, we were able to successfully disrupt the endogenous BCC0 locus in all four of these strains, which was confirmed by IFA and PCR (Figs 6F–6I and S6E). Each of the four mutant strains exhibited obvious morphological and replication defects and a severe reduction in plaque size (Fig 6F–6J). Thus, while just the essential domain of BCC0 (BCC0<sup>701–899</sup>) is sufficient for parasite survival, only BCC0<sup>1–899</sup> is sufficient for full function of the protein.

### BCC0’s essential domain binds to IMC32’s coiled-coil domains

Finally, we wanted to use pairwise Y2H assays to determine which region of IMC32 is involved in binding to BCC0 and to determine whether there are any direct interactions between BCC0 and IMC43. We divided BCC0 into four fragments: BCC0<sup>3–569</sup>, BCC0<sup>570–899</sup>, BCC0<sup>900–1817</sup>, and BCC0<sup>1818–2457</sup> (Fig 7A). For IMC32 and IMC43, we used the same fragments that we had previously used in our investigation of IMC32-IMC43 binding interactions [40]. Each fragment was cloned into either a pB27 (LexA) bait vector or a pP6 (GAL4 activation domain) prey vector. We then co-transformed all 12 possible combinations of the IMC32 and BCC0 bait and prey vectors into yeast and tested each strain’s ability to grow on permissive and restrictive media (Fig 7B). Four of the combinations could not be tested because both fragments were auto-activating in the context of the pB27 vector. Of the remaining eight strains, only the strain expressing BCC0<sup>570–899</sup> and IMC32<sup>Cterm</sup> was able to grow on restrictive media, indicating that BCC0’s essential domain binds to IMC32 at its C-terminal coiled-coil domains. To determine whether BCC0 directly binds to IMC43, we performed the same experiments with all 12 combinations of IMC43 and BCC0 bait and prey vectors. All 12 strains grew robustly on permissive media and were not auto-activating, but none grew on restrictive media, indicating that there are no direct interactions between these two proteins (Fig 7C).

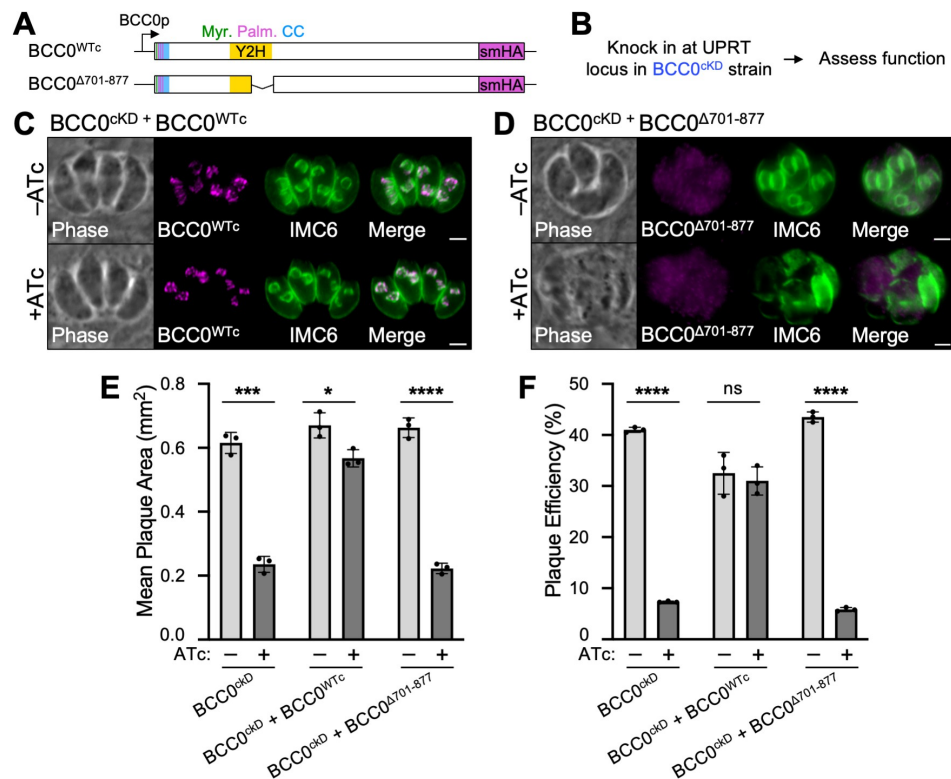


**Fig 5. BCC0 residues 701–877 are essential for function.** A) Diagram of the two constructs used for functional complementation of *BCC0<sup>cKD</sup>*. Both are driven by the endogenous promoter for BCC0 and include a C-terminal smHA tag. “Myr.” = predicted myristoylation site, “Palm.” = predicted palmitoylation site, “CC” = predicted coiled-coil domain, “Y2H” = IMC32-binding domain identified by Y2H screen. B) Workflow used to assess how deleting residues 701–877 affects the function of BCC0 using an ATc-regulatable conditional knockdown strain (*BCC0<sup>cKD</sup>*). C) IFA of *BCC0<sup>cKD</sup> + BCC0<sup>WTc</sup>* parasites grown for 24 hours -/+ ATc showing that *BCC0<sup>WTc</sup>* rescues the morphological defects caused by knockdown of BCC0. Magenta = anti-HA detecting *BCC0<sup>WTc</sup>*, Green = anti-IMC6. D) IFA of *BCC0<sup>cKD</sup> + BCC0<sup>Δ701-877</sup>* parasites grown for 24 hours -/+ ATc showing that *BCC0<sup>Δ701-877</sup>* fails to rescue the morphological defects caused by knockdown of BCC0. Magenta = anti-HA detecting *BCC0<sup>Δ701-877</sup>*, Green = anti-IMC6. E, F) Plaque assays show that *BCC0<sup>Δ701-877</sup>* fails to rescue the defect in both plaque efficiency (number of plaques formed divided by the number of parasites infected) and plaque size caused by knockdown of BCC0. *BCC0<sup>WTc</sup>* does not completely rescue the defect in plaque size due to ATc toxicity which is documented in S5 Fig and previous work [39]. Statistical significance was determined using multiple two-tailed t-tests (\*\*\*\*,  $P < 0.0001$ ; \*\*\*,  $P < 0.001$ ; \*,  $P < 0.05$ ; ns = not significant). Scale bars for all IFAs = 2  $\mu$ m.

<https://doi.org/10.1371/journal.ppat.1012411.g005>

## Discussion

In this study, we identified the essential daughter IMC protein BCC0 as a binding partner of IMC32 and a third component of the essential daughter bud assembly complex (Fig 8A). Using a combination of deletion constructs integrated at an exogenous locus and C-terminal truncations at the endogenous locus, we were able to interrogate how the loss of different regions of BCC0 impacts the protein’s localization and function. One surprising result was that *BCC0<sup>Δ2-169</sup>*, which lacks the predicted N-terminal acylation sites, was able to localize to the daughter IMC and function normally. Several IMC proteins such as IMC32, ISP1-4, GAP45, and HSP20 have been shown to depend on their predicted acylation sites for localization to the IMC [16,17,39,58,59]. However, MORN1 has a predicted palmitoylation site which has been shown to be dispensable for its localization to the basal complex. It is possible that

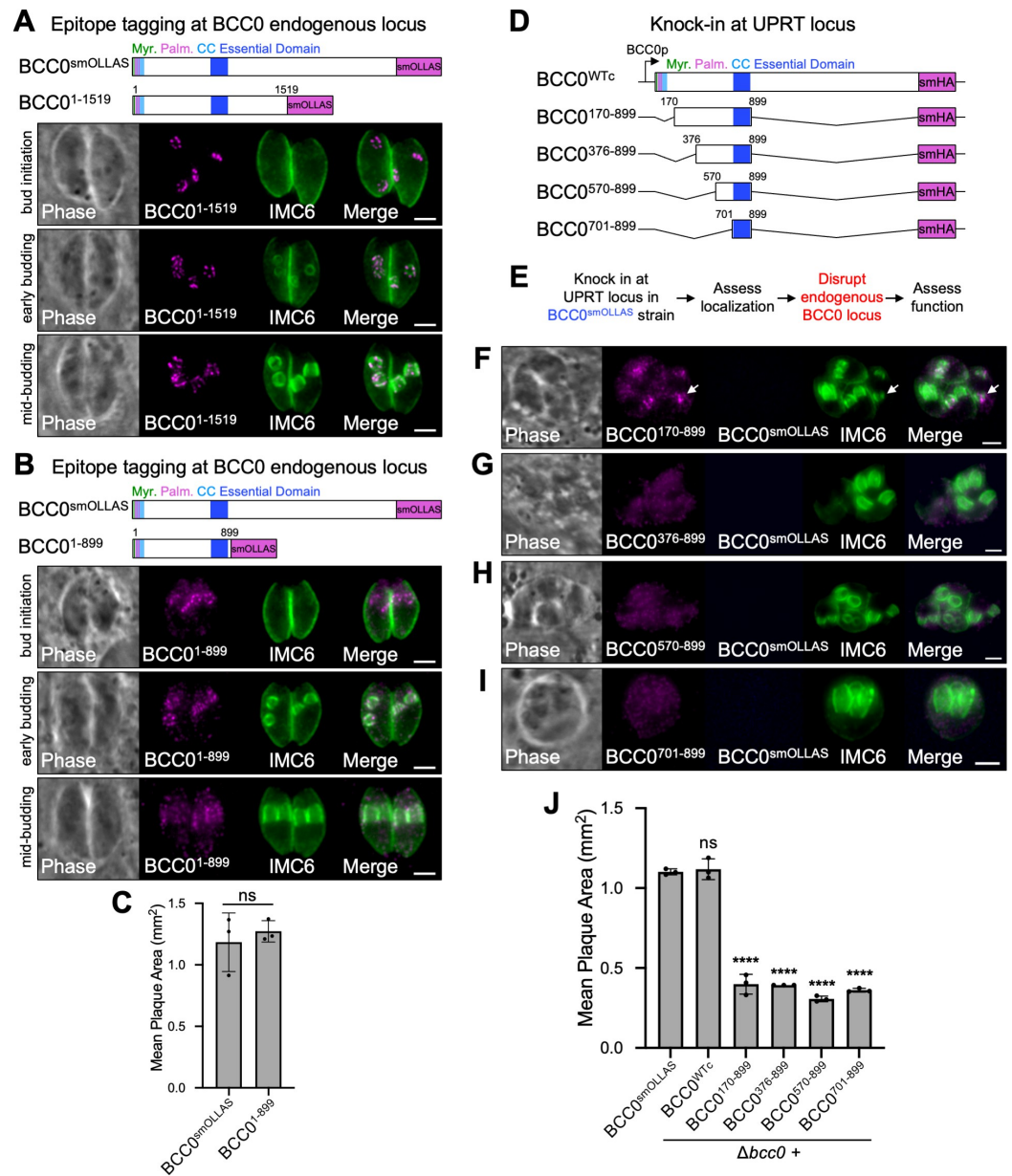


**Fig 6. BCC0 residues 1–899 are sufficient for function.** A) Diagram and IFAs showing that BCC0 can be truncated at residue 1519 without affecting localization of the protein during the bud initiation, early budding, or mid-budding stages of endodyogeny. For diagrams, “Myr.” = predicted myristoylation site, “Palm.” = predicted palmitoylation site, “CC” = coiled-coil domain. For IFAs, Magenta = anti-OLLAS detecting BCC0<sup>1-1519</sup>, Green = anti-IMC6. B) Diagram and IFAs showing that truncation of BCC0 at residue 899 causes partial mislocalization of the protein which is most severe at the mid-budding stage of endodyogeny. Magenta = anti-OLLAS detecting BCC0<sup>1-899</sup>, Green = anti-IMC6. C) Plaque assay comparing full-length BCC0<sup>smOLLAS</sup> with BCC0<sup>1-899</sup> shows that truncation of BCC0 at residue 899 does not affect function. Statistical significance was determined using a two-tailed t-test (ns = not significant). D) Diagram of the four deletion constructs used to determine the minimal region of BCC0 that is sufficient for protein function. All constructs are driven by the endogenous promoter for BCC0 and include a C-terminal smHA tag. E) Workflow used to analyze the localization and function of each of the constructs shown in D. F-I) IFAs of  $\Delta bcc0$  parasites

complemented with each of the constructs shown in D. All four constructs severely mislocalize, and only BCC0<sup>170-899</sup> enriches at daughter buds (arrow). Magenta = anti-HA detecting BCC0 deletions, Blue = anti-OLLAS detecting endogenous BCC0<sup>smOLLAS</sup>, Green = anti-IMC6. J) Plaque assays comparing the size of plaques formed by wild-type BCC0<sup>smOLLAS</sup> parasites with that of  $\Delta bcc0$  parasites complemented with the constructs shown in D. Statistical significance was determined by one-way ANOVA comparing each strain to BCC0<sup>smOLLAS</sup> (\*\*\*\*,  $P < 0.0001$ ; ns = not significant). Scale bars for all IFAs = 2  $\mu$ m.

<https://doi.org/10.1371/journal.ppat.1012411.g006>

these predicted sites on BCC0 are not actually acylated [42]. Alternatively, BCC0 could have bona fide acylation sites which only serve as secondary means of tethering to the IMC.

Our deletion series revealed that residues 701–877 of BCC0 are essential for both its localization and function. Since these residues are contained within the region which we found to be sufficient for IMC32 binding by pairwise Y2H assays and depletion of IMC32 also causes mislocalization of BCC0, this suggests BCC0 is primarily targeted to the daughter cell scaffold by binding to IMC32. We were surprised to find that BCC0 could be truncated down to residue 899 with only minor effects on the protein’s localization and no impact on the protein’s function. Even more surprisingly, expression of just the essential domain of BCC0, residues 701–877, was sufficient for parasite viability, although the protein was severely mislocalized and these parasites exhibited defects in growth and morphology. This suggests that a small

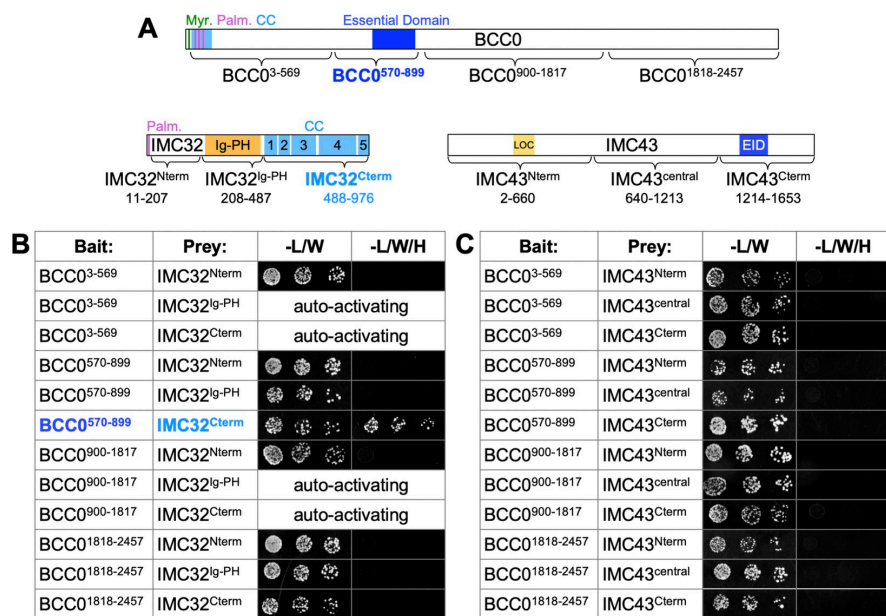


**Fig 7. BCC0 residues 570–899 bind to IMC32’s C-terminal coiled-coil domains.** A) Diagram of the fragments of BCC0, IMC32, and IMC43 used for pairwise Y2H assays. Residues included in each fragment are indicated. “Myr.” = predicted myristoylation site. “Palm.” = predicted palmitoylation site. “CC” = coiled-coil domain. “LOC” = IMC43 localization domain. “EID” = IMC43 essential interaction domain. B) Pairwise Y2H assays testing for binding between fragments of BCC0 and IMC32. Pairs of fragments that were unable to be tested due to auto-activation of both fragments in the pB27 vector are indicated. Growth on permissive (-L/W) media indicates the presence of both the pB27 and pP6 bait and prey plasmids. Growth on restrictive (-L/W/H) media indicates binding between the indicated fragments of each protein. C) Pairwise Y2H assays testing for binding between fragments of BCC0 and IMC43.

<https://doi.org/10.1371/journal.ppat.1012411.g007>

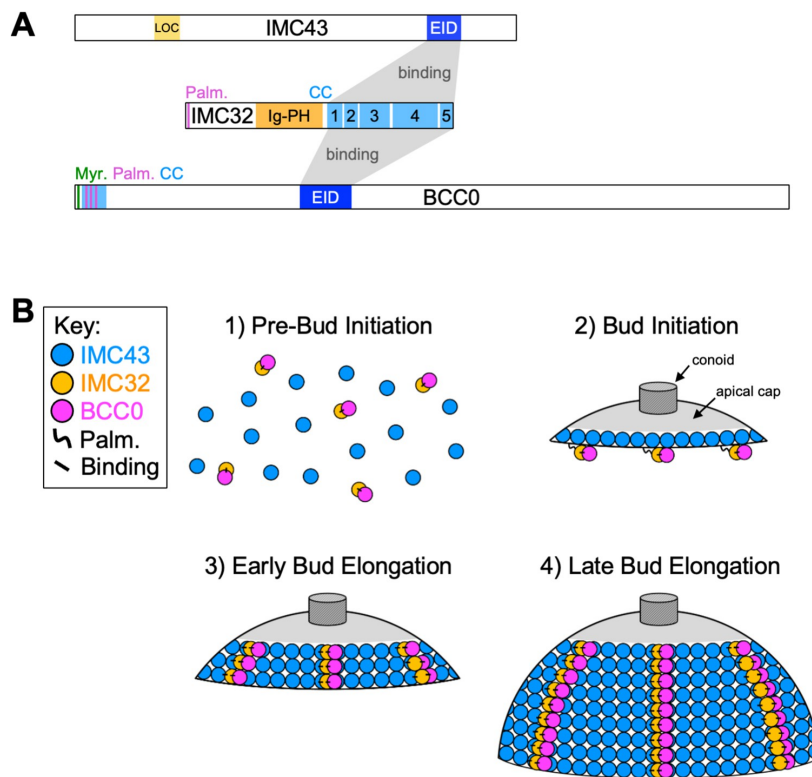


**Fig 8. Summary.** A) Diagram depicting interactions between the components of the essential IMC43-IMC32-BCC0 daughter bud assembly complex. Grey boxes indicate binding interactions between the essential interaction domains (EID) of IMC43 and BCC0 with IMC32's C-terminal coiled-coil domains. "Palm." = predicted palmitoylation site. "CC" = coiled-coil domain. B) Diagram summarizing the current model for how IMC43, IMC32, and BCC0 assemble onto the developing daughter cell scaffold during endodyogeny. Just before bud initiation (step 1) expression of IMC43, IMC32, and BCC0 increases. IMC32 and BCC0 bind to each other at this point. During bud initiation (step 2) IMC43 recruits to the early daughter cell scaffold independently. IMC32 is recruited to the membranes of the early daughter cell scaffold via palmitoylation. BCC0 remains bound to IMC32. During early bud elongation (step 3), IMC32 binds to IMC43, securely locking it into the daughter cell scaffold. BCC0 remains bound to IMC32. Short stripes of IMC32 and BCC0 can be seen at this point, which become more prominent as bud elongation continues (step 4).

<https://doi.org/10.1371/journal.ppat.1012411.g008>

percentage of BCC0<sup>701-899</sup> is able to localize to the daughter cell scaffold and provide sufficient function to support viability. Since  $\Delta bcc0 + BCC0^{170-899}$  and  $\Delta bcc0 + BCC0^{701-899}$  phenocopy each other, it could be possible that BCC0's primary function is carried out by the essential domain within residues 701–877, while a secondary function is carried out by residues 2–169. However, the fact that the BCC0 <sup>$\Delta 2-169$</sup>  mutant was fully functional makes this less likely. Another possibility is that these proteins are more prone to misfolding due to the very large deletions on both the N- and C-termini of the protein. While interpretation of this portion of the data is difficult, the data from the original deletion series and endogenous C-terminal truncations clearly demonstrates that residues 701–877 are necessary and residues 1–899 are sufficient for the function of BCC0.

The data presented in this study and our previous work supports a hierarchical recruitment model for the essential IMC43-IMC32-BCC0 daughter bud assembly complex (Fig 8B). In our

initial studies of IMC32, we demonstrated that mutation of the predicted palmitoylation site causes IMC32 to mislocalize to the cytoplasm [39]. In our recent work in which we identified the IMC43-IMC32 complex, we also demonstrated that IMC32 localizes independently during bud initiation, but once bud elongation begins, IMC32 must bind to IMC43 in order to maintain its striped localization [40]. The data that we present in this study shows that BCC0 becomes mislocalized upon depletion of either IMC32 or IMC43 and that its localization is dependent on its IMC32-binding domain. Together, these data suggest that IMC32 and BCC0 bind to each other either prior to or during bud initiation and recruit to the early daughter cell scaffold via palmitoylation of IMC32. Then, once bud elongation begins, IMC32 binds to IMC43, locking the IMC32-BCC0 subcomplex into the daughter cell scaffold. It remains unclear how IMC43 is recruited to the developing daughter cell scaffold since it localizes normally in the absence of either IMC32 or BCC0 and does not contain any transmembrane domains or predicted acylation sites. It may bind to another IMC protein to tether it to either the alveoli or the cytoskeletal network of the developing daughter bud. Our previous IMC43 Y2H screen identified 28 additional candidate IMC43-binding partners. Future studies will be needed to explore these proteins. Additionally, the stoichiometry of the IMC43-IMC32-BCC0 complex is unclear. It is possible that the complex forms in a 1:1:1 manner, but it is also possible that one or more of the proteins is overrepresented in the complex, potentially allowing for multiple configurations. This would likely be resolved by structural studies of the complex.

Although our work has demonstrated the critical importance of the IMC43-IMC32-BCC0 daughter bud assembly complex and has yielded a model for how each component is recruited, the precise function of the complex remains unknown. Loss of any of the three complex components results in both severe defects in IMC morphology and dysregulation of endodyogeny [39,40,46]. Engelberg et al. additionally observed that loss of BCC0 led to subtle defects in the formation of the basal complex and apical annuli on developing daughter buds, although neither structure was fully disrupted [46]. Our previous work demonstrated that basal complex formation is unaffected by loss of IMC43, so it is possible that the IMC32-BCC0 subcomplex plays a role in recruiting MORN1 to the basal complex during bud initiation, before IMC43 joins the complex. This hypothesis is further supported by the different localizations of each protein during bud initiation. At this stage, both IMC32 and BCC0 are present in five distinct puncta which Engelberg et al. showed lie directly on top of the developing basal complex [39,46]. IMC43, on the other hand, appears as a slightly smaller continuous ring that lies slightly apical to the IMC32-BCC0 puncta [40]. Recent work has demonstrated that during bud initiation, the 22 subpellicular microtubules originally appear as five bundles of microtubules in a 4 + 4 + 4 + 4 + 6 configuration [30,60]. The fact that both the IMC32-BCC0 subcomplex and the nascent SPMTs exhibit the same 5-fold symmetry strongly suggests a functional relationship between these structures. We previously demonstrated that loss of IMC32 does not prevent formation of the conoid or SPMTs [39], but it could be possible that the five bundles of SPMTs act as a foundation for the formation of the IMC32-BCC0 puncta. In future studies it will be intriguing to explore how disruption of the SPMTs at this stage affects localization of the IMC32-BCC0 subcomplex using higher resolution techniques such as ultrastructure expansion microscopy.

Another outstanding question is how the essential daughter bud assembly complex is regulated. Our model suggests that IMC43 does not bind to IMC32 until after bud elongation has begun. How the timing of this binding event is controlled remains unknown. IMC43, IMC32, and BCC0 all have multiple phosphorylation sites which could represent possible means of regulation [61]. Our IMC43 Y2H screen identified three kinases (SRPK, CDPK7, and Ark3) and one phosphatase (PPKL) as candidate binding partners. CDPK7, Ark3, and PPKL have all been shown to play important roles in *T. gondii* endodyogeny [62–64]. SRPK has not been

studied, but its phenotype score suggests it may be essential [65]. Exploring how the activity of these enzymes affects the localization or function of IMC43 and its partners will be an interesting topic of future studies. Identification of additional complex components or regulatory proteins could be achieved by performing TurboID proximity labeling and Y2H screening using BCC0 as bait. BCC0's large size may make Y2H screening challenging due to toxicity, which we observed for IMC43. However, use of an inducible bait vector circumvented this problem for IMC43 and is likely to be successful for BCC0 as well [40]. Alternatively, since residues 1–899 are sufficient for the function of BCC0, it may be more practical to use the truncated protein as bait in a Y2H screen.

Together, the data reported in this study identifies the essential daughter IMC protein BCC0 as the third component of the IMC43-IMC32-BCC0 daughter bud assembly complex and presents a model for how the complex is formed. The functional complementation studies of BCC0 also demonstrate that despite its large size, much of the protein is dispensable and its critical functions are carried out by an essential interaction domain, similar to what we previously observed for IMC43 [40]. As this complex is foundational for the construction of *T. gondii* daughter buds during endodyogeny, a parasite-specific biological function, deepening our understanding of the function and regulation of this complex is likely to facilitate the identification of novel therapeutic targets for this important pathogen.

## Materials and methods

### *T. gondii* and host cell culture

Parental *T. gondii* RH $\Delta$ hxgprt $\Delta$ ku80 (wild-type) and subsequent strains were grown on confluent monolayers of human foreskin fibroblasts (HFFs) (BJ, ATCC, Manassas, VA) at 37°C and 5% CO<sub>2</sub> in Dulbecco's Modified Eagle Medium (DMEM) supplemented with 5% fetal bovine serum (Gibco), 5% Cosmic calf serum (Hyclone), and 1x penicillin-streptomycin-L-glutamine (Gibco). Constructs containing selectable markers were selected using 1  $\mu$ M pyrimethamine (dihydrofolate reductase-thymidylate synthase [DHFR-TS]), 50  $\mu$ g/mL mycophenolic acid-xanthine (HXGPRT), or 40  $\mu$ M chloramphenicol (CAT) [66–68]. Homologous recombination to the UPRT locus was negatively selected using 5  $\mu$ M 5-fluorodeoxyuridine (FUDR) [69]. Knockdown of AID strains was performed by treating parasites with 0.5 mM IAA (Millipore Sigma, I2886). Knockdown of the BCC0<sup>cKD</sup> strain was performed by treating parasites with 1  $\mu$ g/mL ATc (Millipore Sigma, 37919).

### Antibodies

The HA epitope was detected with mouse monoclonal antibody (mAb) HA.11 (BioLegend; 901515). The Ty1 epitope was detected with mouse mAb BB2 [70]. The c-Myc epitope was detected with mouse mAb 9E10 [71]. The OLLAS epitope was detected with rat mAb anti-OLLAS [72]. *Toxoplasma*-specific antibodies include rabbit pAb anti-IMC6 [20] and rabbit anti-Catalase [73].

### Endogenous epitope tagging and knockout

For C-terminal endogenous tagging, a pU6-Universal plasmid containing a protospacer against the 3' untranslated region (UTR) of the target protein approximately 100 bp downstream of the stop codon was generated, as described previously [74,75]. A homology-directed repair (HDR) template was PCR amplified from the  $\Delta$ ku80-dependent LIC vector pmAID3xHA.LIC-HXGPRT, pmAID3xTy.LIC-HXGPRT, p3xHA.LIC-DHFR, p3xMyc.LIC-DHFR, p2xStrep3xTy.LIC-CAT, p2xStrep3xTy.LIC-HXGPRT, psmOLLAS.LIC-DHFR,

psmHA.LIC-DHFR, or pTurboID3xHA.LIC-DHFR, all of which include the epitope tag, 3' UTR, and a selection cassette [76]. The 60-bp primers include 40 bp of homology immediately upstream of the stop codon or 40 bp of homology within the 3' UTR downstream of the CRISPR/Cas9 cut site. For C-terminal truncations at the endogenous locus, the forward primer for amplifying the HDR template was designed using 40 bp of homology within the gene's coding sequence. Primers that were used for the pU6-Universal plasmid as well as the HDR template are listed in S3 Table (primers P1-P14).

For knockout of BCC0, the protospacer was designed to target an intron within the BCC0 locus, ligated into the pU6-Universal plasmid, and prepared similarly to the endogenous tagging constructs. The HDR template was PCR amplified from a pJET vector containing the HXGPRT drug marker driven by the NcGRA7 promoter using primers that included 40 bp of homology immediately upstream of the start codon or 40 bp of homology downstream of the region used for homologous recombination for endogenous tagging of BCC0 (primers P15-P18).

For all tagging and knockout constructs, approximately 50  $\mu$ g of the sequence-verified pU6-Universal plasmid and the PCR-amplified HDR template were electroporated into the appropriate parasite strain. Transfected cells were allowed to invade a confluent monolayer of HFFs overnight, and appropriate selection was applied. Successful tagging or knockout was confirmed by IFA, and clonal lines were obtained through limiting dilution. Knockout of BCC0 was verified by PCR using primers P19-P22.

### Generation of BCC0<sup>cKD</sup> strain

BCC0 was endogenously tagged with a 2xStrep3xTy epitope tag in an RH $\Delta$ ku80-Tati-HXGPRT parent strain as described above. To replace the endogenous promoter with an ATc-regulatable promoter, a pU6-Universal plasmid containing a protospacer against the 5' UTR of BCC0 approximately 250 bp upstream of the start codon was generated, as described previously [74,75]. The HDR template was PCR amplified from the pDHFR-TetO7-SAG4p vector using primers which included 40 bp of homology approximately 1 kb upstream of the start codon and 40 bp of homology immediately downstream of the start codon. Primers that were used for the pU6-Universal plasmid and the HDR template are listed in S3 Table (primers P23-P26). Clones were screened by IFA -/+ ATc (1  $\mu$ g/mL). A clonal strain that was Ty-positive in the -ATc condition and Ty-negative in the +ATc condition was isolated and designated as BCC0<sup>cKD</sup>.

### Knock-in of BCC0 complementation constructs

The BCC0 endogenous promoter (EP) was amplified from genomic DNA using primers P27 and P28. The BCC0 coding region was PCR amplified from cDNA using primers P29 and P30. The smHA tag was PCR amplified from psmHA.LIC-DHFR using primers P31 and P32. The entire plasmid except for the IMC32 promoter, coding region, and 3xHA tag was amplified from pUPRKO-EP-IMC32<sup>WT</sup>-3xHA using primers P33 and P34 [39]. The four fragments were ligated using Gibson assembly to create pUPRKO-EP-BCC0<sup>WTc</sup>-smHA (BCC0<sup>WTc</sup>). This complement vector was then linearized with PsiI-HFv2 and transfected into BCC0<sup>smOL-LAS</sup> or BCC0<sup>cKD</sup> parasites along with a pU6 that targets the UPRT coding region. Selection was performed with 5  $\mu$ g/mL 5-fluorodeoxyuridine (FUDR) for replacement of UPRT. Clones were screened by IFA, and an smHA-positive clone was isolated. BCC0<sup>WTc</sup> was used as the template to generate all deletion constructs using Q5 site-directed mutagenesis with primers P35-P64 (E0552S, NEB). The same processes for linearization, transfection, and selection were

followed for all deletion and mutant constructs. All restriction enzymes were purchased from NEB.

### Immunofluorescence assay

Confluent HFF cells were grown on glass coverslips and infected with *T. gondii*. After 24 hours, the coverslips were fixed with 3.7% formaldehyde in PBS and processed for immunofluorescence as described [77]. Primary antibodies were detected by species-specific secondary antibodies conjugated to Alexa Fluor 594/488/405 (ThermoFisher). Coverslips were mounted in Vectashield (Vector Labs), viewed with an Axio Imager.Z1 fluorescent microscope, and processed with ZEN 2.3 software (Zeiss).

### Western blot

Parasites were lysed in 1x Laemmli sample buffer with 100 mM DTT and boiled at 100°C for 5 minutes. Lysates were resolved by SDS-PAGE and transferred to nitrocellulose membranes, and proteins were detected with the appropriate primary antibody and corresponding secondary antibody conjugated to horseradish peroxidase. Chemiluminescence was induced using the SuperSignal West Pico substrate (Pierce) and imaged on a ChemiDoc XRS+ (Bio-Rad). Signal intensity was quantified using ImageLab. The adjusted volume of the Ty band (detecting BCC0<sup>cKD</sup>) relative to the adjusted volume of the corresponding catalase loading control band was plotted. Raw data for western blot quantification is shown in [S4 Table](#).

### Plaque assay

HFF monolayers were infected with 100–400 parasites and allowed to form plaques for 7 days. Cells were then fixed with ice-cold methanol and stained with crystal violet. All plaque assays were performed in triplicate. To quantify plaque number, the total number of plaques in each condition was counted manually. Plaque efficiency was calculated by dividing the number of plaques formed by the number of parasites infected in each replicate. The number of plaques or plaque efficiency for each replicate was plotted, and error bars were used to show standard deviation. To quantify plaque size, the areas of 30–50 plaques per condition were measured using ZEN software (Zeiss). BCC0<sup>cKD</sup> and BCC0<sup>cKD</sup> + BCC0<sup>Δ701–877</sup> parasites that were treated with ATc exhibited a severe defect in plaque efficiency (<8%). For these experiments, all plaques formed were measured. The mean plaque size for each replicate was plotted, and error bars were used to show standard deviation. Graphical and statistical analyses were performed using Prism GraphPad 8.0. Raw data for plaque assays is shown in [S4 Table](#).

### Affinity capture of biotinylated proteins

For affinity capture of proteins from whole cell lysates, HFF monolayers infected with IMC32<sup>TurboID</sup> or control parasites (RHΔ*hxgprt*Δ*ku80*, WT) were grown in normal media for 25 hours. Then, the media was supplemented with 150 μM biotin and parasites were allowed to grow for an additional 5 hours. Intracellular parasites in large vacuoles were collected by manual scraping, washed in PBS, and lysed in radioimmunoprecipitation assay (RIPA) buffer (50 mM Tris [pH 7.5], 150 mM NaCl, 0.1% SDS, 0.5% sodium deoxycholate, 1% NP-40) supplemented with Complete Protease Inhibitor Cocktail (Roche) for 30 min on ice. Lysates were centrifuged for 15 min at 14,000 x g to pellet insoluble material, and the supernatant was incubated with Streptavidin Plus UltraLink resin (Pierce) overnight at 4°C under gentle agitation. Beads were collected and washed five times in RIPA buffer, followed by three washes in 8 M urea buffer (50 mM Tris-HCl [pH 7.4], 150 mM NaCl) [78]. Samples were submitted for on-

bead digests and subsequently analyzed by mass spectrometry. The experiment was performed in duplicate.

### Mass spectrometry of biotinylated proteins

Purified proteins bound to streptavidin beads were reduced, alkylated, and digested by sequential addition of Lys-C and trypsin proteases. Samples were then desalted using C18 tips (Pierce) and fractionated online using a 75- $\mu\text{m}$  inner-diameter fritted fused silica capillary column with a 5- $\mu\text{m}$  pulled electrospray tip and packed in-house with 25 cm of C18 (Dr. Maisch GmbH) 1.9- $\mu\text{m}$  reversed-phase particles. The gradient was delivered by a 140-minute gradient of increasing acetonitrile and eluted directly into a Thermo Orbitrap Fusion Lumos instrument where MS/MS spectra were acquired by Data Dependent Acquisition (DDA). Data analysis was performed using ProLuCID and DTASelect2 implemented in Integrated Proteomics Pipeline IP2 (Integrated Proteomics Applications) [79–81]. Database searching was performed using a FASTA protein database containing *T. gondii* GT1-translated open reading frames downloaded from ToxoDB. Protein and peptide identifications were filtered using DTASelect and required a minimum of two unique peptides per protein and a peptide-level false positive rate of less than 5% as estimated by a decoy database strategy. Candidates were ranked by spectral count comparing IMC32<sup>TurboID</sup> versus control samples [82]. The results were filtered to include only genes that had at least a two-fold enrichment and a difference of at least 5 when comparing the average spectral counts identified in the IMC32<sup>TurboID</sup> and control samples.

### Yeast two-hybrid

Y2H screening was performed by Hybrigenics Services as previously described [44,45]. Briefly, the full-length coding sequence of IMC32<sup>C7S</sup> was cloned into the pB27 vector (N-LexA-bait-C fusion) and transformed in yeast. This construct was screened for interactions against the *T. gondii* RH strain cDNA library with 23 million interactions tested. Confidence for each interaction was assessed algorithmically (Predicted Biological Score, PBS). Results were filtered to exclude any interactions with antisense or out-of-frame prey proteins.

For pairwise Y2H assays, fragments of BCC0, IMC32, and IMC43 were cloned into the pB27 (N-LexA-bait-C fusion) or pP6 (N-GAL4<sup>AD</sup>-prey-C fusion) vectors (Hybrigenics Services) as N-terminal fusions with the LexA DNA binding domain or GAL4 activation domain, respectively. All pB27 and pP6 constructs were cloned by Gibson Assembly or Q5 site-directed mutagenesis using primers P65-P134. Pairs of pB27 and pP6 constructs were co-transformed into the L40 strain of *S. cerevisiae* [MATa his3D200trp1-901 leu2-3112 ade2 LYS2:::(4lexAop-HIS3) URA3:::(8lexAop-lacZ) GAL4]. Strains were grown overnight in permissive (-Leu/-Trp) medium, normalized to OD<sub>600</sub> = 2, then spotted in six serial dilutions onto permissive (-Leu/-Trp) and restrictive (-Leu/-Trp/-His) media. Growth was assessed after 3–5 days. Auto-activation was tested by co-transforming each pB27 fusion protein with an empty pP6 vector and co-transforming each pP6 fusion protein with an empty pB27 vector and performing spot assays for each strain as described above.

### Bioinformatic analysis of protein features

Coiled-coil domains were predicted using DeepCoil2 using a probability cut-off of 0.5 [50]. Palmitoylation sites were predicted using CSS-Palm 4.0 using a score cut-off of 5 [49]. Myristoylation sites were predicted using GPS-Lipid using a score cut-off of 5 [48]. Alpha helices and beta strands were predicted using PSIPRED using a cut-off of 5 and a minimum length of 4 amino acids for alpha helices or 3 amino acids for beta strands [57].

## Supporting information

**S1 Fig. The AID system does not provide a sufficient knockdown for analysis of BCC0 function.** A) Diagram and IFA of BCC0<sup>AID</sup> parasites grown for 24 hours +/- IAA showing that BCC0<sup>AID</sup> does not provide sufficient protein knockdown (arrow). Magenta = anti-HA detecting BCC0<sup>AID</sup>, Green = anti-IMC6. B) Diagram and IFA of BCC0<sup>IAA7</sup> parasites grown for 24 hours +/- IAA showing that BCC0<sup>IAA7</sup> does not provide sufficient protein knockdown (arrow). Magenta = anti-HA detecting BCC0<sup>IAA7</sup>, Green = anti-IMC6. Scale bars = 2  $\mu$ m. (TIF)

**S2 Fig. Conservation and secondary structure predictions for BCC0.** The amino acid sequence of BCC0 (TG GT1\_294860) was aligned to its *N. caninum* ortholog NCLIV\_001740 using ClustalO 1.2.4. Predicted features are shown above their corresponding sequences. Regions chosen for the deletion series are highlighted. (PDF)

**S3 Fig. Most BCC0 deletion constructs localize normally.** IFAs showing that all BCC0 deletions except for BCC0 <sup>$\Delta$ 701-877</sup> (shown in Fig 4D) colocalize with endogenous BCC0<sup>smOLLAS</sup>. Magenta = anti-HA detecting smHA-tagged BCC0 deletion constructs, Green = anti-OLLAS detecting endogenous BCC0<sup>smOLLAS</sup>. Scale bars = 2  $\mu$ m. (TIF)

**S4 Fig. Validation of BCC0 knockout for strains depicted in Fig 4.** A) PCR verification for genomic DNA of BCC0<sup>smOLLAS</sup> (wild-type parent strain) and complemented  $\Delta bcc0$  parasites. Diagram shows the binding location of primers used to amplify the BCC0 coding sequencing (blue arrows) and the site of recombination for the knockout (red arrows). The strain used in each PCR verification is indicated on the left of each image. B) IFA of complemented  $\Delta bcc0$  parasites confirms loss of BCC0<sup>smOLLAS</sup> signal. Each IFA in panel B corresponds with the PCR verification to the left of it in panel A. Magenta = anti-OLLAS, Green = anti-IMC6. Scale bars = 2  $\mu$ m. (TIF)

**S5 Fig. ATc treatment is toxic to wild-type *T. gondii*.** Quantification of plaque size for RH $\Delta ku80$  parasites grown for seven days +/- ATc. Statistical significance was determined using a two-tailed t-test (\*,  $P < 0.05$ ). (TIF)

**S6 Fig. Localization and PCR verification for strains depicted in Fig 6.** A) IFAs showing that BCC0<sup>170-899</sup>, BCC0<sup>376-899</sup>, BCC0<sup>570-899</sup>, and BCC0<sup>701-899</sup> all mislocalize. Magenta = anti-HA detecting smHA-tagged BCC0 deletion constructs, Green = anti-OLLAS detecting endogenous BCC0<sup>smOLLAS</sup>. Scale bars = 2  $\mu$ m. E) PCR verification for genomic DNA of complemented  $\Delta bcc0$  parasites. Diagram indicates the binding location of primers used to amplify the BCC0 coding sequencing (blue arrows) and the site of recombination for the knockout (red arrows). A control PCR verification performed on BCC0<sup>smOLLAS</sup> (wild-type) parasites can be seen in S4A Fig. (TIF)

**S1 Table. Full IMC32<sup>TurboID</sup> mass spectrometry results.** Full list of genes identified by mass spectrometry in the IMC32<sup>TurboID</sup> experiment. Spectral counts are shown for each gene. “Enrichment Diff” refers to the difference between the average spectral count in IMC32<sup>TurboID</sup> and control parasites. “Enrichment Fold” refers to the average spectral count for IMC32<sup>TurboID</sup> samples divided by the average spectral count for control samples. The second sheet labeled

“Filtered Results” shows the 1,117 genes that were at least two-fold enriched with a difference of at least five spectral counts.  
(XLSX)

**S2 Table. Full IMC32 Y2H screen results.** Full list of binding interactions identified by the Hybrigenics IMC32 Y2H screen. All clones identified for a specific gene are grouped. Clones that were found to be out-of-frame or antisense are greyed out. Global PBS indicates the confidence score assigned to each clone [44,45]. The second sheet labeled “Hits” shows the 15 genes that were identified.  
(XLSX)

**S3 Table. Oligonucleotides used in this study.**  
(XLSX)

**S4 Table. Raw data for quantification of western blot and plaque assays.**  
(XLSX)

## Acknowledgments

We thank Dominique Soldati-Favre for the catalase antibody and Michael Reese for the pP6 and pB27 plasmids, L40 strain of yeast, and protocols for pairwise Y2H assays.

## Author Contributions

**Conceptualization:** Rebecca R. Pasquarelli, Peter J. Bradley.

**Data curation:** Jihui Sha, James A. Wohlschlegel.

**Formal analysis:** Rebecca R. Pasquarelli.

**Funding acquisition:** James A. Wohlschlegel, Peter J. Bradley.

**Investigation:** Rebecca R. Pasquarelli, Jihui Sha.

**Project administration:** James A. Wohlschlegel, Peter J. Bradley.

**Resources:** James A. Wohlschlegel, Peter J. Bradley.

**Supervision:** James A. Wohlschlegel, Peter J. Bradley.

**Validation:** Rebecca R. Pasquarelli.

**Visualization:** Rebecca R. Pasquarelli.

**Writing – original draft:** Rebecca R. Pasquarelli, Jihui Sha, Peter J. Bradley.

**Writing – review & editing:** Rebecca R. Pasquarelli, Peter J. Bradley.

## References

1. Hill DE, Chirukandoth S, Dubey JP. Biology and epidemiology of *Toxoplasma gondii* in man and animals. *Anim Health Res Rev.* 2005; 6: 41–61. <https://doi.org/10.1079/ahr2005100> PMID: 16164008
2. Mackintosh CL, Beeson JG, Marsh K. Clinical features and pathogenesis of severe malaria. *Trends Parasitol.* 2004; 20: 597–603. <https://doi.org/10.1016/j.pt.2004.09.006> PMID: 15522670
3. Sow SO, Muhsen K, Nasrin D, Blackwelder WC, Wu Y, Farag TH, et al. The Burden of *Cryptosporidium* Diarrheal Disease among Children < 24 Months of Age in Moderate/High Mortality Regions of Sub-Saharan Africa and South Asia, Utilizing Data from the Global Enteric Multicenter Study (GEMS). *PLoS Negl Trop Dis.* 2016; 10: e0004729. <https://doi.org/10.1371/journal.pntd.0004729> PMID: 27219054

4. Sharman PA, Smith NC, Wallach MG, Katrib M. Chasing the golden egg: vaccination against poultry coccidiosis. *Parasite Immunol.* 2010; 32: 590–598. <https://doi.org/10.1111/j.1365-3024.2010.01209.x> PMID: 20626814
5. Kivaria FM. Estimated direct economic costs associated with tick-borne diseases on cattle in Tanzania. *Trop Anim Health Prod.* 2006; 38: 291–299. <https://doi.org/10.1007/s11250-006-4181-2> PMID: 17137131
6. Dubey JP. Review of *Neospora caninum* and neosporosis in animals. *Korean J Parasitol.* 2003; 41: 1–16. <https://doi.org/10.3347/kjp.2003.41.1.1> PMID: 12666725
7. Pappas G, Roussos N, Falagas ME. Toxoplasmosis snapshots: global status of *Toxoplasma gondii* seroprevalence and implications for pregnancy and congenital toxoplasmosis. *Int J Parasitol.* 2009; 39: 1385–1394. <https://doi.org/10.1016/j.ijpara.2009.04.003> PMID: 19433092
8. Tenter AM, Heckeroth AR, Weiss LM. *Toxoplasma gondii*: from animals to humans. *Int J Parasitol.* 2000; 30: 1217–1258. [https://doi.org/10.1016/S0020-7519\(00\)00124-7](https://doi.org/10.1016/S0020-7519(00)00124-7) PMID: 11113252
9. Luft BJ, Remington JS. Toxoplasmic Encephalitis in AIDS. *Clin Infect Dis.* 1992; 15: 211–222. <https://doi.org/10.1093/clinids/15.2.211> PMID: 1520757
10. Martin S. Congenital Toxoplasmosis. *Neonatal Netw.* 2001; 20: 23–30. <https://doi.org/10.1891/0730-0832.20.4.23> PMID: 12143899
11. Blader IJ, Coleman BI, Chen C-T, Gubbels M-J. Lytic Cycle of *Toxoplasma gondii*: 15 Years Later. *Annu Rev Microbiol.* 2015; 69: 463–485. <https://doi.org/10.1146/annurev-micro-091014-104100> PMID: 26332089
12. D'Haese J, Mehlhorn H, Peters W. Comparative electron microscope study of pellicular structures in coccidia (*Sarcocystis*, *Besnoitia* and *Eimeria*). *Int J Parasitol.* 1977; 7: 505–518. [https://doi.org/10.1016/0020-7519\(77\)90014-5](https://doi.org/10.1016/0020-7519(77)90014-5) PMID: 413801
13. Agop-Nersesian C, Naissant B, Ben Rached F, Rauch M, Kretzschmar A, Thiberge S, et al. Rab11A-Controlled Assembly of the Inner Membrane Complex Is Required for Completion of Apicomplexan Cytokinesis. Sibley LD, editor. *PLoS Pathog.* 2009; 5: e1000270. <https://doi.org/10.1371/journal.ppat.1000270> PMID: 19165333
14. Chen AL, Kim EW, Toh JY, Vashisht AA, Rashoff AQ, Van C, et al. Novel components of the *Toxoplasma* inner membrane complex revealed by BioID. *mBio.* 2015; 6: e02357–14. <https://doi.org/10.1128/mBio.02357-14> PMID: 25691595
15. Chen AL, Moon AS, Bell HN, Huang AS, Vashisht AA, Toh JY, et al. Novel insights into the composition and function of the *Toxoplasma* IMC sutures. *Cell Microbiol.* 2016; 19: e12678. <https://doi.org/10.1111/cmi.12678> PMID: 27696623
16. Beck JR, Rodriguez-Fernandez IA, Cruz de Leon J, Huynh M-H, Carruthers VB, Morrissette NS, et al. A Novel Family of *Toxoplasma* IMC Proteins Displays a Hierarchical Organization and Functions in Coordinating Parasite Division. Soldati-Favre D, editor. *PLoS Pathog.* 2010; 6: e1001094. <https://doi.org/10.1371/journal.ppat.1001094> PMID: 20844581
17. Fung C, Beck JR, Robertson SD, Gubbels M-J, Bradley PJ. *Toxoplasma* ISP4 is a central IMC sub-compartment protein whose localization depends on palmitoylation but not myristoylation. *Mol Biochem Parasitol.* 2012; 184: 99–108. <https://doi.org/10.1016/j.molbiopara.2012.05.002> PMID: 22659420
18. Mann T, Beckers C. Characterization of the subpellicular network, a filamentous membrane skeletal component in the parasite *Toxoplasma gondii*. *Mol Biochem Parasitol.* 2001; 115: 257–268. [https://doi.org/10.1016/S0166-6851\(01\)00289-4](https://doi.org/10.1016/S0166-6851(01)00289-4) PMID: 11420112
19. Anderson-White BR, Ivey FD, Cheng K, Szatanek T, Lorestani A, Beckers CJ, et al. A family of intermediate filament-like proteins is sequentially assembled into the cytoskeleton of *Toxoplasma gondii*: IMC proteins in *Toxoplasma* cell division. *Cell Microbiol.* 2011; 13: 18–31. <https://doi.org/10.1111/j.1462-5822.2010.01514.x> PMID: 20698859
20. Choi CP, Moon AS, Back PS, Jami-Alahmadi Y, Vashisht AA, Wohlschlegel JA, et al. A photoactivatable crosslinking system reveals protein interactions in the *Toxoplasma gondii* inner membrane complex. *PLoS Biol.* 2019; 17: e3000475. <https://doi.org/10.1371/journal.pbio.3000475> PMID: 31584943
21. Back PSO'Shaughnessy WJ, Moon ASDewangan PS, Reese ML, Bradley PJ Multivalent Interactions Drive the *Toxoplasma* AC9:AC10:ERK7 Complex To Concentrate ERK7 in the Apical Cap. *mBio.* 2022; 13: e0286421. <https://doi.org/10.1128/mbio.02864-21> PMID: 35130732
22. Back PSO'Shaughnessy WJ, Moon AS, Dewangan PS, Hu X, Sha J et al. Ancient MAPK ERK7 is regulated by an unusual inhibitory scaffold required for *Toxoplasma* apical complex biogenesis. *Proc Natl Acad Sci.* 2020; 117: 12164–12173. <https://doi.org/10.1073/pnas.1921245117> PMID: 32409604
23. Gaskins E, Gilk S, DeVore N, Mann T, Ward G, Beckers C. Identification of the membrane receptor of a class XIV myosin in *Toxoplasma gondii*. *J Cell Biol.* 2004; 165: 383–393. <https://doi.org/10.1083/jcb.200311137> PMID: 15123738

24. Back PS, Senthilkumar V, Choi CP, Ly AM, Snyder AK, Lau JG, et al. The Toxoplasma subpellicular network is highly interconnected and defines parasite shape for efficient motility and replication. *BioRxiv Prepr Serv Biol.* 2023; 2023.08.10.552545. <https://doi.org/10.1101/2023.08.10.552545> PMID: 37609316
25. Gubbels M-J, Ferguson DJP, Saha S, Romano JD, Chavan S, Primo VA, et al. Toxoplasma gondii's Basal Complex: The Other Apicomplexan Business End Is Multifunctional. *Front Cell Infect Microbiol.* 2022; 12: 882166. <https://doi.org/10.3389/fcimb.2022.882166> PMID: 35573773
26. Nichols BA, Chiappino ML. Cytoskeleton of Toxoplasma gondii. *J Protozool.* 1987; 34: 217–226. <https://doi.org/10.1111/j.1550-7408.1987.tb03162.x> PMID: 3585817
27. Gubbels M-J, Keroack CD, Dangoudoubiyam S, Worliczek HL, Paul AS, Bauwens C, et al. Fussing About Fission: Defining Variety Among Mainstream and Exotic Apicomplexan Cell Division Modes. *Front Cell Infect Microbiol.* 2020; 10: 269. <https://doi.org/10.3389/fcimb.2020.00269> PMID: 32582569
28. Francia ME, Striepen B. Cell division in apicomplexan parasites. *Nat Rev Microbiol.* 2014; 12: 125–136. <https://doi.org/10.1038/nrmicro3184> PMID: 24384598
29. Frénel K, Jacot D, Hammoudi P-M, Graindorge A, Maco B, Soldati-Favre D. Myosin-dependent cell-cell communication controls synchronicity of division in acute and chronic stages of Toxoplasma gondii. *Nat Commun.* 2017; 8: 15710. <https://doi.org/10.1038/ncomms15710> PMID: 28593938
30. Padilla LFA, Murray JM, Hu K. The initiation and early development of the tubulin-containing cytoskeleton in the human parasite Toxoplasma gondii. *Mol Biol Cell.* 2024; 35: ar37. <https://doi.org/10.1091/mbc.E23-11-0418> PMID: 38170577
31. Chen C-T, Gubbels M-J. The Toxoplasma gondii centrosome is the platform for internal daughter budding as revealed by a Nek1 kinase mutant. *J Cell Sci.* 2013; 126: 3344–3355. <https://doi.org/10.1242/jcs.123364> PMID: 23729737
32. Suvorova ES, Francia M, Striepen B, White MW. A Novel Bipartite Centrosome Coordinates the Apicomplexan Cell Cycle. Pellman D, editor. *PLOS Biol.* 2015; 13: e1002093. <https://doi.org/10.1371/journal.pbio.1002093> PMID: 25734885
33. Anderson-White B, Beck JR, Chen C-T, Meissner M, Bradley PJ, Gubbels M-J. Cytoskeleton assembly in Toxoplasma gondii cell division. *Int Rev Cell Mol Biol.* 2012; 298: 1–31. <https://doi.org/10.1016/B978-0-12-394309-5.00001-8> PMID: 22878103
34. Morrisette NS, Sibley LD. Disruption of microtubules uncouples budding and nuclear division in Toxoplasma gondii. *J Cell Sci.* 2002; 115: 1017–1025. <https://doi.org/10.1242/jcs.115.5.1017> PMID: 11870220
35. Hu K. Organizational Changes of the Daughter Basal Complex during the Parasite Replication of Toxoplasma gondii. Carruthers VB, editor. *PLoS Pathog.* 2008; 4: e10. <https://doi.org/10.1371/journal.ppat.0040010> PMID: 18208326
36. Behnke MS, Wootton JC, Lehmann MM, Radke JB, Lucas O, Nawas J, et al. Coordinated progression through two subtranscriptomes underlies the tachyzoite cycle of Toxoplasma gondii. *PLoS One.* 2010; 5: e12354. <https://doi.org/10.1371/journal.pone.0012354> PMID: 20865045
37. Ouologuem DT, Roos DS. Dynamics of the Toxoplasma gondii inner membrane complex. *J Cell Sci.* 2014; jcs.147736. <https://doi.org/10.1242/jcs.147736> PMID: 24928899
38. Back PS, Moon AS, Pasquarelli RR, Bell HN, Torres JA, Chen AL, et al. IMC29 Plays an Important Role in Toxoplasma Endodyogeny and Reveals New Components of the Daughter-Enriched IMC Proteome. *mBio.* 2023; e0304222. <https://doi.org/10.1128/mbio.03042-22> PMID: 36622147
39. Torres JA, Pasquarelli RR, Back PS, Moon AS, Bradley PJ. Identification and Molecular Dissection of IMC32, a Conserved Toxoplasma Inner Membrane Complex Protein That Is Essential for Parasite Replication. *mBio.* 2021; 12: e03622–20. <https://doi.org/10.1128/mBio.03622-20> PMID: 33593973
40. Pasquarelli RR, Back PS, Sha J, Wohlschlegel JA, Bradley PJ. Identification of IMC43, a novel IMC protein that collaborates with IMC32 to form an essential daughter bud assembly complex in Toxoplasma gondii. *PLoS Pathog.* 2023; 19: e1011707. <https://doi.org/10.1371/journal.ppat.1011707> PMID: 37782662
41. Baptista CG, Lis A, Deng B, Gas-Pascual E, Dittmar A, Sigurdson W, et al. Toxoplasma F-box protein 1 is required for daughter cell scaffold function during parasite replication. Gubbels M-J, editor. *PLOS Pathog.* 2019; 15: e1007946. <https://doi.org/10.1371/journal.ppat.1007946> PMID: 31348812
42. Lorestani A, Sheiner L, Yang K, Robertson SD, Sahoo N, Brooks CF, et al. A Toxoplasma MORN1 null mutant undergoes repeated divisions but is defective in basal assembly, apicoplast division and cytokinesis. *PLoS One.* 2010; 5: e12302. <https://doi.org/10.1371/journal.pone.0012302> PMID: 20808817
43. Branon TC, Bosch JA, Sanchez AD, Udeshi ND, Svinkina T, Carr SA, et al. Efficient proximity labeling in living cells and organisms with TurboID. *Nat Biotechnol.* 2018; 36: 880–887. <https://doi.org/10.1038/nbt.4201> PMID: 30125270

44. Rain JC, Selig L, De Reuse H, Battaglia V, Reverdy C, Simon S, et al. The protein-protein interaction map of *Helicobacter pylori*. *Nature*. 2001; 409: 211–215. <https://doi.org/10.1038/35051615> PMID: 11196647
45. Formstecher E, Aresta S, Collura V, Hamburger A, Meil A, Trehin A, et al. Protein interaction mapping: a *Drosophila* case study. *Genome Res*. 2005; 15: 376–384. <https://doi.org/10.1101/gr.2659105> PMID: 15710747
46. Engelberg K, Bechtel T, Michaud C, Weerapana E, Gubbels M-J. Proteomic characterization of the *Toxoplasma gondii* cytokinesis machinery portrays an expanded hierarchy of its assembly and function. *Nat Commun*. 2022; 13: 4644. <https://doi.org/10.1038/s41467-022-32151-0> PMID: 35941170
47. Amos B, Aurrecochea C, Barba M, Barreto A, Basenko EY, Bazant W, et al. VEuPathDB: the eukaryotic pathogen, vector and host bioinformatics resource center. *Nucleic Acids Res*. 2022; 50: D898–D911. <https://doi.org/10.1093/nar/gkab929> PMID: 34718728
48. Xie Y, Zheng Y, Li H, Luo X, He Z, Cao S, et al. GPS-Lipid: a robust tool for the prediction of multiple lipid modification sites. *Sci Rep*. 2016; 6: 28249. <https://doi.org/10.1038/srep28249> PMID: 27306108
49. Ren J, Wen L, Gao X, Jin C, Xue Y, Yao X. CSS-Palm 2.0: an updated software for palmitoylation sites prediction. *Protein Eng Des Sel*. 2008; 21: 639–644. <https://doi.org/10.1093/protein/gzn039> PMID: 18753194
50. Ludwiczak J, Winski A, Szczepaniak K, Alva V, Dunin-Horkawicz S. DeepCoil—a fast and accurate prediction of coiled-coil domains in protein sequences. *Bioinform Oxf Engl*. 2019; 35: 2790–2795. <https://doi.org/10.1093/bioinformatics/bty1062> PMID: 30601942
51. Lupas A, Van Dyke M, Stock J. Predicting coiled coils from protein sequences. *Science*. 1991; 252: 1162–1164. <https://doi.org/10.1126/science.252.5009.1162> PMID: 2031185
52. Nishimura K, Fukagawa T, Takisawa H, Kakimoto T, Kanemaki M. An auxin-based degron system for the rapid depletion of proteins in nonplant cells. *Nat Methods*. 2009; 6: 917–922. <https://doi.org/10.1038/nmeth.1401> PMID: 19915560
53. Brown KM, Long S, Sibley LD. Plasma Membrane Association by N-Acylation Governs PKG Function in *Toxoplasma gondii*. *mBio*. 2017; 8: e00375–17. <https://doi.org/10.1128/mBio.00375-17> PMID: 28465425
54. Li S, Prasanna X, Salo VT, Vattulainen I, Ikonen E. An efficient auxin-inducible degron system with low basal degradation in human cells. *Nat Methods*. 2019; 16: 866–869. <https://doi.org/10.1038/s41592-019-0512-x> PMID: 31451765
55. Meissner M. Role of *Toxoplasma gondii* Myosin A in Powering Parasite Gliding and Host Cell Invasion. *Science*. 2002; 298: 837–840. <https://doi.org/10.1126/science.1074553> PMID: 12399593
56. Beck JR, Chen AL, Kim EW, Bradley PJ. RON5 Is Critical for Organization and Function of the *Toxoplasma* Moving Junction Complex. *PLoS Pathog*. 2014; 10. <https://doi.org/10.1371/journal.ppat.1004025> PMID: 24651769
57. Buchan DWA, Jones DT. The PSIPRED Protein Analysis Workbench: 20 years on. *Nucleic Acids Res*. 2019; 47: W402–W407. <https://doi.org/10.1093/nar/gkz297> PMID: 31251384
58. Fréchal K, Polonais V, Marq J-B, Stratmann R, Limenitakis J, Soldati-Favre D. Functional dissection of the apicomplexan glideosome molecular architecture. *Cell Host Microbe*. 2010; 8: 343–357. <https://doi.org/10.1016/j.chom.2010.09.002> PMID: 20951968
59. De Napoli MG, de Miguel N, Lebrun M, Moreno SNJ, Angel SO, Corvi MM. N-terminal palmitoylation is required for *Toxoplasma gondii* HSP20 inner membrane complex localization. *Biochim Biophys Acta BBA—Mol Cell Res*. 2013; 1833: 1329–1337. <https://doi.org/10.1016/j.bbamcr.2013.02.022> PMID: 23485398
60. Li Z, Du W, Yang J, Lai D-H, Lun Z-R, Guo Q. Cryo-Electron Tomography of *Toxoplasma gondii* Indicates That the Conoid Fiber May Be Derived from Microtubules. *Adv Sci Weinh Baden-Wuertt Ger*. 2023; 10: e2206595. <https://doi.org/10.1002/advs.202206595> PMID: 36840635
61. Trecek M, Sanders JL, Elias JE, Boothroyd JC. The Phosphoproteomes of *Plasmodium falciparum* and *Toxoplasma gondii* Reveal Unusual Adaptations Within and Beyond the Parasites' Boundaries. *Cell Host Microbe*. 2011; 10: 410–419. <https://doi.org/10.1016/j.chom.2011.09.004> PMID: 22018241
62. Morlon-Guyot J, Berry L, Chen C-T, Gubbels M-J, Lebrun M, Daher W. The *Toxoplasma gondii* calcium-dependent protein kinase 7 is involved in early steps of parasite division and is crucial for parasite survival. *Cell Microbiol*. 2014; 16: 95–114. <https://doi.org/10.1111/cmi.12186> PMID: 24011186
63. Berry L, Chen C-T, Reiningger L, Carvalho TG, El Hajj H, Morlon-Guyot J, et al. The conserved apicomplexan Aurora kinase TgArk3 is involved in endodyogeny, duplication rate and parasite virulence. *Cell Microbiol*. 2016; 18: 1106–1120. <https://doi.org/10.1111/cmi.12571> PMID: 26833682
64. Guttery DS, Poulin B, Ferguson DJP, Szöör B, Wickstead B, Carroll PL, et al. A unique protein phosphatase with kelch-like domains (PPKL) in *Plasmodium* modulates ookinete differentiation, motility and

- invasion. *PLoS Pathog.* 2012; 8: e1002948. <https://doi.org/10.1371/journal.ppat.1002948> PMID: 23028336
65. Sidik SM, Huet D, Ganesan SM, Huynh M-H, Wang T, Nasamu AS, et al. A Genome-wide CRISPR Screen in *Toxoplasma* Identifies Essential Apicomplexan Genes. *Cell.* 2016; 166: 1423–1435. e12. <https://doi.org/10.1016/j.cell.2016.08.019> PMID: 27594426
  66. Donald RG, Roos DS. Stable molecular transformation of *Toxoplasma gondii*: a selectable dihydrofolate reductase-thymidylate synthase marker based on drug-resistance mutations in malaria. *Proc Natl Acad Sci U S A.* 1993; 90: 11703–11707. <https://doi.org/10.1073/pnas.90.24.11703> PMID: 8265612
  67. Kim K, Soldati D, Boothroyd JC. Gene replacement in *Toxoplasma gondii* with chloramphenicol acetyltransferase as selectable marker. *Science.* 1993; 262: 911–914. <https://doi.org/10.1126/science.8235614> PMID: 8235614
  68. Donald RG, Carter D, Ullman B, Roos DS. Insertional tagging, cloning, and expression of the *Toxoplasma gondii* hypoxanthine-xanthine-guanine phosphoribosyltransferase gene: Use as a selectable marker for stable transformation. *J Biol Chem.* 1996; 271: 14010–14019. <https://doi.org/10.1074/jbc.271.24.14010> PMID: 8662859
  69. Donald RG, Roos DS. Insertional mutagenesis and marker rescue in a protozoan parasite: cloning of the uracil phosphoribosyltransferase locus from *Toxoplasma gondii*. *Proc Natl Acad Sci U S A.* 1995; 92: 5749–5753. <https://doi.org/10.1073/pnas.92.12.5749> PMID: 7777580
  70. Bastin P, Bagherzadeh Z, Matthews KR, Gull K. A novel epitope tag system to study protein targeting and organelle biogenesis in *Trypanosoma brucei*. *Mol Biochem Parasitol.* 1996; 77: 235–239. [https://doi.org/10.1016/0166-6851\(96\)02598-4](https://doi.org/10.1016/0166-6851(96)02598-4) PMID: 8813669
  71. Evan GI, Lewis GK, Ramsay G, Bishop JM. Isolation of monoclonal antibodies specific for human c-myc proto-oncogene product. *Mol Cell Biol.* 1985; 5: 3610–3616. <https://doi.org/10.1128/mcb.5.12.3610-3616.1985> PMID: 3915782
  72. Viswanathan S, Williams ME, Bloss EB, Stasevich TJ, Speer CM, Nern A, et al. High-performance probes for light and electron microscopy. *Nat Methods.* 2015; 12: 568–576. <https://doi.org/10.1038/nmeth.3365> PMID: 25915120
  73. Bullen HE, Jia Y, Yamaryo-Botté Y, Bisio H, Zhang O, Jemelin NK, et al. Phosphatidic Acid-Mediated Signaling Regulates Microneme Secretion in *Toxoplasma*. *Cell Host Microbe.* 2016; 19: 349–360. <https://doi.org/10.1016/j.chom.2016.02.006> PMID: 26962945
  74. Sidik SM, Hackett CG, Tran F, Westwood NJ, Lourido S. Efficient Genome Engineering of *Toxoplasma gondii* Using CRISPR/Cas9. Blader LJ, editor. *PLoS ONE.* 2014; 9: e100450. <https://doi.org/10.1371/journal.pone.0100450> PMID: 24971596
  75. Shen B, Brown KM, Lee TD, Sibley LD. Efficient Gene Disruption in Diverse Strains of *Toxoplasma gondii* Using CRISPR/CAS9. Weiss LM, editor. *mBio.* 2014; 5: e01114–14. <https://doi.org/10.1128/mBio.01114-14> PMID: 24825012
  76. Huynh M-H, Carruthers VB. Tagging of endogenous genes in a *Toxoplasma gondii* strain lacking Ku80. *Eukaryot Cell.* 2009; 8: 530–539. <https://doi.org/10.1128/EC.00358-08> PMID: 19218426
  77. Bradley PJ, Ward C, Cheng SJ, Alexander DL, Coller S, Coombs GH, et al. Proteomic analysis of rhoptry organelles reveals many novel constituents for host-parasite interactions in *Toxoplasma gondii*. *J Biol Chem.* 2005; 280: 34245–34258. <https://doi.org/10.1074/jbc.M504158200> PMID: 16002398
  78. Bradley PJ, Rayatpisheh S, Wohlschlegel JA, Nadipuram SM. Using BioID for the Identification of Interacting and Proximal Proteins in Subcellular Compartments in *Toxoplasma gondii*. *Methods Mol Biol Clifton NJ.* 2020; 2071: 323–346. [https://doi.org/10.1007/978-1-4939-9857-9\\_18](https://doi.org/10.1007/978-1-4939-9857-9_18) PMID: 31758461
  79. Xu T, Park SK, Venable JD, Wohlschlegel JA, Diedrich JK, Cociorva D, et al. ProLuCID: An improved SEQUEST-like algorithm with enhanced sensitivity and specificity. *J Proteomics.* 2015; 129: 16–24. <https://doi.org/10.1016/j.jprot.2015.07.001> PMID: 26171723
  80. Tabb DL, McDonald WH, Yates JR. DTASelect and Contrast: Tools for Assembling and Comparing Protein Identifications from Shotgun Proteomics. *J Proteome Res.* 2002; 1: 21–26. <https://doi.org/10.1021/pr015504q> PMID: 12643522
  81. Cociorva D, L. Tabb D, Yates JR. Validation of Tandem Mass Spectrometry Database Search Results Using DTASelect. *Curr Protoc Bioinforma.* 2006; 16: 13.4.1–13.4.14. <https://doi.org/10.1002/0471250953.bi1304s16>
  82. Florens L, Carozza MJ, Swanson SK, Fournier M, Coleman MK, Workman JL, et al. Analyzing chromatin remodeling complexes using shotgun proteomics and normalized spectral abundance factors. *Methods.* 2006; 40: 303–311. <https://doi.org/10.1016/j.ymeth.2006.07.028> PMID: 17101441
  83. Barylyuk K, Koreny L, Ke H, Butterworth S, Crook OM, Lassadi I, et al. A Comprehensive Subcellular Atlas of the *Toxoplasma* Proteome via hyperLOPIT Provides Spatial Context for Protein Functions. *Cell Host Microbe.* 2020; 28: 752–766. e9. <https://doi.org/10.1016/j.chom.2020.09.011> PMID: 33053376

### 3.8 Supplemental Material

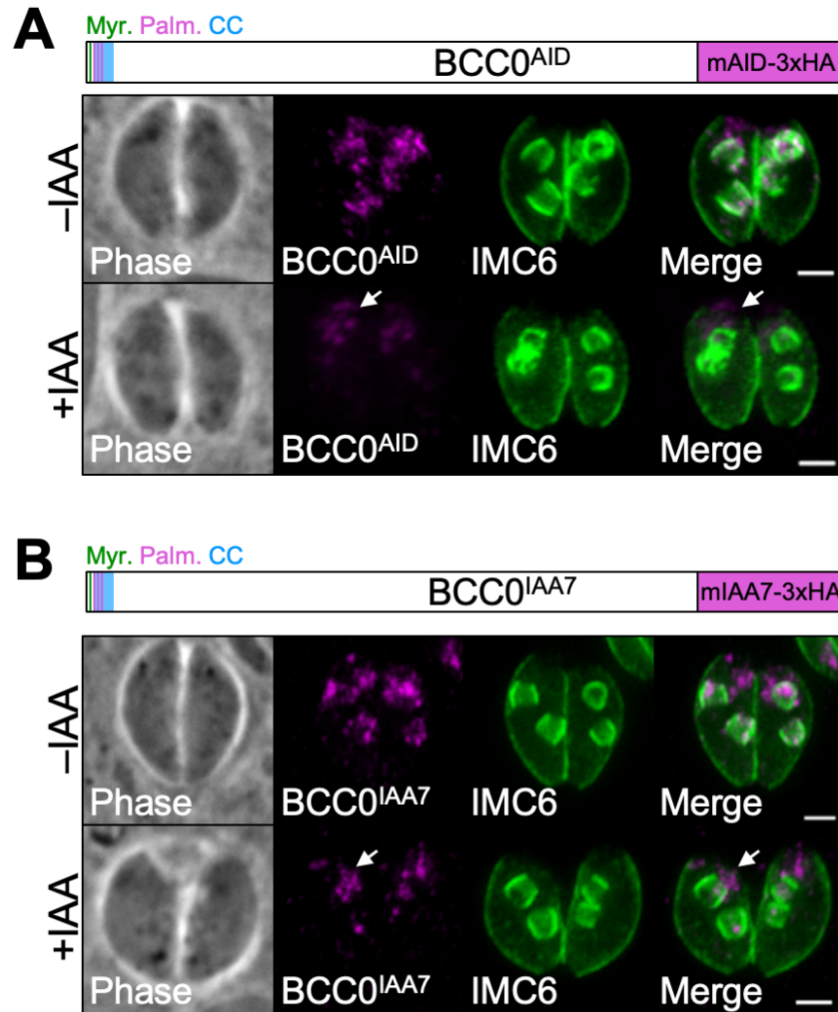


**Figure 3-S1. The AID system does not provide a sufficient knockdown for analysis of BCC0 function.** A) Diagram and IFA of BCC0<sup>AID</sup> parasites grown for 24 hours +/- IAA showing that BCC0<sup>AID</sup> does not provide sufficient protein knockdown (arrow). Magenta = anti-HA detecting BCC0<sup>AID</sup>, Green = anti-IMC6. B) Diagram and IFA of BCC0<sup>IAA7</sup> parasites grown for 24 hours +/- IAA showing that BCC0<sup>IAA7</sup> does not provide sufficient protein knockdown (arrow). Magenta = anti-HA detecting BCC0<sup>IAA7</sup>, Green = anti-IMC6. Scale bars = 2  $\mu$ m.





**Figure 3-S2. Conservation and secondary structure predictions for BCC0.** The amino acid sequence of BCC0 (TGGT1\_294860) was aligned to its *N. caninum* ortholog NCLIV\_001740 using ClustalO 1.2.4. Predicted features are shown above their corresponding sequences. Regions chosen for the deletion series are highlighted.

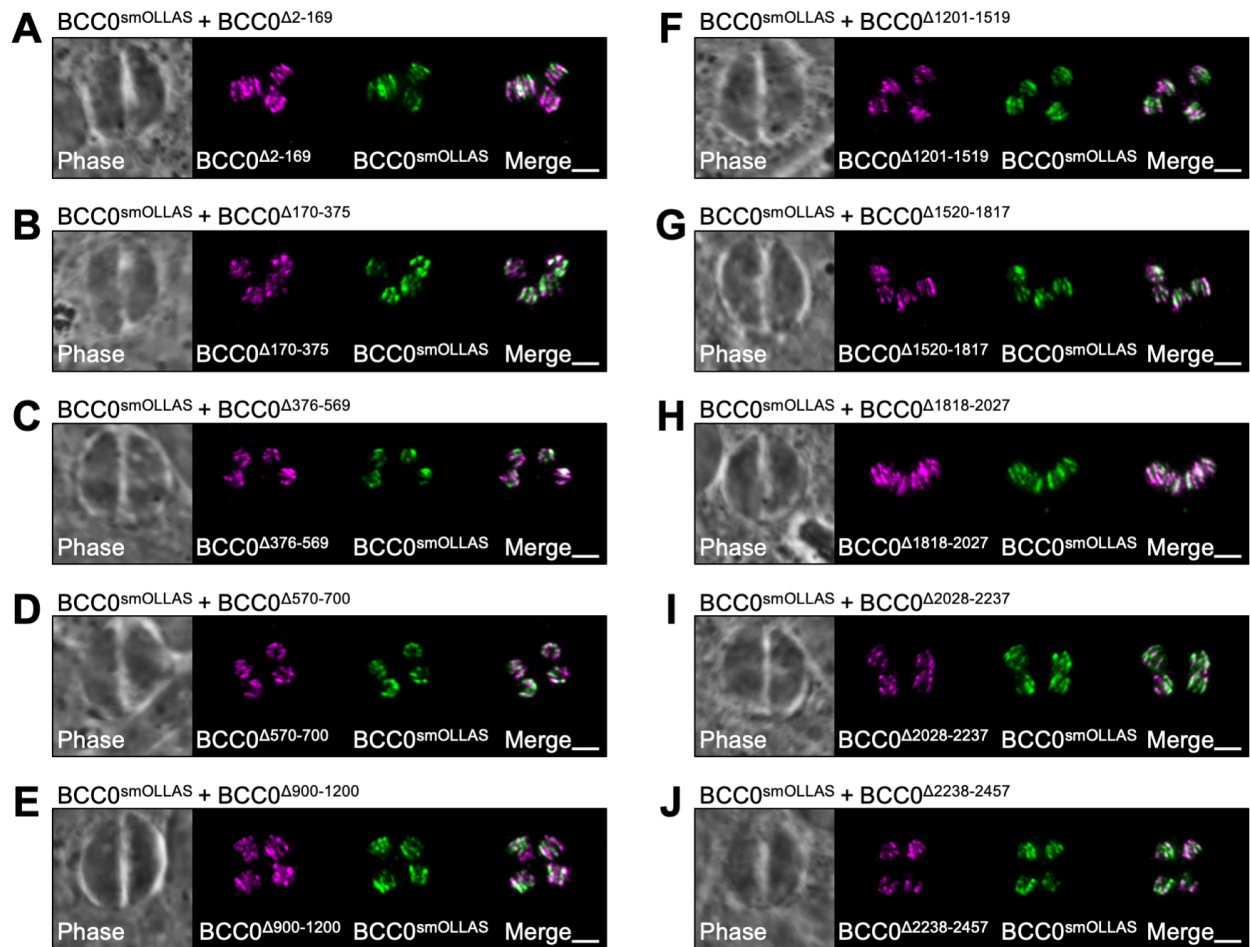


**Figure 3-S3. Most BCC0 deletion constructs localize normally.** IFAs showing that all BCC0 deletions except for  $BCC0^{\Delta 701-877}$  (shown in Fig 3-4D) colocalize with endogenous  $BCC0^{smOLLAS}$ . Magenta = anti-HA detecting smHA-tagged BCC0 deletion constructs, Green = anti-OLLAS detecting endogenous  $BCC0^{smOLLAS}$ . Scale bars = 2  $\mu$ m.



**Figure 3-S4. Validation of BCC0 knockout for strains depicted in Fig 3-4.** A) PCR verification for genomic DNA of BCC0<sup>smOLLAS</sup> (wild-type parent strain) and complemented  $\Delta bcc0$  parasites. Diagram shows the binding location of primers used to amplify the BCC0 coding sequencing (blue arrows) and the site of recombination for the knockout (red arrows). The strain used in each PCR verification is indicated on the left of each image. B) IFA of complemented  $\Delta bcc0$  parasites confirms loss of BCC0<sup>smOLLAS</sup> signal. Each IFA in panel B corresponds with the PCR verification to the left of it in panel A. Magenta = anti-OLLAS, Green = anti-IMC6. Scale bars = 2  $\mu$ m.

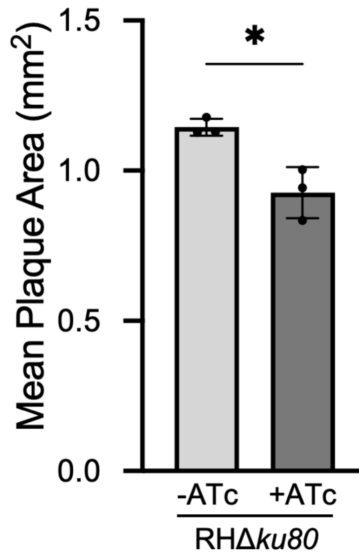


**Figure 3-S5. ATc treatment is toxic to wild-type *T. gondii*.** Quantification of plaque size for RHΔku80 parasites grown for seven days -/+ ATc. Statistical significance was determined using a two-tailed t-test (\*,  $P < 0.05$ ).

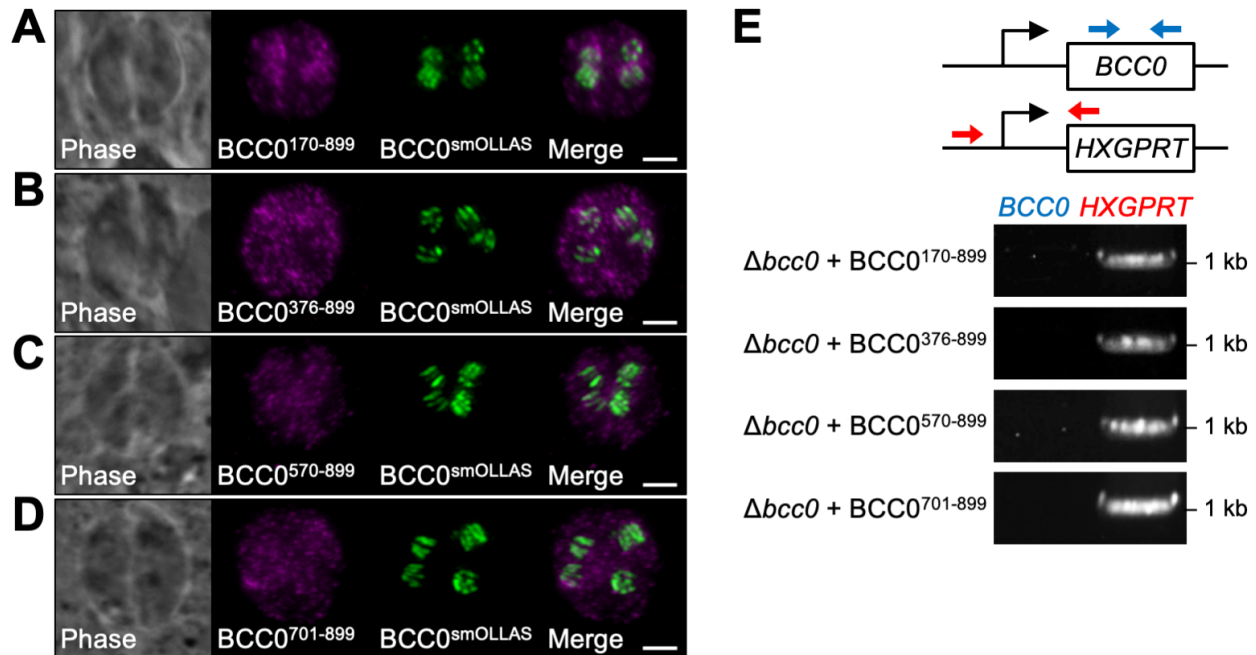


**Figure 3-S6. Localization and PCR verification for strains depicted in Fig 3-6.** A) IFAs showing that BCC0<sup>170-899</sup>, BCC0<sup>376-899</sup>, BCC0<sup>570-899</sup>, and BCC0<sup>701-899</sup> all mislocalize. Magenta = anti-HA detecting smHA-tagged BCC0 deletion constructs, Green = anti-OLLAS detecting endogenous BCC0<sup>smOLLAS</sup>. Scale bars = 2  $\mu$ m. E) PCR verification for genomic DNA of complemented  $\Delta bcc0$  parasites. Diagram indicates the binding location of primers used to amplify the BCC0 coding sequencing (blue arrows) and the site of recombination for the knockout (red arrows). A control PCR verification performed on BCC0<sup>smOLLAS</sup> (wild-type) parasites can be seen in Fig 3-S4A.

**Table 3-S1. Full IMC32<sup>TurboID</sup> mass spectrometry results.** Full list of genes identified by mass spectrometry in the IMC32<sup>TurboID</sup> experiment. Spectral counts are shown for each gene. “Enrichment Diff” refers to the difference between the average spectral count in IMC32<sup>TurboID</sup> and control parasites. “Enrichment Fold” refers to the average spectral count for IMC32<sup>TurboID</sup> samples divided by the average spectral count for control samples. The second sheet labeled “Filtered Results” shows the 1,117 genes that were at least two-fold enriched with a difference of at least five spectral counts.

<https://doi.org/10.1371/journal.ppat.1012411.s007>

**Table 3-S2. Full IMC32 Y2H screen results.** Full list of binding interactions identified by the Hybrigenics IMC32 Y2H screen. All clones identified for a specific gene are grouped. Clones that were found to be out-of-frame or antisense are greyed out. Global PBS indicates the confidence score assigned to each clone [44,45]. The second sheet labeled “Hits” shows the 15 genes that were identified.

<https://doi.org/10.1371/journal.ppat.1012411.s008>

**Table 3-S3. Oligonucleotides used in this study.**

<https://doi.org/10.1371/journal.ppat.1012411.s009>

**Table 3-S4. Raw data for quantification of western blot and plaque assays.**

<https://doi.org/10.1371/journal.ppat.1012411.s010>

## **Chapter 4:**

### Conclusions and Future Directions

## 4.1 Conclusions

This dissertation reveals the existence of an essential daughter bud assembly complex in *T. gondii* composed of the early daughter proteins IMC43, IMC32, and BCC0. It also identifies the dynamically localizing daughter IMC protein IMC44. All four of these proteins are recruited during bud initiation, the earliest stage of endodyogeny (Figure 4-1). We use conditional knockdown approaches to demonstrate that loss of IMC43, IMC32, or BCC0 results in lethal defects in IMC morphology and dysregulation of endodyogeny. Using a combination of deletion analyses and pairwise Y2H assays, we identify which domains of each protein are required for their localization and function and dissect the binding interactions (Figure 3-8A). For IMC43, residues 1441-1561 near the C-terminus of the protein are required for the protein's function, but not its localization. This same region is also involved in binding to IMC32 at its C-terminal coiled-coil domains and

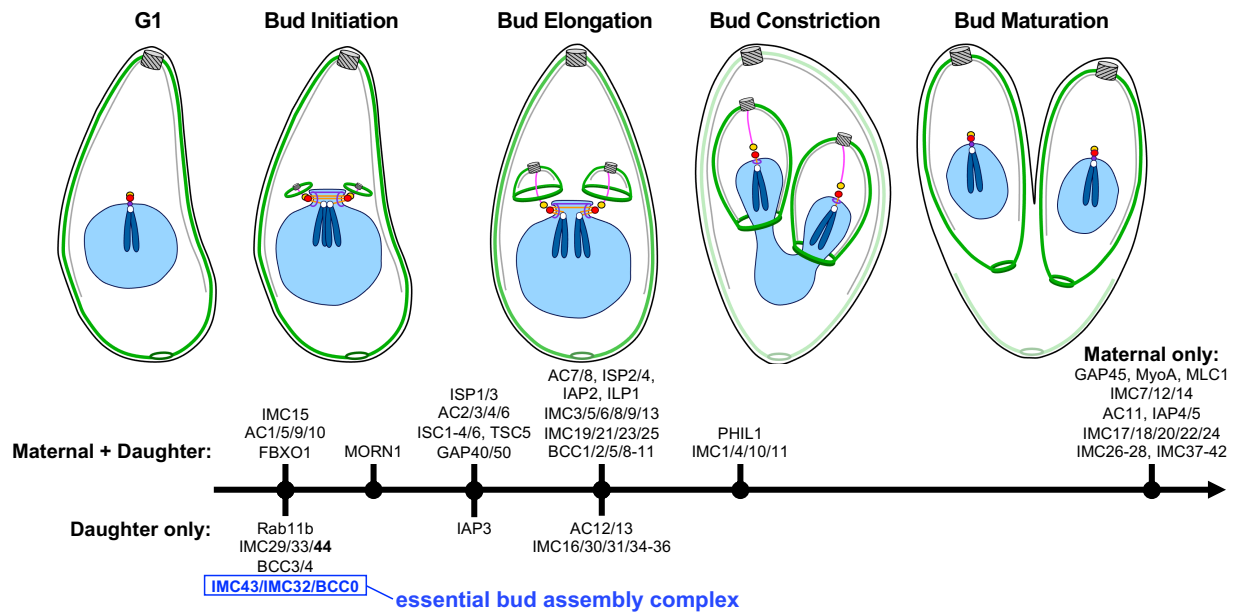


**Figure 4-1. Updated timeline of the sequential recruitment of IMC proteins during endodyogeny.** Timeline showing the sequential recruitment of proteins to the developing daughter cell scaffold, updated to reflect the new data reported in this dissertation. Each node represents the approximate point at which each listed protein is recruited relative to the stages of endodyogeny shown above. Newly identified protein IMC44 is bold. The newly identified IMC43/IMC32/BCC0 essential daughter bud assembly complex is highlighted in blue. Diagram is adapted from Gubbels et al. 2020.

controls IMC32's localization after budding has been initiated. Interestingly, the same domain was also found to bind to IMC44 and control its localization to the body of the daughter IMC. For BCC0, residues 701-877 are required for both localization and function, which is dependent on binding to IMC32's C-terminal coiled-coil domains at this region. Our previous work on IMC32 just prior to the start of this dissertation demonstrated that IMC32's localization and function depend on both its predicted N-terminal palmitoylation site and its C-terminal coiled-coil domains [1].

By combining these data, we constructed a model for how the essential daughter bud assembly complex is formed (Figure 3-8B). The expression of IMC proteins is tightly transcriptionally regulated in a "just-in-time" manner. For all three components of the complex, expression levels are at their lowest during G1 and then peak during S-phase just before bud initiation, at which point an increased cytoplasmic signal is visible by IFA. During this stage, BCC0 likely binds to IMC32. Once budding is initiated, all three components are immediately recruited to the duplicated centrosomes where they form the early daughter cell scaffold. IMC43 is recruited during bud initiation independently of IMC32 and BCC0, possibly by binding to another unidentified complex component. At this stage, IMC43 appears in a small ring. The IMC32-BCC0 subcomplex is likely recruited by palmitoylation of IMC32 and may be secondarily supported by palmitoylation and/or myristoylation of BCC0, although it is not required. At this stage, IMC32 and BCC0 both appear in five distinct puncta which are arranged symmetrically around the slightly smaller IMC43 ring. Since IMC32's localization is not dependent on IMC43 at this stage, it is likely that these two proteins only directly interact once bud elongation has begun. Binding of IMC43 to the IMC32-BCC0 subcomplex during bud elongation is required for the maintenance of both IMC32 and BCC0's organization into five longitudinal stripes on the body of the daughter IMC, indicating that palmitoylation alone is not sufficient to maintain IMC32's association with the alveoli throughout endodyogeny. This suggests that IMC43-IMC32 binding securely locks IMC32 (and therefore also BCC0, which remains bound to IMC32) into the daughter cell scaffold.

## 4.2 Future Directions

This dissertation expanded our understanding of how the early daughter IMC is formed and opened several interesting questions that should be explored in future studies. One of these questions regards the conservation of the essential daughter bud assembly complex in other apicomplexan parasites. While IMC32 is conserved across the phylum, BCC0 is restricted to the family Sarcocystidae (excluding *Sarcocystis* spp.) and IMC43 is restricted even further to only species within the genera *Neospora*, *Hammondia*, and *Besnoitia* [1,2]. The *P. falciparum* ortholog of IMC32 is predicted to be essential in the asexual blood stage [3]. It is therefore curious that IMC43, which is required for the localization of IMC32, is not present in these parasites. It is possible that other apicomplexans do contain an ortholog of IMC43, but it has diverged enough to be unrecognizable by sequence homology. Supporting this, the sequence of IMC32 is highly divergent despite having significant structural homology to *Plasmodium* IMC32 [4,5]. The presence of small proteins in *Sarcocystis neurona* and *Cystoisospora suis* which both have significant homology to the essential interaction domain of IMC43 further supports this hypothesis. However, it is also possible that IMC32 evolved to localize independently in other parasites, or that it relies on binding to a different partner. Studies on the function of IMC32 in *P. falciparum* or other apicomplexan parasites will be needed to answer this question.

Another open question is the functional significance of the five-fold symmetry of IMC32 and BCC0 on the daughter cell scaffold. While it has been suggested that the five stripes of BCC0 correspond to the longitudinal IMC sutures, BCC0 has never been colocalized with an IMC sutures protein and thus this claim is not definitive [6]. In our previous work, we visualized IMC32 alongside the suture marker ISC6 and did not observe a clear colocalization between the two proteins [1]. However, an important caveat to note is that ISC6 is present on the maternal IMC sutures as well, which makes it difficult to visualize the daughter IMC sutures. We also assessed this using widefield fluorescence microscopy, which has limited resolution. In future studies,

IMC32 and BCC0 should be compared to a daughter-specific IMC sutures marker such as BCC3 or DHHC14, and a higher resolution technique such as ultrastructure expansion microscopy (U-ExM) and/or super-resolution microscopy should be used to assess their colocalization.

An important clue towards the relevance of the five IMC32/BCC0 puncta was uncovered in the last year as it was reported that the 22 subpellicular microtubules are initially formed in five bundles during bud initiation in a 4 + 4 + 4 + 4 + 6 configuration [7,8]. These studies demonstrated that the conoid initially appears as a small arc with just a few microtubules extending from it. This arc then extends and closes into a circle, with additional microtubules being nucleated as the conoid arc grows. Since the symmetry of the subpellicular microtubule bundles matches that of the IMC32/BCC0 puncta, it is possible that one lays the foundation for the other. We previously demonstrated that loss of IMC32 does not prevent formation of the conoid or SPMTs [1]. However, it could be possible that the five microtubule bundles serve as a docking site for vesicles transported from the Golgi by Rab11b, thus bringing the membrane-associated IMC32-BCC0 subcomplex to the daughter cell scaffold [9]. Visualization of IMC32 and BCC0 alongside the tubulin structures of the early daughter cell scaffold by U-ExM would help determine which of these structures appears first during bud initiation. It would also be informative to observe how IMC32 and BCC0 are affected by disrupting formation of the subpellicular microtubules either through conditional knockdown of tubulin or treatment with the microtubule depolymerizing drug oryzalin [10,11].

Another open question is how IMC43, IMC32, and BCC0 are regulated, both individually and as a complex. Each of these proteins is transcriptionally upregulated during S-phase, but the mechanism by which this occurs is unclear. The transcription factor AP2IX-5 has been shown to be critical for the proper assembly of the daughter IMC during endodyogeny and was additionally found to bind to and activate the promoters for hundreds of genes involved in budding, including ISP1 and IMC29 [12,13]. The transcriptional repressor AP2XII-2, on the other hand, has been

shown to regulate the cell's progression through S-phase [14]. Therefore, AP2IX-5 or AP2XII-2 seemed to be potential candidates for transcriptional regulation of IMC43, IMC32, and BCC0. However, despite the fact that both AP2IX-5 and AP2XII-2 were found to bind to the promoters of IMC43 and BCC0, neither protein was differentially expressed in response to depletion of these transcription factors [12,15]. Exploration into the many uncharacterized ApiAP2 transcription factors in the future may reveal how transcriptional control of these genes is achieved.

In addition to transcriptional regulation, regulation at the protein level via post-translational modifications is likely to play an important role in the function of these proteins. IMC32 contains a single predicted palmitoylation site which we showed is essential for its localization and function. In *T. gondii*, two palmitoyl acyltransferases (PATs) have been localized to the IMC: DHHC2 and DHHC14 [16]. While DHHC2 is present in both the maternal and daughter IMC, DHHC14 is restricted to the IMC sutures of daughter buds. Transcriptional knockdown of either of these PATs was demonstrated to cause severe defects in IMC morphology. It would be interesting to determine which of these is directly involved in palmitoylating IMC32, as PATs are potentially druggable targets [17]. Another potential means of post-translational regulation is phosphorylation or dephosphorylation. Phosphorylation sites have been identified on IMC43, IMC32, and BCC0 [18]. In addition, in Chapter 2 we identified three kinases (SRPK, CDPK7, and Ark3) and one phosphatase (PPKL) as candidate IMC43 binding partners, further supporting the hypothesis that phosphorylation is used to regulate the essential daughter bud assembly complex. While SRPK has not been studied, its phenotype score suggests it's likely to be essential [19]. Likewise, Ark3, CDPK7, and PPKL have all been shown to play important roles in endodyogeny [20–22]. It is possible that these proteins bind to and modify IMC43 itself, or that IMC43 binding recruits them to the daughter cell scaffold where they act on IMC32, BCC0, or other proteins. Assessing how loss of these proteins affects the components of the essential daughter bud assembly complex (and vice versa) will be an interesting topic of future studies.

Finally, a broader question that warrants investigation is how these and other daughter-specific IMC proteins are removed from the IMC upon bud maturation. A likely mechanism for this would be via the ubiquitin-proteasome system. A study on the ubiquitin proteome of *T. gondii* demonstrated that it encodes many predicted E3 ligases and deubiquitinases and that many ubiquitinated proteins are cell-cycle regulated [23]. While IMC43, IMC32, and BCC0 were not identified in this study, IMC44 was, suggesting a possible mechanism for the release of IMC44 from the body of the IMC during bud constriction. Recently, the putative E3 ligase CSAR1 was shown to be responsible for degradation of the maternal cytoskeleton inside the residual body after bud maturation [24]. However, it was shown to be excluded from daughter buds and thus is unlikely to be involved in the removal of daughter IMC proteins. Better candidates may be the deubiquitinase OTUD3A and the F-box protein FBXO1, both of which have been shown to localize to the daughter IMC and cause serious defects in endodyogeny [25,26]. It would be interesting to assess how loss of either OTUD3A or FBXO1 affects the localization of daughter-specific IMC proteins throughout endodyogeny.

Overall, the detailed investigation of the daughter IMC proteins IMC43, IMC32, BCC0, and IMC44 in this dissertation significantly advances our understanding of the early stages of endodyogeny in *T. gondii*. This work not only provides valuable insights into the molecular basis of daughter bud assembly but also identifies opportunities for future research into the function, regulation, and evolution of these critical proteins in *T. gondii* and other apicomplexan parasites.

### 4.3 References

1. Torres JA, Pasquarelli RR, Back PS, Moon AS, Bradley PJ. Identification and Molecular Dissection of IMC32, a Conserved Toxoplasma Inner Membrane Complex Protein That Is Essential for Parasite Replication. *mBio*. 2021;12: e03622-20. <https://doi.org/10.1128/mBio.03622-20> PMID: 33593973
2. Amos B, Aurrecochea C, Barba M, Barreto A, Basenko EY, Bažant W, et al. VEuPathDB: the eukaryotic pathogen, vector and host bioinformatics resource center. *Nucleic Acids Res*. 2022;50: D898–D911. <https://doi.org/10.1093/nar/gkab929> PMID: 34718728
3. Zhang M, Wang C, Otto TD, Oberstaller J, Liao X, Adapa SR, et al. Uncovering the essential genes of the human malaria parasite *Plasmodium falciparum* by saturation mutagenesis. *Science*. 2018;360: eaap7847. <https://doi.org/10.1126/science.aap7847> PMID: 29724925
4. Jumper J, Evans R, Pritzel A, Green T, Figurnov M, Ronneberger O, et al. Highly accurate protein structure prediction with AlphaFold. *Nature*. 2021;596: 583–589. <https://doi.org/10.1038/s41586-021-03819-2> PMID: 34265844
5. Varadi M, Anyango S, Deshpande M, Nair S, Natassia C, Yordanova G, et al. AlphaFold Protein Structure Database: massively expanding the structural coverage of protein-sequence space with high-accuracy models. *Nucleic Acids Res*. 2022;50: D439–D444. <https://doi.org/10.1093/nar/gkab1061> PMID: 34791371
6. Engelberg K, Bechtel T, Michaud C, Weerapana E, Gubbels M-J. Proteomic characterization of the *Toxoplasma gondii* cytokinesis machinery portrays an expanded hierarchy of its assembly and function. *Nat Commun*. 2022;13: 4644. <https://doi.org/10.1038/s41467-022-32151-0> PMID: 35941170
7. Li Z, Du W, Yang J, Lai D-H, Lun Z-R, Guo Q. Cryo-Electron Tomography of *Toxoplasma gondii* Indicates That the Conoid Fiber May Be Derived from Microtubules. *Adv Sci (Weinh)*. 2023;10: e2206595. <https://doi.org/10.1002/advs.202206595> PMID: 36840635
8. Padilla LFA, Murray JM, Hu K. The initiation and early development of the tubulin-containing cytoskeleton in the human parasite *Toxoplasma gondii*. *Mol Biol Cell*. 2024;35: ar37. <https://doi.org/10.1091/mbc.E23-11-0418> PMID: 38170577
9. Agop-Nersesian C, Egarter S, Langsley G, Foth BJ, Ferguson DJP, Meissner M. Biogenesis of the Inner Membrane Complex Is Dependent on Vesicular Transport by the Alveolate Specific GTPase Rab11B. Sibley LD, editor. *PLoS Pathog*. 2010;6: e1001029. <https://doi.org/10.1371/journal.ppat.1001029> PMID: 20686666
10. Morrissette NS, Sibley LD. Disruption of microtubules uncouples budding and nuclear division in *Toxoplasma gondii*. *J Cell Sci*. 2002;115: 1017–1025. <https://doi.org/10.1242/jcs.115.5.1017> PMID: 11870220

11. Shaw MK, Compton HL, Roos DS, Tilney LG. Microtubules, but not actin filaments, drive daughter cell budding and cell division in *Toxoplasma gondii*. *Journal of Cell Science*. 2000;113: 1241–1254. <https://doi.org/10.1242/jcs.113.7.1241> PMID: 10704375
12. Khelifa AS, Guillen Sanchez C, Lesage KM, Huot L, Mouveaux T, Pericard P, et al. TgAP2IX-5 is a key transcriptional regulator of the asexual cell cycle division in *Toxoplasma gondii*. *Nat Commun*. 2021;12: 116. <https://doi.org/10.1038/s41467-020-20216-x> PMID: 33414462
13. Wang C, Hu D, Tang X, Song X, Wang S, Zhang S, et al. Internal daughter formation of *Toxoplasma gondii* tachyzoites is coordinated by transcription factor TgAP2IX-5. *Cellular Microbiology*. 2021;23. <https://doi.org/10.1111/cmi.13291> PMID: 33217129
14. Srivastava S, White MW, Sullivan WJ. *Toxoplasma gondii* AP2XII-2 Contributes to Proper Progression through S-Phase of the Cell Cycle. *mSphere*. 2020;5: e00542-20. <https://doi.org/10.1128/mSphere.00542-20> PMID: 32938695
15. Srivastava S, Holmes MJ, White MW, Sullivan WJ. *Toxoplasma gondii* AP2XII-2 Contributes to Transcriptional Repression for Sexual Commitment. *mSphere*. 2023;8: e0060622. <https://doi.org/10.1128/msphere.00606-22> PMID: 36786611
16. Dogga SK, Fréna K. Two palmitoyl acyltransferases involved sequentially in the biogenesis of the inner membrane complex of *Toxoplasma gondii*. *Cellular Microbiology*. 2020;22. <https://doi.org/10.1111/cmi.13212> PMID: 32329212
17. Chavda B, Arnott JA, Planey SL. Targeting protein palmitoylation: selective inhibitors and implications in disease. *Expert Opin Drug Discov*. 2014;9: 1005–1019. <https://doi.org/10.1517/17460441.2014.933802> PMID: 24967607
18. Treeck M, Sanders JL, Elias JE, Boothroyd JC. The Phosphoproteomes of *Plasmodium falciparum* and *Toxoplasma gondii* Reveal Unusual Adaptations Within and Beyond the Parasites' Boundaries. *Cell Host & Microbe*. 2011;10: 410–419. <https://doi.org/10.1016/j.chom.2011.09.004> PMID: 22018241
19. Sidik SM, Huet D, Ganesan SM, Huynh M-H, Wang T, Nasamu AS, et al. A Genome-wide CRISPR Screen in *Toxoplasma* Identifies Essential Apicomplexan Genes. *Cell*. 2016;166: 1423-1435.e12. <https://doi.org/10.1016/j.cell.2016.08.019> PMID: 27594426
20. Berry L, Chen C-T, Reininger L, Carvalho TG, El Hajj H, Morlon-Guyot J, et al. The conserved apicomplexan Aurora kinase TgArk3 is involved in endodyogeny, duplication rate and parasite virulence. *Cellular Microbiology*. 2016;18: 1106–1120. <https://doi.org/10.1111/cmi.12571> PMID: 26833682
21. Morlon-Guyot J, Berry L, Chen C-T, Gubbels M-J, Lebrun M, Daher W. The *Toxoplasma gondii* calcium-dependent protein kinase 7 is involved in early steps of parasite division and is crucial for parasite survival. *Cell Microbiol*. 2014;16: 95–114. <https://doi.org/10.1111/cmi.12186> PMID: 24011186

22. Yang C, Doud EH, Sampson E, Arrizabalaga G. The protein phosphatase PPKL is a key regulator of daughter parasite development in *Toxoplasma gondii*. *mBio*. 2023;14: e0225423. <https://doi.org/10.1128/mbio.02254-23> PMID: 37877735
23. Silmon de Monerri NC, Yakubu RR, Chen AL, Bradley PJ, Nieves E, Weiss LM, et al. The Ubiquitin Proteome of *Toxoplasma gondii* Reveals Roles for Protein Ubiquitination in Cell-Cycle Transitions. *Cell Host Microbe*. 2015;18: 621–633. <https://doi.org/10.1016/j.chom.2015.10.014> PMID: 26567513
24. O’Shaughnessy WJ, Hu X, Henriquez SA, Reese ML. *Toxoplasma* ERK7 protects the apical complex from premature degradation. *J Cell Biol*. 2023;222: e202209098. <https://doi.org/10.1083/jcb.202209098> PMID: 37027006
25. Baptista CG, Lis A, Deng B, Gas-Pascual E, Dittmar A, Sigurdson W, et al. *Toxoplasma* F-box protein 1 is required for daughter cell scaffold function during parasite replication. Gubbels M-J, editor. *PLoS Pathog*. 2019;15: e1007946. <https://doi.org/10.1371/journal.ppat.1007946> PMID: 31348812
26. Dhara A, de Paula Baptista R, Kissinger JC, Snow EC, Sinai AP. Ablation of an Ovarian Tumor Family Deubiquitinase Exposes the Underlying Regulation Governing the Plasticity of Cell Cycle Progression in *Toxoplasma gondii*. *mBio*. 2017;8: e01846-17. <https://doi.org/10.1128/mBio.01846-17> PMID: 29162714